universität wien

MASTERARBEIT / MASTER'S THESIS

Titel der Masterarbeit / Title of the Master's Thesis

„Theoretical predictions of the melting point of Si and structure predictions for As, Sb, Se and Te“

verfasst von / submitted by

Florian Dorner BSc

angestrebter akademischer Grad / in partial fulfilment of the requirements for the degree of

Master of Science (MSc)

Wien, 2017 / Vienna, 2017

Studienkennzahl lt. Studienblatt / degree programme code as it appears on the student record sheet:	A 066 876
Studienrichtung lt. Studienblatt / degree programme as it appears on the student record sheet:	Masterstudium Physik
Betreut von / Supervisor:	Univ.-Prof. Dipl.-Ing. Dr. Georg Kresse

Curriculum Vitae

Personal information

Florian Dorner
Obere Amtshausgasse 46/4/2
1050 Wien

Email: dorner3@gmx.at

Date of Birth 04. 05.1991
Place of Birth Oberpullendorf, Austria
Nationality Austria

School education

09/2005–06/2010	HTBLA 7000 Eisenstadt, Austria (Mechatronics)

Civilian service

09/2010–06/2011	Paramedic at Samariterbund 7331 Weppersdorf, Austria

University education

10/2011–06/2013	Studies in Mathematics at the Technical University of Vienna
10/2012–07/2015	Bachelor studies in Physics at the University of Vienna Bachelor thesis: "Level measurement of a caesium oven" Supervisor: Ass.-Prof. Mag. Dr. Peter Steier
10/2015–02/2017	Master's studies in Physics at the University of Vienna Master's thesis: "Crystal structure prediction with the random phase approximation and the melting temperature of silicon" Supervisor: Univ. Prof. Dipl.-Ing. Dr. Georg Kresse

Vienna, 19. February 2017

1 Acknowledgments

I would like to express my deepest appreciation to Univ. Prof. Dr. Georg Kresse, who has offered me the best support I could have ever imagined.

Special thanks to my colleagues Benjamin Ramberger MSc and Tobias Schäfer MSc. They always listened to my problems and helped me to get closer to the solutions.

Michael Pöltl supported me when I had problems with the computer network. Many thanks to him.

Finally, I am grateful for all the encouragement from my parents, my sister, and my friends. With my friend Clemens Etl I could talk about my master's thesis for hours. This enriched my work.

2 Abstract

This Master's thesis is separated into two parts. The first part deals with crystal structure prediction of different materials. The materials of interest are, selenium, tellurium, arsenic and antimony. We are especially interested in Van der Waals (vdW) interactions, which play an important role in these materials. These vdW interactions can lead to problems for density functional calculations (DFT) with a local density approximation (LDA) or a generalized gradient approximation (GGA). To deal with vdW interactions several methods were developed. A class of such methods are the vdW functionals. A vdW functional can be seen as a DFT calculation with an additional energy correcting term. In this master thesis we use three different vdW functionals, the D2 method of Grimme, the method of Tkatchenko-Scheffler and the vdW-DFT method. However there are also other ways to deal with vdW interactions, for example the HSE06 hybrid functional or the random phase approximation (RPA). We tested these methods on the named materials. Using these methods we predicted some structure parameters of these materials and compared them to experimentally measured values.

In the second part we tried to predict the melting temperature of silicon. Previous investigations on this problem led to a melting temperature far below the experimentally measured melting temperature. With the use of the HSE06 functional we improved the melting temperature prediction, compared to previous calculations using DFT-LDA.

3 Zusammenfassung

Diese Masterarbeit besteht aus zwei Teilen. Im ersten Teil wurde die Kristallstruktur von vier verschiedenen Materialien bestimmt. Diese Materialien sind Selen, Tellur, Arsen und Antimon. Dabei interessieren wir uns besonders für Van der Waals (vdW) Wechselwirkungen, die in diesen Materialien auftreten. VdW Wechselwirkungen können durch die Dichtefunktionaltheorie (DFT) mit einer „local density approximation“ (LDA) oder mit einer„generalized gradient approximation“ (GGA) nur schwer beschrieben werden. Um diese vdW Wechselwirkungen dennoch beschreiben zu können wurden mehrere Methoden entwickelt. Eine bestimmte Klasse dieser Methoden sind die vdW Funktionale. Ein vdW Funktional kann als eine DFT Rechnung mit einem zusätzlichen Energie Korrekturterm gesehen werden. In dieser Masterarbeit verwenden wir drei verschiedene vdW Funktionale, die D2 Methode von Grimme, die Methode von Tkatchenko-Scheffler und die vdW-DFT Methode. Jedoch gibt es auch andere Methoden um vdW Wechselwirkungen zu beschreiben. Zum Beispiel das „HSE06 hybrid Funktional“ oder die „Random Phase Approximation“ (RPA). Wir haben all diese Methoden an den hier genannten Materialien getestet. Mit diesen Methoden haben wir einige Strukturparameter von diesen Materialien bestimmt und sie mit experimentell gemessenen Werten verglichen.

Im zweiten Teil haben wir versucht den Schmelzpunkt von Silicium zu bestimmen. Frühere Versuche, den Schmelzpunkt zu bestimmen, resultierten in einer Schmelztemperatur weit unter der experimentell gemessenen Schmelztemperatur. Mit dem „HSE06 hybrid Funktional“ konnten wir die Bestimmung des Schmelzpunktes gegenüber DFT-LDA Rechnungen verbessern.

Contents

4 Introduction

With the big success of the electronic industry, the research of new materials has become a very important function. For example, to produce small and efficient computer processors, it is important to know the properties of the materials, which are used. A special interest exists for the properties of silicon and materials alloyed with silicon. These materials are used in many microelectronic devices.
In materials science, many materials can be modelled by computer simulations based on theoretical solid state physics. The big advantage of computer simulations, compared to experimental measurements, is that a large number of materials can be screened in a rather short time period. Another advantage is that computer models can simulate materials under outside influences, which can not be simulated in a laboratory. One example is very high pressure.
To describe the properties of a material, like the bulk modulus, the heat capacity or the electrical conductivity, it is important to calculate the electronic structure of a material. The electronic structure is relevant for the atomic binding in the solid and therefore relevant for the properties of the material. To give a quantum mechanical description of the electronic structure it is necessary to solve the many body Schrödinger equation. This equation is so complex, that it can not be exactly solved. But there are two approximations of the Schrödinger equation, which have gained a lot of success in the last several decades. These are the Hartree-Fock (HF) theory and the density functional theory (DFT). The HF theory does not fully incorporate electronic correlation and the resulting energies tend to be too high. In the DFT framework there is an unknown term called the exchange and correlation energy. The accuracy of a DFT calculation strongly depends on the approximation of the exchange and the correlation energy. The two most common approximations for the exchange and correlation energy terms are the local density approximation (LDA) and the generalized gradient approximation (GGA). For many materials, a DFT calculation with GGA approximation gives a better approximation to the result of the Schrödinger equation than the HF theory. A problem for the LDA and GGA approximations are materials where Van der Waals (vdW) interactions play a role. By dealing with vdW interactions the dependency of the charge density is nonlocal. Therefore the charge density can not be sufficiently precisely described by the LDA and GGA approximations. Nowadays there are some ways to approximate the exchange and correlation energy of the DFT, to deal with vdW interactions. One of them are the vdW functionals. These methods add a non local energy term to the exchange and correlation energy term, which is calculated by LDA or GGA. This nonlocal energy term consists of empirical parameters, which come from experimental measurements or from atomic theory. Another way to deal with vdW interactions are the so called HF/DFT hybrid functionals. One type of the HF/DFT hybrid functionals is the HS06 functional. This functional separates the energy exchange and correlation term into a short range part and into a long range part. In the short range part the HSE06 functional adds a Hartree-Fock exchange energy term to the GGA exchange energy term. In the long range part the exchange and correlation energy is approximated by the GGA functional. There is also another way, where the exchange and correlation energy is approximated with the use of linear response functions. These response functions react on small changes in the external potential and correct the charge density. This is described by the adiabatic connection fluctuation-dissipation theorem (ACFDT).

5 Born Oppenheimer approximation

The Born Oppenheimer approximation is a method to simplify the many body Schrödinger equation. The idea of this approximation is to separate the motions of the atomic nuclei from the motions of the electrons. Due to the large difference between nuclear and electronic masses, the variations of electronic motions happen on a different time scale than the variations of nuclear motions. Therefore the separation leads to an acceptable approximation of the Schrödinger equation. The Hamiltonian for the hole system can then be written as

$$\hat{H} = \hat{T}_{\mathrm{e}} + \hat{T}_{\mathrm{N}} + \hat{V}_{\mathrm{ee}} + \hat{V}_{\mathrm{NN}} + \hat{V}_{\mathrm{eN}}. \tag{1}$$

In the last equation $\hat{T}_{\mathrm{e}}$ is the kinetic energy operator for the electrons, $\hat{T}_{\mathrm{N}}$ is the kinetic energy operator for the atomic nuclei, $\hat{V}_{\mathrm{ee}}$ is an operator, which describes the interactions between electrons, the $\hat{V}_{\mathrm{NN}}$ operator describes the interactions between atomic nuclei and the $\hat{V}_{\mathrm{eN}}$ operator describes the interactions between electrons and atomic nuclei. In some cases only the electronic structure is interesting, then this can be described by the Hamiltonian

$$\hat{H}_{\mathrm{e}} = \hat{T}_{\mathrm{e}} + \hat{V}_{\mathrm{ee}} + \hat{V}_{\mathrm{eN}} \tag{2}$$

$$\hat{H}_{\mathrm{e}} = \sum_{i}^{N}(-\frac{1}{2}\nabla_i^2 - \sum_{j=1}^{M}\frac{Z_j e}{|\mathbf{r}_i - \mathbf{R}_j|}) + \frac{e^2}{2}\sum_{i}^{N}\sum_{j\neq i}^{N}\underbrace{\frac{1}{|\mathbf{r}_i - \mathbf{r}_j|}}_{\hat{v}}. \tag{3}$$

In the last equation the vector $\mathbf{r}$ describes the position of an electron, the vector $\mathbf{R}$ describes the position of an atomic nuclei, e is the elementary charge and Z is the charge of the atomic nuclei. The Born Oppenheimer approximation is usually the basis, which is used in density functional theory as well as in Hartree-Fock theory.

6 Density functional theory (DFT)

Hohenberg and Kohn dealt with the theoretical description of an inhomogeneous electron gas. In 1964 they published a paper, where they proved that for an interacting electron gas in an external potential $v(\mathbf{r})$, there exists an energy functional of the electron density, $F[n(\mathbf{r})]$, which corresponds to the total energy E of the system. By minimizing the total energy $E[n(\mathbf{r})]$ the ground state energy E_0 is obtained.

$$E_0 = \min_{n(\mathbf{r})} E[n(\mathbf{r})] = \min_{n(\mathbf{r})} \int v(\mathbf{r})n(\mathbf{r}) + F[n(\mathbf{r})]. \tag{4}$$

The mathematical proof of this theorem won't be shown in this work, it can be found in reference [**1**]. The theorem (4) says, that for every external potential there is a certain electron density.

In a paper of Kohn and Sham [**2**], they published a theorem to rewrite the energy functional of the Hohenberg-Kohn theorem. The idea of this new form is to find an effective potential, which includes the contribution of the electron-electron interaction. In this effective potential the electrons can be treated as non-interacting particles.

$$E[n(\mathbf{r})] = \underbrace{\int v(\mathbf{r})n(\mathbf{r})d^3r}_{E_{\mathrm{ext}}} + \underbrace{\frac{1}{2}\int\int \frac{n(\mathbf{r})n(\mathbf{r}')}{|\mathbf{r}-\mathbf{r}'|}d^3r d^3r'}_{E_{\mathrm{H}}} + G[n(\mathbf{r})] \tag{5}$$

$$G[n(\mathbf{r})] \equiv F[n(\mathbf{r})] - \frac{1}{2}\int\int \frac{n(\mathbf{r})n(\mathbf{r}')}{|\mathbf{r}-\mathbf{r}'|}d^3r d^3r'. \tag{6}$$

When we plug equation (6) in equation (5) we obtain equation (4). In equation (5) it can be seen, that the Coulomb term of the electrons, which is commonly termed as the Hartree term E_{H}, is written explicitly and a new functional $G[n(\mathbf{r})]$ is introduced (6). The energy functional $G[n(\mathbf{r})]$ can also be written as

$$G[n(\mathbf{r})] = T_{\mathrm{s}}[n(\mathbf{r})] + E_{\mathrm{xc}}[n(\mathbf{r})], \tag{7}$$

here $T_{\mathrm{s}}[n(\mathbf{r})]$ is the kinetic energy of the non-interacting particles and we define $E_{\mathrm{xc}}[n(\mathbf{r})]$ as exchange and correlation energy. According to the Hohenberg and Kohn theorem for every $v(\mathbf{r})$ there is a certain $T_{\mathrm{s}}[n(\mathbf{r})]$. The $E_{\mathrm{xc}}[n(\mathbf{r})]$ cannot be written in a simple exact expression. There are many ways to approximate this term, which will be shown in section 2. From equation (5) the following variational equation can be obtained

$$\int \delta n(\mathbf{r}) (\underbrace{v(\mathbf{r}) + \int \frac{n(\mathbf{r}')}{|\mathbf{r}-\mathbf{r}'|} d^3r' + \mu_{\mathrm{xc}}[n(\mathbf{r})]}_{v_{\mathrm{eff}}^{\mathrm{KS}}} + \frac{\delta T_{\mathrm{s}}[n(\mathbf{r})]}{\delta n(\mathbf{r})}) d^3r = 0 \tag{8}$$

$$\mu_{\mathrm{xc}}[n(\mathbf{r})] = \frac{\delta E_{\mathrm{xc}}[n(\mathbf{r})]}{\delta n(\mathbf{r})}. \tag{9}$$

According to the theory of Hohenberg and Kohn [**1**], we can interpret equation (8) as a variational equation that stems from the Hamiltonian

$$\hat{H}^{\mathrm{KS}} = \hat{V}_{\mathrm{eff}}^{\mathrm{KS}} + \hat{T}. \tag{10}$$

Using the field operators $\psi(\mathbf{r})$ and $\psi^\dagger(\mathbf{r})$ we obtain

$$\hat{H}^{\mathrm{KS}} = \int v_{\mathrm{eff}}^{\mathrm{KS}}(\mathbf{r}) \psi^\dagger(\mathbf{r}) \psi(\mathbf{r}) d^3r - \frac{1}{2} \int \psi^\dagger(\mathbf{r}) \triangle \psi(\mathbf{r}) d^3r. \tag{11}$$

With the ground state wave function Ψ_0 and

$$n(\mathbf{r}) = \langle \Psi | \, \psi^\dagger(\mathbf{r}) \psi(\mathbf{r}) \, | \Psi \rangle \tag{12}$$

we obtain

$$E_0 = \langle \Psi_0 | \, \hat{H}^{\mathrm{KS}} \, | \Psi_0 \rangle = \int v_{\mathrm{eff}}^{\mathrm{KS}} n(\mathbf{r}) d^3r + T[n(\mathbf{r})] \tag{13}$$

So the Hohenberg and Kohn theorem holds for our Hamiltonian H^{KS}, therefore we can formulate the time-independent Schrödinger for a system of non-interacting particles.

$$(-\frac{1}{2}\nabla^2 + \underbrace{v(\mathbf{r}) + \int \frac{n(\mathbf{r}')}{|\mathbf{r}-\mathbf{r}'|} d^3r' + \mu_{\mathrm{xc}}(\mathbf{r})}_{v_{\mathrm{eff}}^{\mathrm{KS}}}) \phi_m^{\mathrm{KS}}(\mathbf{r}) = \epsilon_m \phi_m^{\mathrm{KS}}(\mathbf{r}) \tag{14}$$

$$n(\mathbf{r}) = 2 \sum_{i=1}^{N} |\phi_m^{\mathrm{KS}}(\mathbf{r})|^2. \tag{15}$$

Equations (14) and (15) have to be solved iterative.

6.1 Exchange and correlation energy

In the last section we showed that the many body Schrödinger equation for an electron gas in an external potential can be rewritten to a Schrödinger equation of non-interacting particles in an effective potential. The new equation (14) can be solved, but there is the exchange and correlation term. This $E_{\mathrm{xc}}[n(r)]$ term is a functional of the electron density and is unknown. There are several ways to approximate this term that we will discuss in this section.

6.1.1 Local density approximation (LDA)

In a system where the variations of the electron density are small, the exchange and correlation energy can be approximated by

$$E_{\mathrm{xc}}(n) \approx E_{\mathrm{xc}}^{\mathrm{LDA}}(n) = \int n(\mathbf{r}) \epsilon_{\mathrm{xc}}^{LDA}(n(\mathbf{r})) d^3r \tag{16}$$

$$E_{\mathrm{xc}} = E_{\mathrm{x}} + E_{\mathrm{c}} \tag{17}$$

where $\epsilon_{\mathrm{xc}}^{\mathrm{LDA}}$ is the local exchange correlation energy per particle of a homogeneous electron gas with the density $n(\mathbf{r})$. For a homogeneous electron gas, the contribution of the exchange energy per particle $\epsilon_{\mathrm{x}}^{\mathrm{hom}}(n)$ can be calculated in an analytical way [**3**].

$$\epsilon_{\mathrm{x}}^{\mathrm{hom}}(n) = -\frac{3}{4}(\frac{3}{\pi})^{\frac{1}{3}} n^{\frac{1}{3}} \tag{18}$$

For the correlation energy per particle $\epsilon_{\mathrm{c}}^{\mathrm{hom}}(n)$ analytical expressions are not known. Therefore quantum Monte Carlo simulations for the energy of an homogeneous electron gas have been performed for different densities [**4**]. The usual approach for the LDA calculation is to interpolate the data points of the quantum Monte Carlo simulations and parameterize $\epsilon_{\mathrm{c}}^{\mathrm{hom}}(n)$. An analytical expression for the interpolation was suggested by Perdew and Wang [**5**].

6.1.2 Generalized gradient approximation (GGA)

A more advanced way to approximate the exchange and correlation energy functional is the generalized gradient approximation GGA. In the GGA the exchange and correlation energy functional is approximated by an integral over a function. The function depends on the density and the gradient of the density

$$E_{\mathrm{xc}}(n) \approx E_{\mathrm{xc}}^{\mathrm{GGA}}(n) = \int f(n, \nabla n) d^3r. \tag{19}$$

In a paper of Perdew, Burke and Ernzerhof (PBE) [**6**] they show a concrete implementation of the generalized gradient approximation GGA. In this master thesis we used the PBE and the B88 functionals.

6.2 Limitations of density function theory

Density functional theory has a wide field of applications and it is often used for electronic structure calculations in science and engineering. The quality of these calculations strongly depends on the approximation of the exchange and correlation energy. A famous example where LDA and GGA lead to big errors are Van der Waals (vdW) interactions. The problem of vdW interactions is that they always correlate electrons at two points in space. With other words to approximate the vdW interactions, a functional would have to know the electron density at two points in space at each time and this is something that the local functionals (LDA and GGA) do not do. In the next chapter we present some DFT correction methods for vdW interactions.

7 vdW functionals

To use DFT for problems which include vdW interactions, some vdW functionals methods have been developed. Some of them are also semi empirical. We call a method semi empirical, when a energy correction E_{corr} term is add to a DFT calculation. The energy correcting therm includes empirical parameters.

$$E = E_{\mathrm{DFT}} + E_{\mathrm{corr}}. \tag{20}$$

In the following sections some of these methods will be presented.

7.1 Method of Grimme (D2)

In the D2 method of Grimme [**7**] the energy correction term is called energy dispersion term E_{disp} and has the form of

$$E_{\mathrm{disp}} = -\frac{1}{2}\sum_{i=1}^{N_{at}}\sum_{j=1}^{N_{at}}\sum_{L}\frac{C_{6ij}}{r_{ij,\mathbf{L}}^{6}} f_{d,6}(r_{ij},\mathbf{L}). \tag{21}$$

where N_{at} is the number of atoms and $\mathbf{L} = (l_1, l_2, l_3)$ are the translational vectors of the unit cell. So in the reference cell $\mathbf{L} = 0$. $r_{ij,\mathbf{L}}$ is the distance between atom i in the reference cell and atom j in cell L. C_{6ij} is the dispersion coefficient between atom i and j. The coefficient can be calculated by

$$C_{6ij} = \sqrt{C_{6ii}C_{6jj}}. \tag{22}$$

Where C_6's are called dispersion coefficients. They can be theoretical calculated for different element. The function

$$f_{d,6}(r_{ij}) = \frac{s_6}{1 + e^{-d(r_{ij}/(s_R R_{0ij})-1)}} \tag{23}$$

is called a damping function. Where s_6 is a global scaling factor which depends on the density functional (PBE $s_6 = 0.75$) that is used. d is a damping parameter. It's usually set to a small number, like $d = 20$. s_R is another scaling factor and R_{0ij} is set to

$$R_{0ij} = \sqrt{R_{0i}R_{0j}} \tag{24}$$

Where R_0's are the experimentally determined values for the atomic vdW radii. They are different for each element.

7.2 Tkatchenko-Scheffler method (TS)

Tkatchenko and Scheffler published another method [**8**]. In this method the energy correction term is identical to the term of the D2 method of Grimme. The idea from Tkatchenko and Scheffler was to rescale the dispersion coefficient and the vdW radius by the volume of an atom in a solid divided by the volume of an atom in free space.

$$C_{6ii}^{\mathrm{TS}} = (\frac{V_A^{\mathrm{eff}}}{V_A^{\mathrm{free}}})^2 C_{6ii}^{\mathrm{free}}. \tag{25}$$

The ratio of volume of an atom in a solid and the atom in free space can be calculated by using the Hirschfeld partitioning of electron density:

$$\frac{V_A^{\mathrm{eff}}}{V_A^{\mathrm{free}}} = \frac{\int r^3 \omega_A(\mathbf{r}) n(\mathbf{r}) d^3r}{\int r^3 n_A^{\mathrm{free}}(\mathbf{r}) d^3r}, \tag{26}$$

where $\omega_A(r)$ is the Hirschfeld weight:

$$\omega_A(\mathbf{r}) = \frac{n_A^{\mathrm{free}}(\mathbf{r})}{\sum_B n_B^{\mathrm{free}}(\mathbf{r})}. \tag{27}$$

Where $n^{\mathrm{free}}(r)$ is the electron density of a free atom. By defining a rule for the strength of the dipole-dipole dispersion interaction between different species, Tkatchenko and Scheffler obtained

$$C_{6ij} = \frac{2 C_{6ii} C_{6jj}}{[\frac{\alpha_j}{\alpha_i} C_{6ii} + \frac{\alpha_i}{\alpha_j} C_{6jj}]}. \tag{28}$$

The polarizability can be rescaled to

$$\alpha_i^{\mathrm{TS}} = (\frac{V_A^{\mathrm{eff}}}{V_A^{\mathrm{free}}})_i \alpha_i^{\mathrm{free}}, \tag{29}$$

and the vdW radius can be rescaled to

$$R_{0i} = (\frac{\alpha_i}{\alpha_i^{\mathrm{free}}})^{\frac{1}{3}} R_{0i}^{\mathrm{free}} \tag{30}$$

with

$$R_{0ij} = R_{0i} + R_{0j}. \tag{31}$$

7.3 vdW-DFT

An other method for dealing with vdW interactions is the vdW-DFT. It has been proposed by Dion et al [**9**]. The idea is, to write the exchange-correlation energy like

$$E_{\mathrm{xc}} = E_{\mathrm{x}}^{\mathrm{GGA}} + E_{\mathrm{c}}^{\mathrm{LDA}} + E_{\mathrm{c}}^{\mathrm{nl}}, \tag{32}$$

where $E_{\mathrm{c}}^{\mathrm{nl}}$ is a nonlocal exchange-correlation energy.

$$E_{\mathrm{c}}^{\mathrm{nl}} = \frac{1}{2} \int \int d^3r d^3r' n(\mathbf{r}) \phi(\mathbf{r}, \mathbf{r}') n(\mathbf{r}'). \tag{33}$$

Here $n(\mathbf{r})$ is the electron density at $\mathbf{r}$ and $\phi(\mathbf{r}, \mathbf{r}')$ is called the nonlocal exchange-correlation kernel. The exchange-correlation kernel has a complicated form and depends on $\frac{1}{|\mathbf{r}-\mathbf{r}'|}$ and on additional parameters.

8 Hybrid functionals

8.1 Hartree-Fock (HF)

The Hartree-Fock theory [**10**] is like the DFT theory, an approximation for the many body Schrödinger equation. In this approximation we start with the Born Oppenheimer approximation. In the next formula we write down the stationary Schrödinger equation for the electronic system.

$$\hat{H}\psi(\mathbf{r}_i) = E\psi(\mathbf{r}_i) \tag{34}$$

with the Hamiltonian:

$$\hat{H} = \sum_i^N (-\frac{1}{2}\nabla_i^2 - \sum_{j=1}^M \frac{Z_j e}{|\mathbf{r}_i - \mathbf{R}_j|}) + \frac{e^2}{2}\sum_i^N \sum_{j\neq i}^N \underbrace{\frac{1}{|\mathbf{r}_i - \mathbf{r}_j|}}_{\hat{v}} \tag{35}$$

For equation (34) with the Hamiltonian of (35) the resulting wave function is too complex, to find an exact result. The idea of the Hartree theory is to separate the wave function in a product of orthonormal one-electron wave functions $\chi_i(x_n)$.

$$\psi(\mathbf{r}_i) = \chi_j(\mathbf{r}_1)\chi_k(\mathbf{r}_2)...\chi_l(\mathbf{r}_N) \tag{36}$$

These are called spin orbitals and include the spin coordinates. We can also separate the Hamiltonian $\hat{H}$.

$$\hat{H} = \sum_{i=1}^N \hat{h}_i \tag{37}$$

with,

$$\hat{h}_i = \underbrace{-\frac{1}{2}\nabla_i^2 - \sum_{j=1}^M \frac{Z_j e}{|\mathbf{r}_i - \mathbf{R}_j|}}_{\hat{o}_i} + \frac{e^2}{2}\sum_{j\neq i}^N \hat{v}_i. \tag{38}$$

Here $\hat{o}$ describes the one particle part of the operator $\hat{h}$ and $\hat{v}$ describes the interaction between the particles. With this operator and the spin orbitals we can calculate the eigenvalues ϵ_j.

$$\hat{h}_i\chi_j(\mathbf{r}_i) = \epsilon_j\chi_j(\mathbf{r}_i) \tag{39}$$

with,

$$E = \sum_i^N \epsilon_i. \tag{40}$$

Now we can write the stationary Schrödinger equation in the following way

$$\hat{H}\prod_j^l \chi_j = E\prod_j^l \chi_j. \tag{41}$$

The problem of this Hartree product ansatz is that it just describes symmetric wave functions, but electrons are Fermions and they have to be described by an antisymmetric wave function. The wave function has to be antisymmetric for exchange of two coordinates.

$$\psi(x_1, ..., x_i, ..., x_j, ...x_n) = -\psi(x_1, ..., x_j, ..., x_i, ...x_n). \tag{42}$$

When we now write the product ansatz for two electrons.

$$\psi_{12}(x_1, x_2) = \chi_i(x_1)\chi_j(x_2) \tag{43}$$

$$\psi_{21}(x_1, x_2) = \chi_i(x_2)\chi_j(x_1). \tag{44}$$

It is easy to see, that this product is not antisymmetric. The proper ansatz must account for the Fock part, that electrons are indistinguishable particles. So we have to modify the Hartree product ansatz to a Hartree-Fock product ansatz. A linear combination of the products was used.

$$\psi(x_1, x_2) = \frac{1}{\sqrt{2}}[\chi_i(x_1)\chi_j(x_2) - \chi_i(x_2)\chi_j(x_1)]. \tag{45}$$

Here the factor $\frac{1}{\sqrt{2}}$ is the normalization constant and in formula (45) we can see that the wave function disappears, if both electrons occupy the same spin orbital. This fulfills the Pauli exclusion principle. We can write this modified product ansatz in a more general way.

$$\psi(x_1, x_2, ..., x_N) = \frac{1}{\sqrt{N!}} \sum_{v=1}^{N!} (-1)^{pv} \hat{P}_v \prod_j^l \chi_j \tag{46}$$

Where $\frac{1}{\sqrt{N!}}$ is the normalization constant and $\hat{P}_v$ is the particle-permutation operator. We also can write the wave function in an alternative way, with the so called Slater-Determinant.

$$\psi(x_1, x_2, ..., x_N) = \frac{1}{\sqrt{N!}} \begin{vmatrix} \chi_j(x_1) & \chi_k(x_1) & \cdots & \chi_l(x_1) \\ \chi_j(x_2) & \chi_k(x_2) & \cdots & \chi_l(x_2) \\ \vdots & \vdots & \ddots & \vdots \\ \chi_j(x_N) & \chi_k(x_N) & \cdots & \chi_l(x_N) \end{vmatrix} \tag{47}$$

When we exchange two rows of a determinant the sign changes, this fulfills the antisymmetric principle. If two columns of a determinant are equal, the result is 0. This rule forbids that two electrons are in the same spin orbital. For calculating the wave function, we can separate the spin orbital in an orbital function ϕ and a spin component s.

$$\chi_i(x_i) = \phi(x_i) \cdot s_i \tag{48}$$

These orbitals are calculated by linear combination of a set of basis function.

$$\phi_i = \sum_k^M c_{ik}\psi_k \tag{49}$$

For the basis functions ψ_k, plane wave and Gaussian functions are commonly used. We will now look at the expected value of $\hat{H}$.

$$\begin{aligned} E &= \langle\psi|\hat{H}|\psi\rangle = \\ &= \sum_i^N (\sum_\alpha^N \underbrace{\int \chi_\alpha^*(\mathbf{r}_i)\hat{o}_i\chi_\alpha(\mathbf{r}_i)d^3\mathbf{r}_i}_{1} + \\ &\frac{e^2}{2}\sum_\alpha^N\sum_{\gamma\neq\alpha}^N (\underbrace{\int\int \chi_\alpha^*(\mathbf{r}_i)\chi_\gamma^*(\mathbf{r}_j)\hat{v}_{ij}\chi_\gamma(\mathbf{r}_j)\chi_\alpha(\mathbf{r}_i)d^3r_i d^3r_j}_{2} - \\ &\underbrace{\int\int \chi_\alpha^*(\mathbf{r}_i)\chi_\gamma^*(\mathbf{r}_j)\hat{v}_{ij}\chi_\gamma(\mathbf{r}_i)\chi_\alpha(\mathbf{r}_j)d^3r_i d^3r_j}_{3})) \end{aligned} \tag{50}$$

Part 2 and 3 of formula (50) describe the interactions between electrons and contribution 1 describes the kinetic energy. Here 2 is the exchange interaction energy between electrons and 3 describes the coulomb interaction between electrons. The disadvantage of the Hartree-Fock theory is that one particle only sees the average potential of all other particles and not the current potential of all other particles and the Hartree-Fock theory does not incorporate the correlation energy between electrons. Therefore in some cases DFT is more accurate, because the theory incorporate the correlation energy of electrons by the approximation of the E_{xc} term.

8.2 Hybrid functionals HSE06

With the use of hybrid functionals, the exchange and correlation energy E_{xc} for density functional theory can be approximated. The approximation of E_{xc}, with the HSE hybrid functional, can be written in the following way.[**11**]

$$E_{\mathrm{xc}}^{\mathrm{HSE}} = \frac{1}{4}E_{\mathrm{x}}^{\mathrm{SR}}(\mu) + \frac{3}{4}E_{\mathrm{x}}^{\mathrm{PBE,SR}}(\mu) + E_{\mathrm{x}}^{\mathrm{PBE,LR}}(\mu) + E_{\mathrm{c}}^{\mathrm{PBE}}(\mu) \tag{51}$$

In this approximation we separate the electron-electron interaction into a short ranged SR and a long ranged part LR. This separation is only realized in the exchange part of the interaction, the correlation energy is approximated by the PBE density functional theory. The separation of the coulomb kernel is realized in the following way.

$$\frac{1}{r} = SR_{\mu}(r) + LR_{\mu}(r) = \frac{erfc(\mu r)}{r} + \frac{erf(\mu r)}{r} \tag{52}$$

In this formula μ is a parameter, which defines the separation range. The parameter is related to a characteristic distance of $\frac{2}{\mu}$. At this distance the short range interaction becomes insignificant. It has been shown that the optimal range of μ is between $(0.2 - 0.3)$Å. The parameter μ can be set by the `HFSCREEN` flag in the `INCAR` file. By setting `HFSCREEN=0.2` the HSE06 method is obtained. The exchange part of PBE density functional theory is calculated for the short and long range ($E_x^{\mathrm{PBE,SR}}(\mu)$,$E_x^{\mathrm{PBE,LR}}(\mu)$) part. For the short range part the exchange energy is also calculated by Hartree-Fock theory $E_x^{\mathrm{SR}}(\mu)$.

$$E_{\mathrm{x}}^{\mathrm{SR}}(\mu) = \frac{e^2}{2}\sum_{\alpha}^{N}\sum_{\gamma\neq\alpha}^{N}\int\int d^3r_i d^3r_j \frac{erfc(\mu|\mathbf{r}_i - \mathbf{r}_j|)}{|\mathbf{r}_i - \mathbf{r}_j|}\chi_{\alpha}^{*}(\mathbf{r}_i)\chi_{\gamma}^{*}(\mathbf{r}_j)\chi_{\gamma}(\mathbf{r}_j)\chi_{\alpha}(\mathbf{r}_i) \tag{53}$$

9 The Random Phase Approximation (RPA)

9.1 The Adiabatic Connection Fluctuation-Dissipation Theorem (ACFDT)

In this section we show another approximation for the exchange and correlation energy term. The idea of the adiabatic connection fluctuation dissipation theorem is to approximate E_{xc} [**12**], by observing a system which turns from the Kohn Sham Hamiltonian into the fully interacting Hamiltonian. To obtain this we have to introduce a parameter λ and the corresponding Hamiltonian $H(\lambda)$.

$$H(\lambda) = T + V(\lambda) + \lambda V_{\mathrm{ee}} \tag{54}$$

In this Hamiltonian $V(\lambda)$ is an external potential, and V_{ee} is the potential of the electron-electron interaction. The parameter is $\lambda \in [0, 1]$. For $\lambda = 1$ we deal with the fully interacting system and for $\lambda = 0$ we have a non interacting Kohn Sham system $V(0) = V_{\mathrm{eff}}^{\mathrm{KS}}$. Now we have to require that the electron densities for all different ground states $|\psi(\lambda)\rangle$ of the Hamiltonians $H(\lambda)$ are equal.

$$\langle\psi(\lambda)|\,\psi(\mathbf{r})^\dagger\psi(\mathbf{r})\,|\psi(\lambda)\rangle \doteq \langle\psi(1)|\,\psi(\mathbf{r})^\dagger\psi(\mathbf{r})\,|\psi(1)\rangle = n(\mathbf{r})\forall\lambda \tag{55}$$

So the external potential $V(\lambda)$ has to be chosen in such a way, that the electron density $n(\mathbf{r})$ is independent of λ.

In the following, we like to derive the adiabatic connection fluctuation-dissipation theorem. First it will be shown that an integral over the expectation value of the electron-electron interaction of the λ dependent ground state will lead to the exchange and correlation energy. This is known as adiabatic connection. Then this integral is expressed by an analytic continuation of a linear response function $\chi^\lambda(\mathbf{r}, \mathbf{r}', i\omega)$, which represents the fluctuation-dissipation part. The fluctuation-dissipation theorem [**13**] predicates that the response of a system to a small external perturbation is the same, as its spontaneous fluctuation.

With the equations (5) and (7) we can write

$$E_{\mathrm{H}} + E_{\mathrm{xc}} = E - E_{\mathrm{ext}} - T_{\mathrm{s}}. \tag{56}$$

The energies for the fully interacting system and the Kohn-Sham system have to be equal to the Hohenberg-Kohn theorems. Therefore we can write,

$$E - E_{\mathrm{ext}} = \langle\psi(1)|\,H(1)\,|\psi(1)\rangle - \langle\psi(1)|\,V(1)\,|\psi(1)\rangle \tag{57}$$

and T_s can be written as

$$T_{\mathrm{s}} = \langle\psi(0)|\,H(0)\,|\psi(0)\rangle - \langle\psi(0)|\,V(0)\,|\psi(0)\rangle\,. \tag{58}$$

When we now insert equation (57) and (58) into (56) we obtain

$$\begin{aligned} E_{\mathrm{Hxc}} &\equiv E_{\mathrm{H}} + E_{\mathrm{xc}} \\ &= \langle\psi(1)|\,H(1)\,|\psi(1)\rangle - \langle\psi(1)|\,V(1)\,|\psi(1)\rangle - \langle\psi(0)|\,H(0)\,|\psi(0)\rangle - \langle\psi(0)|\,V(0)\,|\psi(0)\rangle \\ &= \int_0^1 d\lambda \frac{d}{d\lambda}\,\langle\psi(\lambda)|\,H(\lambda)\,|\psi(\lambda)\rangle - \langle\psi(\lambda)|\,V(\lambda)\,|\psi(\lambda)\rangle \end{aligned} \tag{59}$$

With the help of the Hellmann-Feynman theorem,

$$\frac{d}{d\lambda}E(\lambda) = \frac{d}{d\lambda}\,\langle\psi(\lambda)|\,H(\lambda)\,|\psi(\lambda)\rangle = \langle\psi(\lambda)|\,\frac{d}{d\lambda}H(\lambda)\,|\psi(\lambda)\rangle\,. \tag{60}$$

Equation (59) can be written as,

$$E_{\mathrm{Hxc}} = \int_0^1 d\lambda \left\langle \psi(\lambda) \right| V_{\mathrm{ee}} \left| \psi(\lambda) \right\rangle . \tag{61}$$

Now we like to introduce the linear response function χ. This response function describes the reaction of the system to a small perturbation to the external potential δV_{ext}. In the case of non-interacting particles the response function is called the independent particle polarizability χ^0 and this function describes the response of the system to a small change in the Kohn Sham potential $\delta V_{\mathrm{eff}}^{\mathrm{KS}}$. In the perturbed system there is also a change in the electron density, which depends on the time t and is denoted by $\delta n(\mathbf{r},t) \equiv n_{\mathrm{per}}(\mathbf{r},t) - n_0(\mathbf{r})$. The change in the electron density which depends on the perturbation $\delta V(\mathbf{r},t)$ can be described by the linear response function $\chi(\mathbf{r},\mathbf{r}',t-t')$.

$$\delta n(\mathbf{r},t) = \int dt' \int d^3r \chi(\mathbf{r},\mathbf{r}',t-t')\delta V(\mathbf{r},t') \tag{62}$$

From this equation follows, that the response function $\chi(\mathbf{r},\mathbf{r}',t-t')$ is the derivative of $n(\mathbf{r},t)$ with respect to $\delta V(\mathbf{r}',t')$.

$$\chi(\mathbf{r},\mathbf{r}',t-t') = \frac{\delta n(\mathbf{r},t)}{\delta V(\mathbf{r}',t')} \tag{63}$$

An explicit expression for the response function $\chi(\mathbf{r},\mathbf{r}',t-t')$ can be found in [**14**], it is

$$\chi(\mathbf{r},\mathbf{r}',t-t') = -i\theta(t-t') \left\langle \Psi_0 \right| \left[n(\mathbf{r},t), n(\mathbf{r}',t') \right] \left| \Psi_0 \right\rangle . \tag{64}$$

In this formula Ψ_0 is the ground state of the unperturbed system and [,] is the commutator and $\theta(t-t')$ is a step function. Now we like to change this response function which depends on $t-t'$ to a function which depends on a fixed frequency ω. For this we use a Fourier transformation.

$$\chi(\mathbf{r},\mathbf{r}',i\omega) = \int_{-\infty}^{\infty} dt e^{i\omega t} \chi(\mathbf{r},\mathbf{r}',t) \tag{65}$$

$$= \sum_{j\neq 0} \frac{\left\langle \Psi_0 \right| n(\mathbf{r}) \left| \Psi_j \right\rangle \left\langle \Psi_j \right| n(\mathbf{r}') \left| \Psi_0 \right\rangle}{i\omega - \omega_j} - \frac{\left\langle \Psi_0 \right| n(\mathbf{r}') \left| \Psi_j \right\rangle \left\langle \Psi_j \right| n(\mathbf{r}) \left| \Psi_0 \right\rangle}{i\omega + \omega_j} \tag{66}$$

The derivation of the last equation can be found in [**14**]. In the last equation Ψ_j are excited states and $\omega_j = E_j - E_0$.

Now the response function $\chi^0(\mathbf{r},\mathbf{r}',\omega)$ of a non-interacting system of N fermions shall be introduced. This response function can be written with single particle energy eigenfunctions $\phi_n(\mathbf{r})$ and the corresponding eigenvalues ϵ_n. In the ground state the lowest N energy eigenstates are occupied with one particle and all other states are unoccupied. The expectation value of the density can be written as.

$$\left\langle \Psi_j \right| n(\mathbf{r}) \left| \Psi_0 \right\rangle = \sum_{n,m} \phi_n^*(\mathbf{r})\phi_m(\mathbf{r}) \left\langle \Psi_j \right| a_n^\dagger a_m \left| \Psi_0 \right\rangle \tag{67}$$

Here the creation and annihilation operators, $a_n^\dagger$ and a_m have been used. This expression is zero for $m > N$, because in the ground state there are no occupied states that are higher than ϕ_N. Unoccupied states can't be annihilated. For the next step we need the anticommutator relation for $a_n^\dagger$ and a_m which is

$$\{a_n^\dagger, a_m\} = \delta_{m,n} \tag{68}$$

with that we can rewrite equation (67) in

$$\left\langle \Psi_j \right| n(\mathbf{r}) \left| \Psi_0 \right\rangle = \sum_{n,m\leq N} \phi_n^*(\mathbf{r})\phi_m(\mathbf{r})(\left\langle \Psi_j \right| \delta_{m,n} \left| \Psi_0 \right\rangle - \left\langle \Psi_j \right| a_m a_n^\dagger \left| \Psi_0 \right\rangle). \tag{69}$$

For $j \neq 0$, the term $\langle \Psi_j | \, \delta_{m,n} \, | \Psi_0 \rangle$ vanishes, because the Ψ_j are orthogonal to each other. The term $\langle \Psi_j | \, a_m a_n^\dagger \, | \Psi_0 \rangle$ vanishes for $n \leq N$, because the states below ϕ_{N+1} are already occupied in the ground state. Now we obtain:

$$\langle \Psi_j | \, n(\mathbf{r}) \, | \Psi_0 \rangle = - \sum_{n>N, m \leq N} \phi_n^*(\mathbf{r}) \phi_m(\mathbf{r}) \, \langle \Psi_j | \, a_m a_n^\dagger \, | \Psi_0 \rangle \, \forall j \neq 0 \tag{70}$$

We denote $m \leq N$ as "$m \in occ$", which are the energy levels occupied in the ground state and we denote $n > N$ as "$n \in uocc$", which are the unoccupied energy levels in the ground state. Now we have to consider the term $a_m a_n^\dagger \, | \Psi_0 \rangle$. Therefore we introduce a "single" excited state $| \Psi_{nm} \rangle$. This state is by a single excited particle, from one energy ϵ_m to ϵ_n, different to the ground state. In a set of such states, the states are orthonormal to each other. When we use equation (70) and set Ψ_j=Ψ_{nm}, we obtain

$$\langle \Psi_{nm} | \, n(\mathbf{r}) \, | \Psi_0 \rangle = - \sum_{k,l} \phi_k^*(\mathbf{r}) \phi_l(\mathbf{r}) \, \langle \Psi_{nm} | \, a_l a_k^\dagger \, | \Psi_0 \rangle = - \phi_n^*(\mathbf{r}) \phi_m(\mathbf{r}) \tag{71}$$

This means that we can reduce the response function $\chi^0(\mathbf{r}, \mathbf{r}', \omega)$ from a sum over all excited states as in equation (66), to a sum over all "single" excited states Ψ_{nm}. The next equation shows the final expression of the response function at imaginary frequency.

$$\chi^0(\mathbf{r}, \mathbf{r}', i\omega) = \sum_{n \in uocc, m \in occ} \frac{\phi_n(\mathbf{r}) \phi_m^*(\mathbf{r}) \phi_n^*(\mathbf{r}') \phi_m(\mathbf{r}')}{i\omega - \epsilon_n + \epsilon_m} - \frac{\phi_n(\mathbf{r}') \phi_m^*(\mathbf{r}') \phi_n^*(\mathbf{r}) \phi_m(\mathbf{r})}{i\omega + \epsilon_n - \epsilon_m} \tag{72}$$

In the last equation we had used, that the frequency ω_j depends on the energy difference of a single excitation $\omega_j = \epsilon_n - \epsilon_m$.

After this introduction of the response functions, we can consider the Hartree-exchange-correlation energy.

$$E_{\mathrm{Hxc}} = \int_0^1 d\lambda \, \langle \psi(\lambda) | \, V_{\mathrm{ee}} \, | \psi(\lambda) \rangle = \frac{1}{2} \int_0^1 d\lambda \int d^3r d^3r' \frac{n^{2,\lambda}(\mathbf{r}, \mathbf{r}')}{|\mathbf{r} - \mathbf{r}'|}. \tag{73}$$

Where the electron density operator can be written as $\hat{n}(\mathbf{r}) = \sum_i \delta(\mathbf{r} - \mathbf{r}_i)$ and the pair density as:

$$n^{2,\lambda}(\mathbf{r}, \mathbf{r}') = \langle \Psi(\lambda) | \sum_{ij, i \neq j} \delta(\mathbf{r} - \mathbf{r}_i) \delta(\mathbf{r}' - \mathbf{r}_j) \, | (\lambda) \rangle = \tag{74}$$

$$= \langle \Psi(\lambda) | \sum_{ij} \delta(\mathbf{r} - \mathbf{r}_i) \delta(\mathbf{r}' - \mathbf{r}_j) \, | \Psi(\lambda) \rangle - \delta(\mathbf{r} - \mathbf{r}') \, \langle \Psi(\lambda) | \sum_i \delta(\mathbf{r} - \mathbf{r}_i) \, | \Psi(\lambda) \rangle = \tag{75}$$

$$= \langle \Psi(\lambda) | \, \hat{n}(\mathbf{r}) \hat{n}(\mathbf{r}') \, | \Psi(\lambda) \rangle - \hat{n}(\mathbf{r}) \delta(\mathbf{r} - \mathbf{r}') \tag{76}$$

$$= \langle \Psi(\lambda) | \, \frac{\hat{n}(\mathbf{r}) \hat{n}(\mathbf{r}') + \hat{n}(\mathbf{r}') \hat{n}(\mathbf{r})}{2} \, | \Psi(\lambda) \rangle - n(\mathbf{r}) \delta(\mathbf{r} - \mathbf{r}'). \tag{77}$$

Now the last term of equation (77) should be expressed by the linear response function. To obtain this, it is useful to consider the following expression:

$$\chi(\mathbf{r}, \mathbf{r}', i\omega) + \chi(\mathbf{r}', \mathbf{r}, i\omega) = \tag{78}$$

$$= \sum_{j \neq 0} \frac{\langle \Psi_0 | \, n(\mathbf{r}) \, | \Psi_j \rangle \, \langle \Psi_j | \, n(\mathbf{r}') \, | \Psi_0 \rangle}{i\omega + i\eta - \omega_j} - \frac{\langle \Psi_0 | \, n(\mathbf{r}') \, | \Psi_j \rangle \, \langle \Psi_j | \, n(\mathbf{r}) \, | \Psi_0 \rangle}{i\omega + i\eta + \omega_j} \tag{79}$$

$$+ \frac{\langle \Psi_0 | \, n(\mathbf{r}') \, | \Psi_j \rangle \, \langle \Psi_j | \, n(\mathbf{r}) \, | \Psi_0 \rangle}{i\omega + i\eta - \omega_j} - \frac{\langle \Psi_0 | \, n(\mathbf{r}) \, | \Psi_j \rangle \, \langle \Psi_j | \, n(\mathbf{r}') \, | \Psi_0 \rangle}{i\omega + i\eta + \omega_j} \tag{80}$$

$$
\begin{aligned}
&= \sum_{j\neq 0} \langle\Psi_0|\, n(\mathbf{r})\, |\Psi_j\rangle \langle\Psi_j|\, n(\mathbf{r}')\, |\Psi_0\rangle + \langle\Psi_0|\, n(\mathbf{r}')\, |\Psi_j\rangle \langle\Psi_j|\, n(\mathbf{r})\, |\Psi_0\rangle \\
&\cdot \left(\frac{1}{i\omega + i\eta - \omega_j} - \frac{1}{i\omega + i\eta + \omega_j}\right)
\end{aligned} \tag{81}
$$

$$
\begin{aligned}
&= -\sum_{j\neq 0} \langle\Psi_0|\, n(\mathbf{r})\, |\Psi_j\rangle \langle\Psi_j|\, n(\mathbf{r}')\, |\Psi_0\rangle + \langle\Psi_0|\, n(\mathbf{r}')\, |\Psi_j\rangle \langle\Psi_j|\, n(\mathbf{r})\, |\Psi_0\rangle \\
&\cdot \left(\frac{2\omega_j}{(\omega+\eta)^2 + \omega_j^2}\right)
\end{aligned} \tag{82}
$$

The integration of this expression is:

$$
\begin{aligned}
&\int_0^\infty \chi(\mathbf{r},\mathbf{r}',i\omega) + \chi(\mathbf{r}',\mathbf{r},i\omega) d\omega = \\
&-\pi \sum_{j\neq 0} \langle\Psi_0|\, \hat{n}(\mathbf{r})\, |\Psi_j\rangle \langle\Psi_j|\, \hat{n}(\mathbf{r}')\, |\Psi_0\rangle + \langle\Psi_0|\, \hat{n}(\mathbf{r}')\, |\Psi_j\rangle \langle\Psi_j|\, \hat{n}(\mathbf{r})\, |\Psi_0\rangle \\
&= -\pi(\langle\Psi_0|\, \hat{n}(\mathbf{r})\hat{n}(\mathbf{r}')\, |\Psi_0\rangle + \langle\Psi_0|\, \hat{n}(\mathbf{r}')\hat{n}(\mathbf{r})\, |\Psi_0\rangle) + 2\pi \langle\Psi_0|\, \hat{n}(\mathbf{r})\, |\Psi_0\rangle \langle\Psi_0|\, \hat{n}(\mathbf{r}')\, |\Psi_0\rangle \\
&= -\pi(\langle\Psi_0|\, \hat{n}(\mathbf{r})\hat{n}(\mathbf{r}')\, |\Psi_0\rangle + \langle\Psi_0|\, \hat{n}(\mathbf{r}')\hat{n}(\mathbf{r})\, |\Psi_0\rangle) + 2\pi n(\mathbf{r}) n(\mathbf{r}') \\
&\Rightarrow \langle\Psi(0)|\, \frac{\hat{n}(\mathbf{r})\hat{n}(\mathbf{r}') + \hat{n}(\mathbf{r}')\hat{n}(\mathbf{r})}{2}\, |\Psi(0)\rangle = -\frac{1}{\pi}\int_0^\infty \frac{\chi(\mathbf{r},\mathbf{r}'i\omega) + \chi(\mathbf{r}',\mathbf{r},i\omega)}{2} d\omega + n(\mathbf{r})n(\mathbf{r}')
\end{aligned} \tag{83}
$$

This last relation holds for all systems. By replacing Ψ_0 with Ψ_λ and χ with χ^λ, we can write:

$$
\begin{aligned}
E_{\mathrm{Hxc}} &= \frac{1}{2}\int_0^1 d\lambda \int d^3r d^3r' \frac{1}{|\mathbf{r}-\mathbf{r}'|} \cdot \left(-\frac{1}{\pi}\int_0^\infty \frac{\chi^\lambda(\mathbf{r},\mathbf{r}'i\omega) + \chi^\lambda(\mathbf{r}',\mathbf{r},i\omega)}{2} d\omega + n(\mathbf{r})n(\mathbf{r}') - n(\mathbf{r})\delta(\mathbf{r}-\mathbf{r}')\right) \\
&= \frac{1}{2}\int_0^1 d\lambda \int d^3r d^3r' \frac{1}{|\mathbf{r}-\mathbf{r}'|} \cdot \left(-\frac{1}{\pi}\int_0^\infty \chi^\lambda(\mathbf{r},\mathbf{r}'i\omega) d\omega + n(\mathbf{r})n(\mathbf{r}') - n(\mathbf{r})\delta(\mathbf{r}-\mathbf{r}')\right)
\end{aligned} \tag{84}
$$

In equation (84), the integration variables, for the term $\chi^\lambda(\mathbf{r}',\mathbf{r},i\omega)$, were interchanged. The Hartree term can be written as:

$$
E_{\mathrm{H}} = \frac{1}{2}\int d^3r d^3r' \frac{1}{|\mathbf{r}-\mathbf{r}'|} n(\mathbf{r})n(\mathbf{r}'). \tag{85}
$$

We finally obtain the exchange-correlation energy, by subtracting the Hartree energy from the Hartree-exchange-correlation energy.

$$
\begin{aligned}
E_{\mathrm{xc}} &= E_{\mathrm{Hxc}} - E_{\mathrm{H}} \\
&= -\frac{1}{2}\int_0^1 d\lambda \int d^3r d^3r' \frac{1}{|\mathbf{r}-\mathbf{r}'|} \cdot \left(\frac{1}{\pi}\int_0^\infty \chi^\lambda(\mathbf{r},\mathbf{r}'i\omega) d\omega + n(\mathbf{r})\delta(\mathbf{r}-\mathbf{r}')\right)
\end{aligned} \tag{86}
$$

The last equation shows the ACFDT exchange-correlation energy. For the following RPA method it is common to use the ACFDT correlation energy. To obtain the correlation energy, we have to prove the following expression.

$$
-\frac{1}{2}\int d^3r d^3r' \frac{n(\mathbf{r})\delta(\mathbf{r}-\mathbf{r}')}{|\mathbf{r}-\mathbf{r}'|} = E_{\mathrm{EXX}} + \frac{1}{2}\int d^3r d^3r' \frac{1}{\pi}\int_0^\infty \frac{\chi^0(\mathbf{r},\mathbf{r}',i\omega)}{|\mathbf{r}-\mathbf{r}'|} d\omega \tag{87}
$$

Now the expression for the response function for non-interacting systems from equation (72) and formula (83) are used.

$$\frac{1}{2}\int d^3rd^3r'\frac{1}{\pi}\int_0^\infty \frac{\chi^0(\mathbf{r},\mathbf{r}',i\omega)}{|\mathbf{r}-\mathbf{r}'|}d\omega = -\int d^3rd^3r' \sum_{n\in uocc, m\in occ} \frac{\phi_n(\mathbf{r})\phi_m^*(\mathbf{r})\phi_n^*(\mathbf{r}')\phi_m(\mathbf{r}')}{|\mathbf{r}-\mathbf{r}'|} \tag{88}$$

The exact exchange energy, for the Kohn-Shan orbitals is given by [**2**]

$$E_{\mathrm{EXX}} = -\int d^3rd^3r' \sum_{n\in occ, m\in occ} \frac{\phi_n(\mathbf{r})\phi_n^*(\mathbf{r}')\phi_m(\mathbf{r}')\phi_m^*(\mathbf{r})}{|\mathbf{r}-\mathbf{r}'|} \tag{89}$$

When we now express the right side of equation (87), with (88) and (89).

$$2E_{\mathrm{EXX}} + \int d^3rd^3r'\frac{1}{\pi}\int_0^\infty \frac{\chi^0(\mathbf{r},\mathbf{r}',i\omega)}{|\mathbf{r}-\mathbf{r}'|}d\omega \tag{90}$$

$$= -\Big(\int d^3rd^3r'\Big(\sum_{n\in uocc, m\in occ} \frac{\phi_n(\mathbf{r})\phi_m^*(\mathbf{r})\phi_n^*(\mathbf{r}')\phi_m(\mathbf{r}')}{|\mathbf{r}-\mathbf{r}'|} + \sum_{n\in occ, m\in occ} \frac{\phi_n(\mathbf{r})\phi_n^*(\mathbf{r}')\phi_m(\mathbf{r}')\phi_m^*(\mathbf{r})}{|\mathbf{r}-\mathbf{r}'|}\Big)\Big) \tag{91}$$

$$= -\int d^3rd^3r' \sum_{n,m\in occ} \frac{\phi_n(\mathbf{r})\phi_n^*(\mathbf{r})\phi_m(\mathbf{r}')\phi_m^*(\mathbf{r}')}{|\mathbf{r}-\mathbf{r}'|} \tag{92}$$

$$= -\int d^3rd^3r'\frac{1}{|\mathbf{r}-\mathbf{r}'|}\sum_n \phi_n(\mathbf{r})\phi_n^*(\mathbf{r}')\sum_{m\in occ}\phi_m(\mathbf{r}')\phi_m^*(\mathbf{r}) \tag{93}$$

$$= -\int d^3rd^3r'\frac{n(\mathbf{r})\delta(\mathbf{r}-\mathbf{r}')}{|\mathbf{r}-\mathbf{r}'|} \tag{94}$$

From equation (93) to (94) the fact that the ϕ_n are orthonormal and the definition of a density (15) have been used. Now we finally obtain the correlation energy.

$$\begin{aligned} E_{\mathrm{c}} &= E_{\mathrm{xc}} - E_{\mathrm{EXX}} \\ &= -\frac{1}{2}\int_0^1 d\lambda \int d^3rd^3r'\frac{1}{|\mathbf{r}-\mathbf{r}'|}\cdot\Big(\frac{1}{\pi}\int_0^\infty \chi^\lambda(\mathbf{r},\mathbf{r}'i\omega)d\omega - \chi^0(\mathbf{r},\mathbf{r}',i\omega)d\omega\Big) \end{aligned} \tag{95}$$

The correlation energy per unit cell can also be written in the reciprocal space.

$$\begin{aligned} E_{\mathrm{c}} &= -\frac{1}{2\pi}\int_0^1\int_0^\infty d\omega \sum_{\mathbf{q}\in BZ}\sum_{\mathbf{G}}\frac{4\pi}{|\mathbf{q}+\mathbf{G}|^2}\{\chi^\lambda_{\mathbf{G},\mathbf{G}}(\mathbf{q},i\omega) - \chi^0_{\mathbf{G},\mathbf{G}}(\mathbf{q},i\omega)\} \\ &= -\frac{1}{2\pi}\int_0^1 d\lambda\int_0^\infty d\omega Tr\{v[\chi^\lambda(i\omega)-\chi^0(i\omega)]\} \end{aligned} \tag{96}$$

For the last expression we have used the Coulomb kernel, $v_{\mathbf{G},\mathbf{G}'}(\mathbf{q}) = \frac{4\pi}{|\mathbf{G}+\mathbf{q}|^2}\delta_{\mathbf{G},\mathbf{G}'}$. In real space this kernel depends on $\frac{1}{|\mathbf{r}-\mathbf{r}'|}$.

9.2 Random phase approximation (RPA)

The RPA [**15**] is a way to approximate the response function χ^λ, to solve the ACFDT correlation energy. The response function χ^0 of a non-interacting system is connected to the response function of an interacting system χ^λ, through the Dyson equation.

$$\chi^\lambda(\mathbf{r},\mathbf{r}',i\omega) = \chi^0(\mathbf{r},\mathbf{r}',i\omega) + \int d^3r''d^3r'''\chi^0(\mathbf{r},\mathbf{r}'',i\omega)(\frac{\lambda}{|\mathbf{r}''-\mathbf{r}'''|} + K_{\mathrm{xc}}^\lambda)\chi^\lambda(\mathbf{r}''',\mathbf{r}',i\omega) \quad (97)$$

Where K_{xc}^λ is the exchange-correlation kernel. In the random phase approximation the exchange-correlation kernel is set to zero.

$$\begin{aligned}\chi^\lambda(\mathbf{r},\mathbf{r}',i\omega) &\approx \chi^{\lambda,\mathrm{RPA}}(\mathbf{r},\mathbf{r}',i\omega) \\ &= \chi^0(\mathbf{r},\mathbf{r}',i\omega) + \int d^3r''d^3r'''\chi^0(\mathbf{r},\mathbf{r}'',i\omega)\frac{\lambda}{|\mathbf{r}''-\mathbf{r}'''|}\chi^{\lambda,\mathrm{RPA}}(\mathbf{r}''',\mathbf{r}',i\omega).\end{aligned} \quad (98)$$

We can formulate equation (98) in the reciprocal space,

$$\chi_{\mathbf{G},\mathbf{G}'}^{\lambda,\mathrm{RPA}}(\mathbf{q},i\omega) = \chi_{\mathbf{G},\mathbf{G}'}^0(\mathbf{q},i\omega) + \sum_{\mathbf{G}''}\chi_{\mathbf{G},\mathbf{G}''}^0(\mathbf{q},i\omega)\frac{4\pi\lambda}{|\mathbf{q}+\mathbf{G}''|^2}\chi_{\mathbf{G}'',\mathbf{G}'}^{\lambda,\mathrm{RPA}}(\mathbf{q},i\omega) \quad (99)$$

which can be solved explicitly for $\chi^{\lambda,\mathrm{RPA}}$, we obtain

$$\chi_{\mathbf{G},\mathbf{G}'}^{\lambda,\mathrm{RPA}}(\mathbf{q},i\omega) = \sum_{\mathbf{G}''}(1 - \frac{4\pi\lambda\chi^0(\mathbf{q},i\omega)}{|\mathbf{q}+\mathbf{G}''|^2})_{\mathbf{G},\mathbf{G}''}^{-1}\chi_{\mathbf{G}'',\mathbf{G}'}^0(\mathbf{q},i\omega). \quad (100)$$

To avoid the λ integral in equation (97) we can use:

$$Tr\{\chi^{\lambda,\mathrm{RPA}}v\} = Tr\{(1-\lambda\chi^0(i\omega)v)^{-1}\chi^0(\mathbf{q},i\omega)v\} = -\frac{\delta}{\delta\lambda}Tr\{\ln(1-\lambda\chi^0(i\omega)v)\} \quad (101)$$

With this expression and equation (97) we finally obtain:

$$E_{\mathrm{c}}^{\mathrm{RPA}} = \frac{1}{2\pi}\int_0^\infty d\omega Tr\{\ln(1-\chi^0(i\omega)v) + \chi^0(i\omega)v\} \quad (102)$$

9.3 Calculations with RPA

The total ACFDT energy in the RPA is given by

$$E_{\mathrm{RPA}} = T_{\mathrm{s}} + E_{\mathrm{H}} + E_{\mathrm{EXX}} + E_{\mathrm{c}}^{\mathrm{RPA}} = E_{\mathrm{HF}} + E_{\mathrm{c}}^{\mathrm{RPA}}. \tag{103}$$

As it is seen in formula (103) the Hartree-Fock energy for the Kohn-Sham wave functions and the RPA correlation energy have to be calculated. In `VASP`, the RPA energy is calculated in four steps. The first step is a standard DFT run, with a high precision. In the second step the Hartree-Fock energy E_{HF} is calculated with the DFT orbitals. To obtain a HF energy, the flag `LHFCALC=.TRUE.` and `AEXX=1.0` has to be set. The flag `NELM=1` sets the number of electronic self-consistency steps to one, because the DFT orbitals need to be used. The `AEXX=1` (section 12) flag specifies that the whole exact exchange energy is calculated. To allow to recalculate electron energies and perform selected postprocessing using the current orbitals specified in the `WAVECAR` file, `ALGO=Eigenval` was set. To prevent the program form overwriting the orbitals from step one, the flag `LWAVE=.FALSE.` was set. For insulators and materials with a sizeable band gap, the flag `HFRCUT=-1`, for a faster convergence of the Hartree-Fock energy, can be set. In the third step, all virtual states are determined by an exact diagonalization of the DFT Hamiltonian. We obtain this by setting `ALGO=Exact`. Also the flag `NBANDS` has to be set to the 'maximum number of plane-waves' which were used in the first step. Additionally `LOPTICS=.TRUE.` is used to calculate the frequency dependent dielectric matrix [**16**]. In the fourth step the RPA correlation energy is calculated. This is obtained by setting `ALGO=ACFDT`. Additionally the flag `NOMEGA=8` is set, which determines the grid which is used for Fourier transforms between imaginary time and imaginary frequency domains. For the RPA correlation energy formula (102) is used, which is in the reciprocal space

$$E_{\mathrm{c}}^{\mathrm{RPA}} = \frac{1}{2\pi}\int_0^\infty d\omega \sum_{\mathbf{q}\in BZ}\sum_{\mathbf{G}}\{ln(1-\chi^0(\mathbf{q},i\omega)v(\mathbf{q}))_{\mathbf{G},\mathbf{G}} + \chi^0(\mathbf{q},i\omega)_{\mathbf{G},\mathbf{G}}v(\mathbf{q})_{\mathbf{G},\mathbf{G}}\} \tag{104}$$

The sum over G is truncated at a certain $G_{\max}$, which is determined by the `ENCUTGW` flag.

$$\frac{\hbar|\mathbf{q}+\mathbf{G}_{\max}|^2}{2m_e} < \mathrm{ENCUTGW} \tag{105}$$

After these four steps the Hartree-Fock and the RPA correlation energy per unit cell have been calculated.

In the case of metals, `HFRCUT` in step two is not set and an additional correction energy for the E_{HF}, related to partial occupancies has to be added.

$$E_{\mathrm{RPA}} = E_{\mathrm{c}}^{\mathrm{RPA}} + E_{\mathrm{HF}} + E_{\mathrm{HFc}} \tag{106}$$

This additional energy term is calculated for any Hartree-Fock type calculation, like in step two.

10 Performing a DFT calculation

When we simulate materials, we are not interested in electrons that are near the atomic core. We are predominantly interested in electrons in valence bands, because they are essential for chemical bonding. Electrons can be described through Bloch waves. The Bloch waves are realized by a linear combination of plane waves[**17**].

$$\phi_{n,k}(\mathbf{r}) = \sum_{\mathbf{G}} c_{n,k}(\mathbf{G}) e^{i(\mathbf{k}+\mathbf{G})\mathbf{r}}, \tag{107}$$

where $\mathbf{G}$ is a reciprocal vector. The reciprocal vectors have the right periodicity to fulfill the boundary conditions of a crystal and there is an infinit set of reciprocal vectors $\mathbf{G}$. For computational reasons we have to define a cut-off energy E_{cut}.

$$E_{\text{cut}} > \frac{\hbar}{2m}|\mathbf{k}+\mathbf{G}|^2 \tag{108}$$

This expression limits the set of $\mathbf{G}$ vectors.

For calculating the electron density, we have to integrate over all possible $\mathbf{k}$ vectors in the Brillouin-Zone.

$$n(\mathbf{r}) = \sum_n \int_{BZ} |\phi_{n,k}(\mathbf{r})|^2 d^3k \tag{109}$$

To approximate the integral, a set of k points is used.

$$n(\mathbf{r}) \approx \sum_n \sum_k \omega_k |\phi_{n,k}(\mathbf{r})|^2 \tag{110}$$

This approximation depends on how the k points are set and therefore on the symmetry of the Brillouin-Zone. In `VASP` there are two automatic ways to set the k points [**18**]. One of them is called the Gamma centered k point mesh. Here it is necessary to set subdivisions N_1 , N_2 and N_3. The k points are then calculated in the following way.

$$\mathbf{k} = \mathbf{b}_1 \frac{n_1+s_1}{N_1} + \mathbf{b}_2 \frac{n_2+s_2}{N_2} + \mathbf{b}_3 \frac{n_3+s_3}{N_3} \tag{111}$$

with,

$$n_1 = 0..., N_1 - 1 \quad n_2 = 0..., N_2 - 1 \quad n_3 = 0..., N_3 - 1. \tag{112}$$

Where $\mathbf{b}_1$, $\mathbf{b}_2$ and $\mathbf{b}_3$ are reciprocal lattice vectors. s_1, s_2 and s_3 can be set to obtain an additional shift away from the Γ point. Normally these shifts are set to zero.

The other method is called the Monkhorst-Pack k point mesh. Here the k points are calculated in the following way.

$$\mathbf{k} = \mathbf{b}_1 \frac{n_1+s_1+\frac{1}{2}}{N_1} + \mathbf{b}_2 \frac{n_2+s_2+\frac{1}{2}}{N_2} + \mathbf{b}_3 \frac{n_3+s_3+\frac{1}{2}}{N_3} \tag{113}$$

The choice of the k mesh depends on the symmetry of the Brillouin-Zone. A good choice of the k points leads to convergence with fewer k points and therefore it also leads to less computing time.

10.1 Pseudopotentials

To describe the wave function of the core electrons and the rapid oscillations of valence electrons a very large plane wave basis set would be necessary [**17**]. With the use of a pseudopotentials we can reduce the basis set and give a sufficiently accurate description of the electronic system. The idea of the pseudopotential approximation is that most of the properties of solids are predominantly determined by the valence electrons and much less by the core electrons. The pseudopotential contains both, the Coulomb potential of the nucleus and the effects of core electrons on the valence electrons. If a pseudopotential is used, the true wave functions are replaced by pseudo wave functions. A pseudo wave function can be different to the true wave function in the core region, but outside the core region the pseudo wave function has to be identical to the true wave function of the valence electrons. In this master thesis we mainly use the projected augmented wave (PAW) pseudopotential. Valence wave functions tend to have rapid oscillations near the ion core. The PAW approach replaces these wave functions with smooth pseudo wave functions. This leads to less computational requirement[**19**].

11 Free energy calculations

The free energy can not be calculated directly from a single molecular dynamics simulation (MD), because the free energy cannot be expressed by an ensemble average. In this section some methods to calculate free energy differences between two systems will be presented. And in the end of this section lattice vibrations and the free energy in crystals will be discussed.

11.1 Thermodynamic Integration (TI)

The free energy difference ΔF between a reference system and a final system can be calculated by different methods. Thermodynamic Integration (TI) [**20**] is such a method to calculate the free energy difference ΔF. In TI we require that the two systems have different potential energies. We denote the reference system with U_A and the final system with U_B. To apply TI we need to construct a potential energy function which describes the system going from the reference state to the final state. The most convenient choice is a linear function

$$U(\lambda) = U_A + \lambda(U_B - U_A), \tag{114}$$

with the parameter $\lambda \in [0,1]$. To write the free energy difference $\Delta F = F_B - F_A$ in an integral form we used the fundamental theorem of calculus [**21**]

$$\Delta F = \int_0^1 \frac{\partial F(\lambda)}{\partial \lambda} d\lambda. \tag{115}$$

This integral can be calculated by using the free energy formula for the canonical ensemble

$$F(\lambda) = -\frac{1}{\beta} \ln Z(\lambda). \tag{116}$$

Z is the partition function

$$Z(\lambda) = \sum_i e^{-\beta U_i(\lambda)}. \tag{117}$$

When we now use equation (116) and (117), we can find an expression for the derivation of the free energy.

$$\frac{\partial F(\lambda)}{\partial \lambda} = \frac{1}{Z} \sum_i e^{-\beta U_i(\lambda)} \frac{\partial U(\lambda)}{\partial \lambda} \tag{118}$$

The expression of (118) can be written as the expected value in the canonical ensemble

$$\frac{\partial F(\lambda)}{\partial \lambda} = \langle \frac{\partial U(\lambda)}{\partial \lambda} \rangle_\lambda. \tag{119}$$

When we now insert equation (119) in equation (115) we obtain the final form of our integral

$$\Delta F = \int_0^1 \langle \frac{\partial U(\lambda)}{\partial \lambda} \rangle_\lambda d\lambda. \tag{120}$$

With the use of formula (114) we obtain

$$\Delta F = \int_0^1 \langle \Delta U \rangle_\lambda d\lambda, \tag{121}$$

with $\Delta U = U_B - U_A$.

The value of $\langle \Delta U(\lambda) \rangle_\lambda$ for a fixed λ can be calculated, by performing a molecular dynamics (MD) simulation. In the MD simulation $U(\lambda)$ is the potential energy, which moves the atoms in the simulation. U_A and U_B have to be evaluated for each resulting configuration, to calculate ΔU. For integral (121) multiple simulations for different values of λ have to be performed. After that a numerical integral scheme has to be used.

11.2 Thermodynamic Perturbation Theory (TPT)

Thermodynamic perturbation theory (TPT) [**22**] is another method to calculate the free energy difference ΔF between two systems. For presenting the method, we start with the partition function.

$$Z = \sum_i e^{-\beta U_i}. \tag{122}$$

Using (116) we can write the free energy difference as:

$$\Delta F = F_B - F_A = -\frac{1}{\beta} \ln(\frac{Z_B}{Z_A}). \tag{123}$$

With the equation (122) we obtain:

$$\Delta F = -\frac{1}{\beta} \ln(\frac{1}{Z_A} \sum_i e^{-\beta U_{B,i}}). \tag{124}$$

We can multiply the integrand with $e^{\beta U_{A,i}}$ and $e^{-\beta U_{A,i}}$

$$\begin{aligned} \Delta F &= -\frac{1}{\beta} \ln(\frac{1}{Z_A} \sum_i e^{-\beta(U_{B,i} - U_{A,i})} e^{-\beta U_{A,i}}) \\ &= -\frac{1}{\beta} \ln(\sum_i e^{-\beta \Delta U_i} P_0(U_A)) \\ &= -\frac{1}{\beta} \ln \langle e^{-\beta \Delta U} \rangle_A. \end{aligned} \tag{125}$$

Where $P_0(U_A)$ is the probability density to find the system A in a certain state $U_{A,i}$. It can also be seen as a function of ΔU. The probability density $P_0(\Delta U)$ is often a Gaussian distribution and can be approximately written as:

$$P_0(\Delta U) = \frac{1}{\sqrt{2\pi}\sigma} e^{-\frac{(\Delta U - \langle \Delta U \rangle_0)^2}{2\sigma^2}}. \tag{126}$$

With the standard deviation,

$$\sigma = \langle \Delta U^2 \rangle - \langle \Delta U \rangle_0^2. \tag{127}$$

By multiplying the probability density with the Boltzmann distribution $e^{-\beta \Delta U} P_0(\Delta U)$ a new shifted Gaussian distribution is obtained. It can be show that the mean value of this new function is shifted by $-\frac{1}{2}\beta\sigma^2$ from $\langle \Delta U \rangle_0$.

$$\Delta F = \langle \Delta U \rangle_0 - \frac{1}{2} \beta \sigma^2 \tag{128}$$

This can be seen in figure 1.

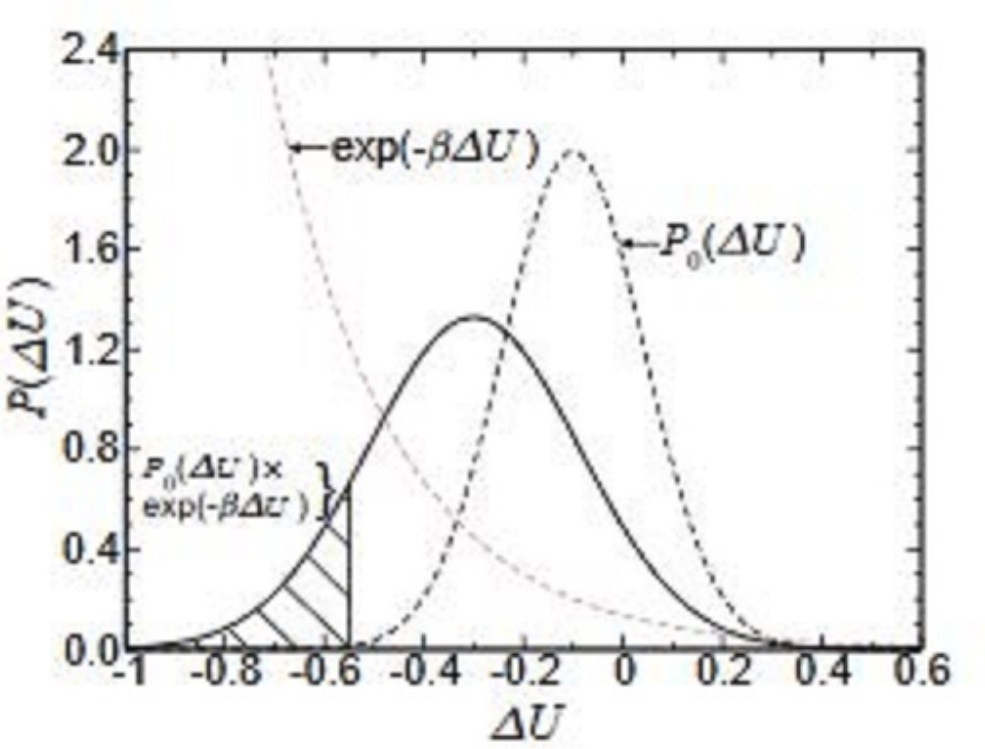

Figure 1: *Probability density $P_0(\Delta U)$, Boltzmann distribution $e^{-\beta\Delta U}$ and $e^{-\beta\Delta U}P_0(\Delta U)$ as a function of ΔU* [**37**]

Figure 1 shows the probability to find system A and system B in certain configurations where the energy is $\Delta U = U_B - U_A$. If the distribution $P_0(\Delta U)$ has a large standard deviation σ compared to $\frac{1}{\beta}$, the shift $-\frac{1}{2}\beta\sigma^2$ is large and then there are not many configurations which sample the $e^{-\beta\Delta U}P_0(\Delta U)$ distribution. But this distribution is used to calculate the free energy difference ΔF. In other words, if there are no configurations in the hatched area of figure 1 than the result for ΔF will be inaccurate.

To calculate this expected value from equation (125), it is necessary to perform an MD simulation with the potential U_A and a calculation for the resulting configurations with potential U_B. For calculating $\Delta U = U_B - U_A$ it is more efficient to use statistically independent configurations for the calculation of U_B. In this way if the calculation of U_B is much more expensive than of U_A, U_B does not have to be calculated for every simulation step.

The thermodynamic perturbation theory can take less computing time than the TI, because only one MD is required. The problem of the TPT is that it becomes inaccurate if U_A and U_B are too different. When U_A and U_B are very different the probability distribution $P_0(\Delta U)$ has a large standard deviation σ. Therefore the calculation of ΔF is inaccurate. To test if U_A and U_B are close enough, we use the 2nd order Taylor expansion of equation (125)

$$\Delta F = -\beta \ln\langle e^{-\beta\Delta U}\rangle_A \approx \langle\Delta U\rangle_A - \frac{\beta}{2}\langle(\Delta U)^2\rangle_A + \frac{\beta}{2}\langle\Delta U\rangle_A^2. \tag{129}$$

If this approximation is very close to the value of the logarithm, the result for ΔF can be often used.

11.3 Lattice vibrations and free energy in crystals

In this section we like to describe the lattice vibrations in crystals [**23**]. First we have to make an assumption about all displacements, that the atoms can adopt through the lattice

vibrations. The displacements have to be small compared to the lattice constant. The position $\mathbf{r}_i$ of each atom is then given by

$$\mathbf{r}_i = \mathbf{R}_i + \mathbf{u}_i, \tag{130}$$

with $\mathbf{R}_i$ the positions in a Bravais lattice and $\mathbf{u}_i$ the displacements. With this relation we can write the potential U as

$$U = \phi(\mathbf{r}_i) = \phi(\mathbf{R}_i + \mathbf{u}_i). \tag{131}$$

We can now apply a Taylor expansion around $\mathbf{R}_i$. We expand this series to the third order and neglect all the higher order terms. The error than is proportional to $\mathcal{O}(\Delta u^4)$.

$$U = \phi(\mathbf{r}_i) + \sum_{i,j} \frac{\partial}{\partial \mathbf{r}_i}\phi(\mathbf{r}_i)\cdot\mathbf{u}_i + \frac{1}{2}\sum_{i,j}\frac{\partial^2}{\partial \mathbf{r}_i \partial \mathbf{r}_j}\phi(\mathbf{r}_i)\cdot\mathbf{u}_i\cdot\mathbf{u}_j + \frac{1}{6}\sum_{i,j,k}\frac{\partial^3}{\partial \mathbf{r}_i \partial \mathbf{r}_j \partial \mathbf{r}_k}\phi(\mathbf{r}_i)\cdot\mathbf{u}_i\cdot\mathbf{u}_j\cdot\mathbf{u}_k \tag{132}$$

Now we apply a harmonic approximation to this potential. In the harmonic approximation we describe the potential just for small displacements around the equilibrium. For these small displacements the potential from (132) can be replaced by a harmonic potential.

$$U_{\text{harm}} = \phi(\mathbf{r}_i) + \frac{1}{2}\sum_{i,j}\frac{\partial^2}{\partial \mathbf{r}_i \partial \mathbf{r}_j}\phi(\mathbf{r}_i)\cdot\mathbf{u}_i\cdot\mathbf{u}_j. \tag{133}$$

With this potential we can calculate a coupling constant

$$C_i^j = \frac{\partial^2}{\partial \mathbf{r}_i \partial \mathbf{r}_j} U_{\text{harm}}. \tag{134}$$

The coupling constant describes how the displacement of atom j acts on atom i and the constant has the dimension of a spring constant

$$F_i = -C_i^j \mathbf{u}_j. \tag{135}$$

With this relation we can write the equation of motion. In this equation the displacements from all atoms in the system act on the atom i and m_i denotes the mass of atom i

$$m_i \ddot{\mathbf{u}}_i = -\sum_j C_i^j \mathbf{u}_j. \tag{136}$$

To solve this equation we use a plane wave ansatz $\mathbf{u}_i = \frac{1}{\sqrt{m}}\mathbf{A}(\mathbf{k})\cdot e^{i(\mathbf{k}\cdot\mathbf{R}_i - \omega t)}$ for the displacements. Where $\mathbf{k}$ is the wave vector. When we plug this ansatz into the equation of motion, we obtain

$$-\omega^2 \mathbf{A}_i(\mathbf{k}) + \sum_j \sum_{n,m} \frac{1}{\sqrt{m_i m_j}} C_i^j e^{i\mathbf{k}\cdot(\mathbf{R}_n - \mathbf{R}_m)} \mathbf{A}_j(\mathbf{k}) = 0. \tag{137}$$

This equation can be rewritten, by using the dynamic matrix D

$$D_i^j(\mathbf{k}) = \sum_{n,m} \frac{1}{\sqrt{m_i m_j}} C_i^j e^{i\mathbf{k}\cdot(\mathbf{R}_n - \mathbf{R}_m)}. \tag{138}$$

With D we obtain the equation of motion

$$-\omega^2 \mathbf{A}_i(\mathbf{k}) + \sum_j D_i^j(\mathbf{k})\mathbf{A}_j(\mathbf{k}) = 0. \tag{139}$$

This equation of motion can be seen as a homogeneous equation system and the coefficients can be determined by solving

$$det[\mathbf{D} - \omega^2 \mathbb{1}] = 0. \tag{140}$$

This equation has $s = 3 \cdot r$ results of $\omega(\mathbf{k})$ for each wave vector $\mathbf{k}$. r is the number of basis atoms and $\omega(\mathbf{k})$ is known as the dispersion relation. The s different solutions of $\omega(\mathbf{k})$ are known as the dispersion branches. These branches can be separated in acoustic branches and optic branches. The difference between these branches are their frequency ranges. In a crystal there are 3 acoustic branches and $3 \cdot r - 3$ optical branches. A crystal with a one atom basis only has 3 acoustic branches, one of them is a longitudinal wave and two of them are transversal waves.

11.3.1 Quantum mechanical description of the harmonic lattice vibrations

To obtain a quantum mechanical description, we have to quantize the lattice vibration modes into phonons. Each one of the $3 \cdot N$ frequency modes of $\omega_s(\mathbf{k})$ are connected to a harmonic oscillator with the frequency $\omega_s(\mathbf{k})$. s describes the dispersion branch. For a one atomic basis $s \in [1, 3]$ and N is the total number of atoms in the system. The energy for one mode is given by,

$$\epsilon_{k,s} = \hbar\omega_s(\mathbf{k}) \cdot (n_{k,s} + \frac{1}{2}). \tag{141}$$

We can say that $n_{k,s}$ phonons are in the state of the energy $\hbar\omega_s(\mathbf{k})$. Now we can write the energy of a crystal as

$$E_{\text{dyn}} = \frac{1}{N} \sum_{k,s} \hbar\omega_s(\mathbf{k}) \cdot (n_{k,s} + \frac{1}{2}). \tag{142}$$

The last formula also describes the zero point energy of

$$E_0 = \sum_{k,s} \frac{\hbar\omega_s(\mathbf{k})}{2}. \tag{143}$$

This is the vibrational energy, which the crystal has at zero temperature. Phonons are bosons, therefore the occupation number $n_{k,s}$ for each energy state is calculated through the Bose-Einstein statistic. The average of the occupation value for a given state is given by

$$\langle n_{k,s} \rangle = \frac{1}{\exp(\beta\hbar\omega_s(\mathbf{k})) - 1}. \tag{144}$$

We can use equation (144) and plug it into formula (142) for the energy of the crystal, which gives us

$$E_{\text{dyn}} = \frac{1}{N}(\sum_{k,s} \frac{\hbar\omega_s(\mathbf{k})}{2} + \sum_{k,s} \frac{\hbar\omega_s(\mathbf{k})}{\exp(\beta\hbar\omega_s(\mathbf{k})) - 1}), \tag{145}$$

and the internal energy is given by

$$U = E_{\text{eq}} + \frac{1}{N}(\sum_{k,s} \frac{\hbar\omega_s(\mathbf{k})}{2} + \sum_{k,s} \frac{\hbar\omega_s(\mathbf{k})}{\exp(\beta\hbar\omega_s(\mathbf{k})) - 1}). \tag{146}$$

11.3.2 Free energy of a harmonic oscillating crystal

The free energy of a harmonic oscillating crystal can be calculated through the partition function Z [**24**].

$$F = -k_B T \ln(Z) \tag{147}$$

The canonical partition function for one quantum mechanical oscillator $Z_{k,s}$ is given by

$$Z_{k,s} = \sum_{n=0}^{\infty} \exp[-\beta\hbar\omega_s(\mathbf{k}) \cdot (n + \frac{1}{2})]. \tag{148}$$

This is a geometric series and can be written as,

$$Z_{k,s} = \frac{\exp(\frac{-\beta\hbar\omega_s(\mathbf{k})}{2})}{1 - \exp(-\beta\hbar\omega_s(\mathbf{k}))} = \frac{\exp(\frac{\beta\hbar\omega_s(\mathbf{k})}{2})}{\exp(-\beta\hbar\omega_s(\mathbf{k})) - 1}. \tag{149}$$

For a crystal of N atoms the partition function is a product of the partition functions of 3N different quantum mechanical oscillators

$$Z = \prod_{k,s} \frac{\exp(\frac{\beta\hbar\omega_s(\mathbf{k})}{2})}{\exp(\beta\hbar\omega_s(\mathbf{k})) - 1}. \tag{150}$$

With this we obtain the free energy of a harmonic oscillating crystal

$$F_{\text{harm}} = -\frac{1}{\beta}\ln(Z) = \sum_{k,s}[\frac{\hbar\omega_s(\mathbf{k})}{2} + k_B T \cdot \ln(1 - \exp(-\beta\hbar\omega_s(\mathbf{k}))]. \tag{151}$$

To obtain the free energy per unit cell. We can rewrite the sum over the **k** vectors to an integral over the Brillouin zone.

$$F_{\text{harm}} = \frac{1}{\Omega_{BZ}} \sum_s \int_{BZ} [\frac{\hbar\omega_s(\mathbf{k})}{2} + k_B T \cdot \ln(1 - exp(-\beta\hbar\omega_s(\mathbf{k}))] d\mathbf{k} \tag{152}$$

11.3.3 Anharmonic oscillations

In every crystal there are also anharmonic oscillations. These oscillations are seen as the deviation from a system to the harmonic oscillation. To deal with anharmonic oscillation, we have to consider all terms of equation (132). In the phonon picture this means that the phonons interact with each other and can be scattered. In practise anharmonic oscillations are calculated by a full interacting ab-initio molecular dynamic simulation.

12 Thermostat

The MD method is an approach to simulate a micro-canonical (NVE) ensemble. When we want to simulate a canonical (NVT) ensemble we have to use a thermostat. There are two kinds of thermostats. Some of them use stochastic particle collisions, which should simulate the heat bath. Other thermostats modify the equations of motion in the MD simulation, to simulate a canonical ensemble. In this master thesis both types of thermostats had been used. Here we present the Langevin thermostat and the Nosé-Hoover thermostat.

12.1 Langevin thermostat

The Langevin thermostat is a stochastic thermostat [**25**]. We can write the equation of motion in the following way

$$\dot{\mathbf{r}}_i = \frac{\mathbf{p}_i}{m_i} \tag{153}$$

$$\dot{\mathbf{p}}_i = F_i - \gamma_i \mathbf{p}_i + f_i. \tag{154}$$

In equation (154) F_i is the force acting on atom i and γ_i is a friction coefficient. f_i is a random force chosen from a Gauss distribution, with an mean value of zero and a variance of σ_i^2.

$$\sigma_i^2 = \frac{2 m_i \gamma_i k_B T}{\Delta t} \tag{155}$$

The variance σ_i^2 depends on the friction coefficient γ_i, on the temperature T and on the time-step Δt of the MD simulation. In `VASP` this method can be set with following flags. `MDALGO=3` to set the Langevin thermostat, the flag `TEBEG` is used to set the temperature and with the `LANGEVIN_GAMMA` flag the friction coefficient γ_i can be set.

12.2 Nosé-Hoover thermostat

The idea of the Nosé-Hoover thermostat is to extend phase space from a normal $6N$ to a $6N + 2$ dimensional system [**26**]. Here 6 stands for 3 space coordinates and 3 momentum coordinates. The value N stands for the number of particles. So in the Nosé-Hoover thermostat there are two additional phase coordinates. This system can be described with the following Hamiltonian

$$H_{\mathrm{N}}(\mathbf{p}^N, \mathbf{r}^N, p_s, s) = \sum_{i=1}^{N} \frac{\mathbf{p}_i^2}{2 m_i s^2} + U(\mathbf{r}^N) + \frac{p_s^2}{2Q} + \frac{g}{\beta} \ln(s). \tag{156}$$

Here the parameter Q determines how quickly the thermostat reacts. This relates to the common notion that the parameter Q is often called the thermostat mass. T is the parameter for the temperature of the ensemble and g is a scaling constant. This Hamiltonian leads to the following equations of motion.

$$\dot{\mathbf{r}}_i = \frac{\delta H_{\mathrm{N}}}{\delta \mathbf{p}_i} = \frac{\mathbf{p}_i}{m_i s^2} \tag{157}$$

$$\dot{\mathbf{p}}_i = -\frac{\delta H_{\mathrm{N}}}{\delta \mathbf{r}_i} = \mathbf{F}_i \tag{158}$$

$$\dot{s} = \frac{\delta H_{\mathrm{N}}}{\delta p_s} = \frac{p_s}{Q} \tag{159}$$

$$\dot{p}_s = -\frac{\delta H_{\mathrm{N}}}{\delta s} = \frac{1}{s}[\sum_{i=1}^{N} \frac{\mathbf{p}_i^2}{m_i s^2} - \frac{g}{\beta}] \tag{160}$$

In these equations it is easy to see that s controls the velocities of the particles, but the change of s corresponds to p_s. On the other hand the change of p_s corresponds to the momentum of the particles $\mathbf{p}_i$ scaled by the temperature T. With this method an MD simulation for a canonical ensemble can be performed. To set this thermostat in `VASP`, the following flags are required. `MDALGO=2` to set the Nosé thermostat, `SMASS` to set the thermostats mass and `TEBEG` to set the temperature of the simulation.

13 Block averages

In an MD simulation the averages are calculated over a finite time. Therefore these averages are affected by statistical errors. These errors can be described through the autocorrelation function C_A and the correlation length τ_A [**27**]. The correlation length is the number of time steps between two configurations that they require to become statistical uncorrelated. The sample size M is the number of time steps which are made in the MD simulation. With the correlation length τ_A and the sample size M. There is a relation between the variance of a finite sample $\sigma^2(\bar{A})$ and the variance of the ensemble $\sigma^2(A)$

$$\sigma^2(\bar{A}) = \frac{2\tau_A}{M}\sigma^2(A). \tag{161}$$

The block average method is one way to obtain the correlation length τ_A. Imagine your sample has M different configurations and you separate this sample in n_B blocks, which have all the same size M_B.

$$n_B = \frac{M}{M_B} \tag{162}$$

For these blocks we can calculate the block averages

$$\bar{A}_B^{(i)} = \frac{1}{M_B}\sum_{j=1}^{M_B} A((i-1)M_B + j). \tag{163}$$

Where i denotes the number of the block and A(...) is the element of the sample. Using the block averages we can calculate the average of the entire sample

$$\bar{A} = \frac{1}{n_B}\sum_{i=1}^{n_B} \bar{A}_B^{(i)}. \tag{164}$$

Now we can use formula (161) for the variance. We use this formula to compute $2 \cdot \tau_A$,

$$P(M_B) = M_B\frac{\sigma^2(\bar{A}_B)}{\sigma^2(A_s)}. \tag{165}$$

In formula (165) $\sigma^2(A_s)$ is the variance of the entire sample with A_s the average of the sample and $\sigma^2(\bar{A_B})$ is the variance of the block averages $\bar{A}$.

$$\sigma^2(A_s) \approx \frac{1}{M}\sum_{i=1}^{M}(A(i) - A_s)^2 \tag{166}$$

$$\sigma^2(\bar{A}_B) \approx \frac{1}{n_B}\sum_{i=1}^{n_B}(\bar{A}_B^{(i)} - \bar{A})^2 \tag{167}$$

If the block size MB is larger than the correlation length τ, then $P(M_B)$ from formula (162) should converge towards $2\tau_A$. $P(M_B)$ will be also called the statistical inefficiency s.

$$\lim_{M_B\to\infty} P(M_B) = 2\tau_A \tag{168}$$

This block average method is a powerful tool to check if a simulation is sufficiently long. If $P(M_B)$ keeps changing as M_B approaches M, the simulation is too short. If our simulation is long enough we can calculate the variance σ^2 and the standard deviation $\sigma_s = \frac{\sigma}{\sqrt{N}}$ for the sample. In the last expression for the standard deviation N is the number of elements in the sample. This method will be often used in this master thesis.

14 List of VASP flags

Here we describe some `VASP INCAR` flags, which are used for this master thesis [**28**].

- **ISMEAR & SIGMA**

  `ISMEAR` determines how the partial occupancies f_{nk} are set for each orbital. `ISMEAR=-1` means that the Fermi-Dirac-Statistic is used, for the partial occupancies, with `ISMEAR=0` a Gaussian distribution is used. `SIGMA` determines the width of the smearing in eV and it can be calculated through the temperature which is used in a simulation.

- **NKRED**

  `NKRED` is a flag which can be used with the HSE hybrid functionals. With `NKRED` we can set a considerably coarser mesh of points in the BZ $\{q_k\}$, which is used for the calculation of the short range exchange potential.

  $$q_k = \mathbf{b}_1 \frac{n_1 C_1}{N_1} + \mathbf{b}_2 \frac{n_2 C_2}{N_2} + \mathbf{b}_3 \frac{n_3 C_3}{N_3} \tag{165}$$

  with $(n_i = 0, .., N_i - 1)$

  Where $\mathbf{b}_{1,2,3}$ are the reciprocal lattice vectors and C_i is the integer grid reduction factor. This leads to a reduction of the computational costs by a factor.

  $$\frac{1}{C_1 C_2 C_3} \tag{166}$$

  $C_{1,2,3}$ can be set through the `NKRED` flags (`NKREDX`, `NKREDY`, `NKREDZ`).

- **IBRION, NSW & POTIM**

  `IBRION` determines how the ions are updated and moved. The default value of `IBRION` is zero. With `IBRION=0` a standard ab-initio molecular dynamic simulation with a Verlet algorithm will be performed. `NSW` sets the number of steps which are used and `POTIM` sets the time step. In the case of lattice vibrations we set `IBRION` to 6. `IBRION=6` determines the energy for harmonic oscillations and the phonon frequencies.

- **ISIF**

  `ISIF` determines if the stress tensor is calculated and which degrees-of-freedom are allowed to change in a molecular dynamic simulation. We use `ISIF=2`. With this setting the forces and the Stress tensor is calculated and the positions are free to move. With `ISIF=3` also the cell shape can be relaxed. This flag has to be set if the external pressure should be calculated.

- **ISPIN**

  `ISPIN` determines whether in the calculations the electrons can be spin polarized. With `ISPIN=2` spin polarized calculations are performed.

- **ALGO**

  The ALGO flag specifies which electronic minimisation algorithm is used in the calculations. With ALGO=VeryFast a RMM-DIIS (residual minimization method direct inversion in the iterative subspace) is used, which makes the calculation fast but might result in instabilities. By setting ALGO=Normal a blocked Davidson iteration scheme is used. And with setting ALGO=Fast then a mixture of the Davidson and RMM-DIIS algorithms is used. With ALGO=All a conjugate gradient algorithm is used.

- **LUSE_VDW,GGA & AGGAC**

  These are flags, which are used for vdW-DFT. LUSE_VDW=.TRUE. switches on vdW corrections. GGA sets the type of the generalized gradient approximation. If the GGA flag is unset, the generalized gradient approximation is chosen from the POTCAR file. By setting GGA=BO, the B88 functional is used. And with AGGAC=0 the generalized gradient approximation is removed from the correlation energy part.

- **LHFCALC, HFSCREEN & AEXX**

  These flags are used for HT/DFT hybrid functionals. The method of hybrid functionals is set by LHFCALC=.TRUE. With HFSCREEN the separation range can be set. The AEXX flag sets the fraction of Hartree-Fock exchange energy in the hybrid functional. The default value is AEXX=0.25.

- **PRECFOCK**

  In a HF/DFT hybrid functional calculation, it is possible to choose different FFT grids for the Hartree Fock exchange part and the DFT potentials. The PRECFOCK flag controls the FFT grid of the Hartree-Fock exchange routines. By PRECFOCK=Fast the smallest possible FFT grid is used, it is determined by the plane wave cutoff. This accelerates the calculations by a factor of two or three, but causes slight changes in the total energies and some noise in the calculated forces. For PRECFOCK=Normal, the FFT grid for the Hartree Fock exchange is identical to the FFT grid in the DFT part. This results in high quality calculations.

- **IVDW**

  This flag selects a special semi empirical method. Fot IVDW=1 the D2 method of Grimme is set and for IVDW=2 the Tkatchenko-Scheffler method is set.

- **EDIFF, EDIFFG & ENCUT**

  EDIFF is a condition to stop the electronic selfconsistent loop. The relaxation of the electronic degrees of freedom will be stopped if the total free energy change and the band structure energy change between two steps are both smaller than EDIFF. EDIFFG is a condition to stop the ionic relaxation loop. If the total free energy is smaller than EDIFFG between two ionic steps the relaxation will be stopped. With ENCUT the energy cutoff for a plane wave basis set can be set.

15 Crystal structure prediction

In this section we try to predict crystal structure properties of different materials. We are particularly interested in materials, where vdW interactions play a decisive role. As mentioned before DFT methods with a GGA functional have problems describing vdW interactions. Therefore materials, where vdW interactions play a part, are good examples for comparing different DFT methods with each other. The materials of interest are selenium (Se), tellurium (Te), arsenic (As) and antimony (Sb). The properties of these materials have been calculated with five different methods and the following settings.

To predict the crystal structure we tried to relax all parameters of the crystal structure to their ground state values. By setting `IBRION=2`, a conjugate-gradient algorithm is used to relax the ions into their energy ground states. All simulations were performed with 6×6×6 k-points, an energy cutoff of 400 eV, the accuracy of the ionic relaxation was set to `EDIFFG=10`$^{-4}$ and the allowed error in total energy was set to `EDIFF=10`$^{-8}$. The calculations of this section are all performed using the `VASP` version *vasp.5.4.2*. Here the different methods are listed. The flags which are used are described in section 11.

- **PBE** is a DFT calculation with a generalized gradient approximation, as described in section 5.1.2.
- **Method of Grimme (D2)** is the D2 method of Grimme, which is described in section 6.1. In `VASP` we obtain this method, by setting `IVDW=1`.
- **Tkatchenko-Scheffler (TS)** is the method of Tkatchenko-Scheffler, which is described in section 6.2. In `VASP` we obtain this method, by setting `IVDW=2`.
- **vdW-DFT** is described in section 6.3. Here we used the optB88 exchange functional. We obtained this by setting `GGA=BO`, `LUSE _VDW=.TRUE.`, `AGGAC=0` and the vdW-kernel (*vdW_kernel.bindat*) have been used.
- **Hybrid functional HSE06** is described in section 7.2. For the HSE06 the flags `LHFCALC=.TRUE.`, `HFSCREEN=0.2` and `AEXX=0.25` were set.
- **Random phase approximation (RPA)** How to perform the RPA calculation and the flags which are used, can be seen under section 8.3.

15.1 Selenium Se

The materials selenium and tellurium have both the same crystal structure. It is a hexagonal structure, which is described by the Pearson symbol hP3. The structure is presented by the following vectors.

Primitive lattice vectors:

$$\mathbf{a}_1 = \frac{1}{2}a \cdot \mathbf{x} - \frac{1}{2}3^{\frac{1}{2}}a \cdot \mathbf{y} \tag{169}$$

$$\mathbf{a}_2 = \frac{1}{2}a \cdot \mathbf{x} + \frac{1}{2}3^{\frac{1}{2}}a \cdot \mathbf{y} \tag{170}$$

$$\mathbf{a}_3 = c \cdot \mathbf{z} \tag{171}$$

Basis vectors:

$$\mathbf{b}_1 = x \cdot \mathbf{a}_1 + \frac{1}{3} \cdot \mathbf{a}_3 = \frac{1}{2}ax \cdot \mathbf{x} - \frac{1}{2}3^{\frac{1}{2}}ax \cdot \mathbf{y} + \frac{1}{3}c \cdot \mathbf{z} \tag{172}$$

$$\mathbf{b}_2 = x \cdot \mathbf{a}_2 + \frac{2}{3} \cdot \mathbf{a}_3 = \frac{1}{2}ax \cdot \mathbf{x} + \frac{1}{2}3^{\frac{1}{2}}ax \cdot \mathbf{y} + \frac{2}{3}c \cdot \mathbf{z} \tag{173}$$

$$\mathbf{b}_3 = -x \cdot \mathbf{a}_1 - x \cdot \mathbf{a}_2 = -ax \cdot \mathbf{x} \tag{174}$$

In the last equations, the vectors $\mathbf{x}$, $\mathbf{y}$ and $\mathbf{z}$ are the unit vectors of the Cartesian coordinate system. a,c and x are scalars. The following figure shows the hP3 crystal structure.

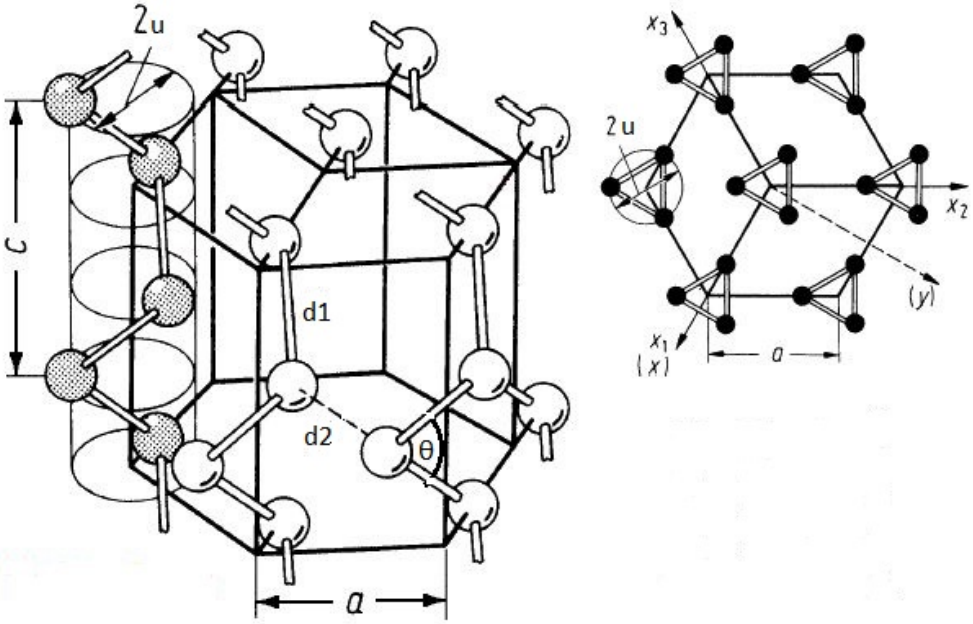

Figure 2: *Properties of crystal structure hP3* [**38**]

The hP3 structure can be seen as a hexagonal structure with an atomic chain on each corner. Figure 2 shows some properties which were calculated for the selenium structure. In the picture c and a are the lattice constants. The distance d_1 is called the intrachain distance, it describes the length from one atom to the neighbor atom in the same chain. d_2 is called the interchain distance and it describes the nearest distance from one atom to another atom of a different chain. θ is the binding angle and the parameter u is the radius of an atomic chain. Another important property, which was calculated, is the volume per atom.

For calculating these structure properties we pursue the following strategy. To calculate the total energy of the selenium unit cell at different c/a-ratios and different cell volumes, several simulations were performed. Overall 56 points of a uniform grid, of different c/a-ratios and different volumes were simulated. For these simulations the flag `ISIF=2` was used, which does not change the cell shape and the cell volume. For the calculations, the `POTCAR` file *PAW Se_GW 20Mar2012* was used. This leads to the following energy plots.

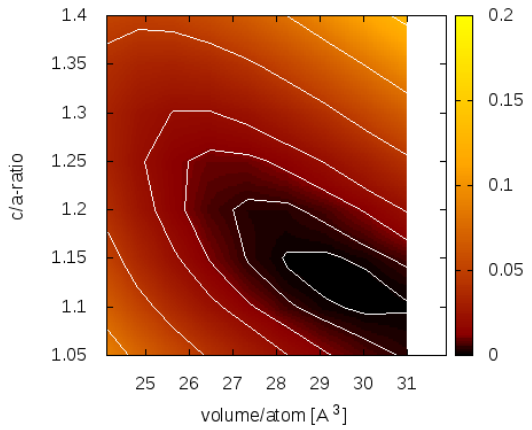

Figure 3: *Total energy of selenium as a function of the volume/atom and the c/a-ratio, calculated with PBE.*

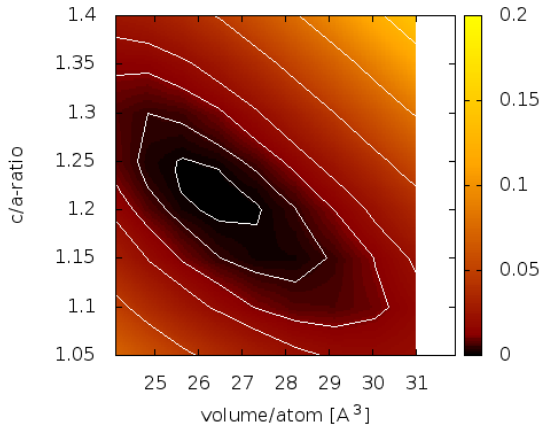

Figure 4: *Total energy of selenium as a function of the volume/atom and the c/a-ratio, calculated with D2.*

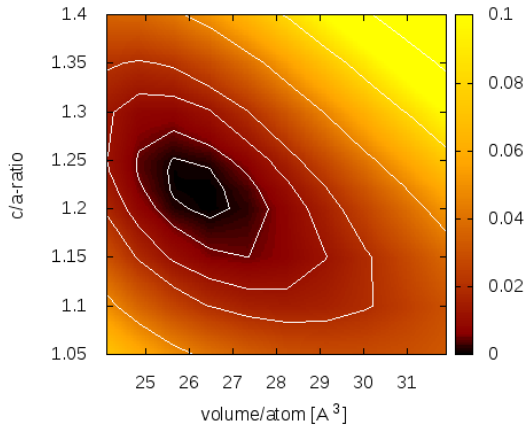

Figure 5: *Total energy of selenium as a function of the volume/atom and the c/a-ratio, calculated with TS.*

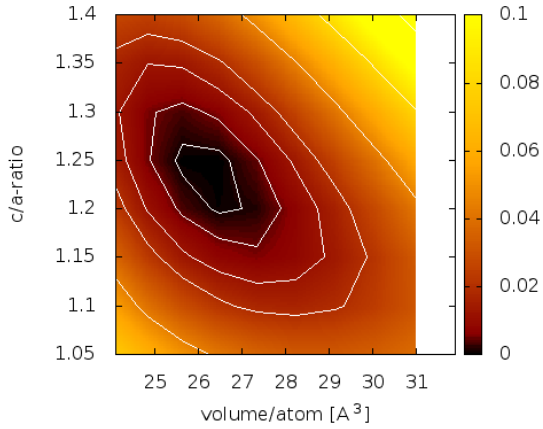

Figure 6: *Total energy of selenium as a function of the volume/atom and the c/a-ratio, calculated with vdW-DFT.*

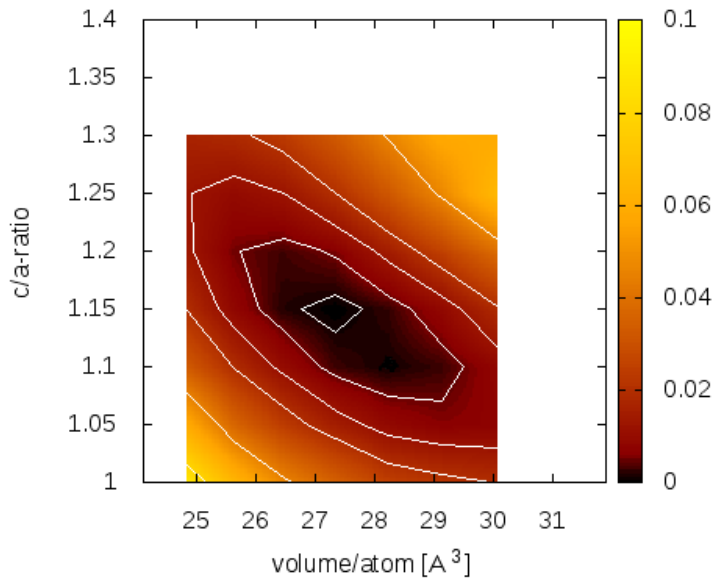

Figure 7: *Total energy of selenium as a function of the volume/atom and the c/a-ratio, calculated with the RPA.*

The smallest energy of these plots, is the black area. The structure properties for the smallest energy corresponds to the structure properties of the relaxed ground state. For PBE, D2, TS, vdW-DFT and RPA, the ground state energy has been predicted through the interpolation of 56 points. For PBE, D2, TS and vdW-DFT, another simulation with `ISIF=3` was performed, to verify the solutions. `ISIF=3` also relaxes the shape of the cell and the volume of the cell. But the manual scan of the c/a-ratio and the volume, as described before, was more accurate. In the following table we like to present the structure properties of the selenium calculations and compare them to experimental data of [**29**]. The properties are the volume per atom, the c/a-ratio, the u parameter, the binding angle θ and the ratio of intrachain and interchain distances $\frac{d_2}{d_1}$. Note that in the RPA calculations, selenium was treated as an insulator and for the RPA calculations the parameter u was determined for each c/a-ratio and each volume using the PBE functional.

Table 1: *Crystal structure properties of selenium calculated with different methods compared with the experimental values (Expt).*

	volume/atom (Å^3)	c/a-ratio (Å)	u	θ (deg)	$\frac{d_2}{d_1}$
PBE	29.03	1.208	0.223	104.4	1.462
D2	26.51	1.208	0.236	103.6	1.384
TS	26.12	1.215	0.234	103.8	1.377
vdW	26.33	1.227	0.238	105.1	1.358
RPA	27.33	1.15	0.232	102.5	1.411
Expt	27.27	1.136	0.229	102.5	1.43

15.1.1 Atomization energy

To calculate the atomization energy in a crystal structure. It is necessary to calculate the total energy of an atom in a crystal structure and the total energy of a free atom. The difference of these two energies is the binding energy or cohesive energy. We obtain the total energy of an atom in a crystal structure from the calculations before. The energy of the ground state calculations was used. To predict the energy of a free atom, we put one atom in the middle of a cubic cell and increased the volume until the energy value started to converge. For the calculation of the free atom we also set `ISPIN=2`, to perform a spin polarized calculation.

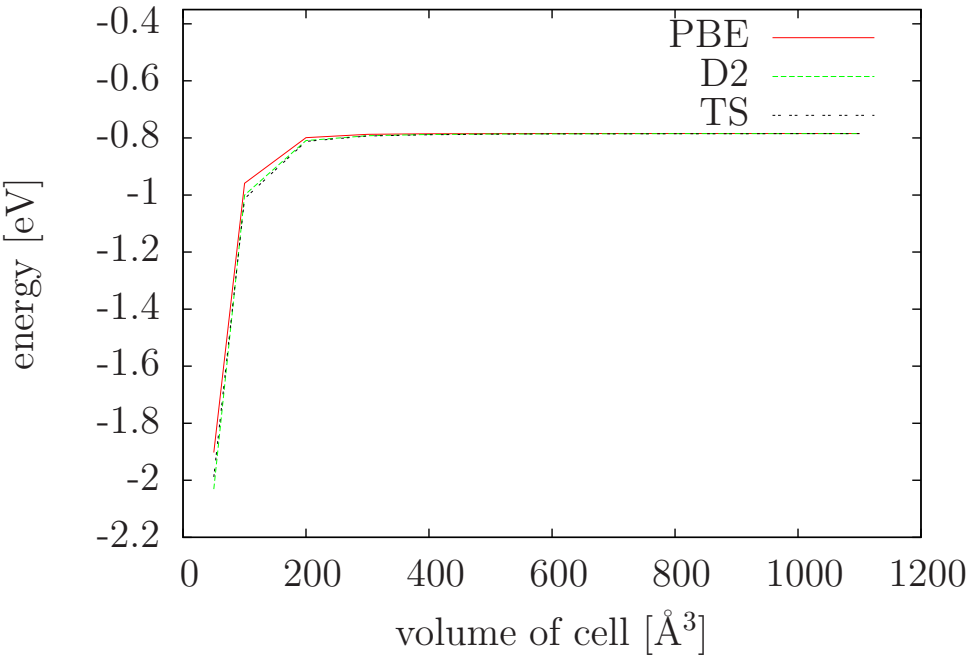

Figure 8: *Convergence of the total energy with increasing volume of the unit cell and calculated with PBE, D2 and TS*

Figure 8 shows the converge of the energies, calculated with PBE, D2 and TS, by increasing the volume of the cubic cell. It is easy to see, that these three methods converge to the same value. That is, because the energy correcting term of D2 and TS vanishes for large atomic distances. The energy of an atom in a 500 Å^3 cubic cell, is $E_{\text{free}} = 0.7848$ eV. This leads to following binding energies. $\Delta E_{\text{PBE}} = 2.718$ eV, $\Delta E_{\text{D2}} = 2.914$ eV and $\Delta E_{\text{TS}} = 2.888$ eV

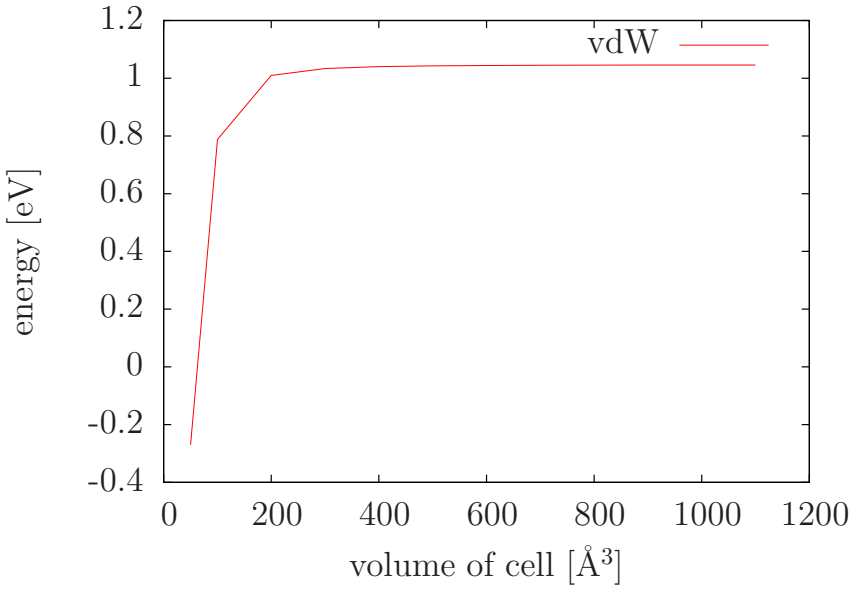

Figure 9: *Convergence of the total energy with increasing volume of the unit cell and calculated with the vdW-DFT.*

Figure 9 shows the calculations for the vdW-DFT. The energy calculated for a free atom is $E_{\text{free}} = 1.046$ eV. This leads to the binding energy of $\Delta E_{\text{vdW}} = 2.891$ eV.

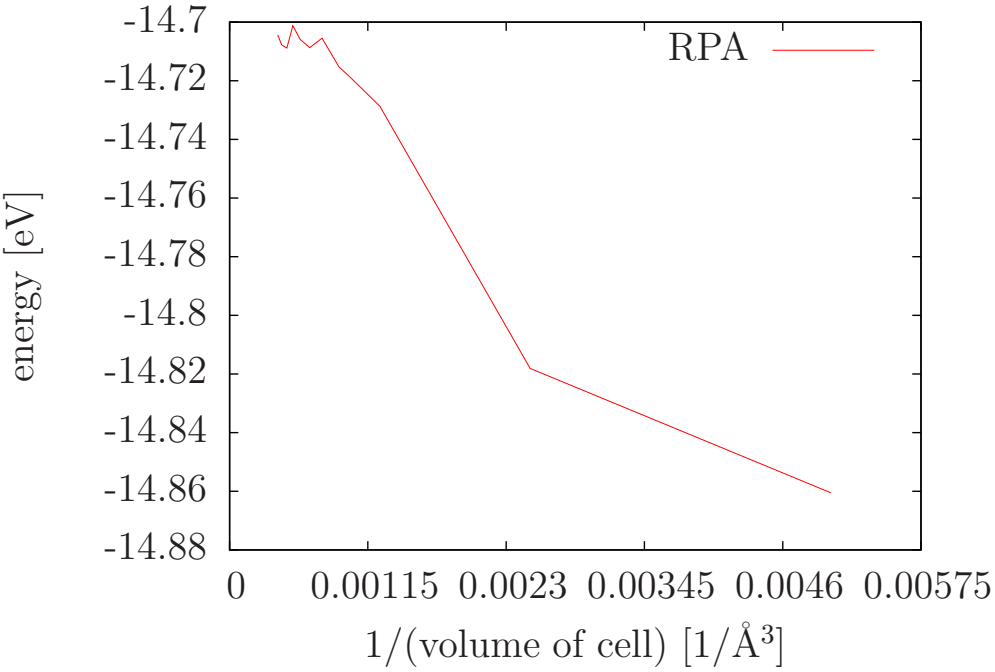

Figure 10: *Convergence of the RPA correlation energy plus the Hartree-Fock energy as a function of 1/(volume of the unit cell).*

The calculations of figure 10 show the RPA energy as a function of 1/V. This energy converges at a volume of 2000 Å^3. This leads to $E_{\text{free}} = 14.708$ eV and to the cohesive energy of $\Delta E_{\text{RPA}} = 2.319$ eV.

In the following table we list the cohesive energies predicted with every method compared to the experimental values [**30**].

Table 2: *Cohesive energies of selenium calculated with different methods and compared with the experimental values (Expt).*

	cohesive energies [eV]
PBE	2.718
D2	2.914
TS	2.888
vdW	2.891
HSE06	2.641
RPA	2.319
Expt	2.25

15.1.2 Conclusion

We now discuss the results of table 1 and 2. When we look at the PBE calculations it can be seen that two parameters, the volume/atom and the $\frac{d_2}{d_1}$-ratio are large compared to the experimental values [**29**]. In selenium we expect a vdW interaction between the atomic chains. This interaction should have an influence on the interchain distance d_2. The PBE functional does not consider vdW interactions leading to a large $\frac{d_2}{d_1}$-ratio and a too large volume/atom. The vdW functionals D2, TS and vdW-DFT predict small $\frac{d_2}{d_1}$-ratios, small volumes/atom and large c/a-ratios, as expect from the vdW functionals. The vdW interaction pulls the atomic chains together, which result in a small $\frac{d_2}{d_1}$-ratio. In the case of the vdW functionals the vdW interaction is overestimated. These vdW corrections also lead to smaller volumes/atom and to larger c/a-ratios than using PBE. The RPA is for the values of the volume/atom, the c/a-ratio, the binding angle θ and the $\frac{d_2}{d_1}$-ratio very close to the experimental values. In the case of cohesive energies the vdW functionals predict the largest values. We expect this behavior from the vdW functionals, because they add an energy correction term to the DFT calculation. This correction term is zero for one atom in a large cubic cell. Therefore the cohesive energy is too large. The RPA predicts the best cohesive energy compared to the experiment.

15.2 Tellurium

Tellurium has the same crystal structure as selenium. The calculations were performed in the same way as described in the section before, except of the RPA calculations. In these calculations tellurium was treated as a metal. For the calculations, the `POTCAR` file *PAW_PBE Te_GW 22Mar2012* was used. These calculations lead to the following energy plots.

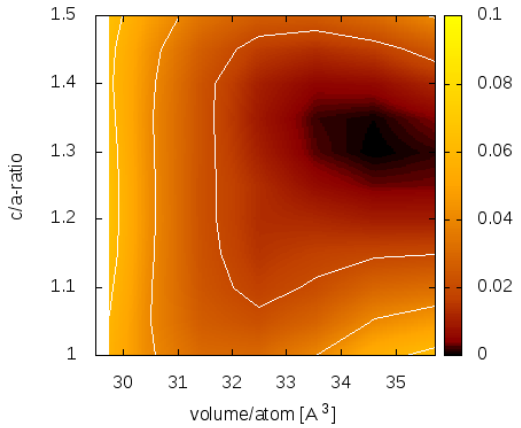

Figure 11: *Total energy of tellurium as a function of the volume/atom and the c/a-ratio, calculated with PBE.*

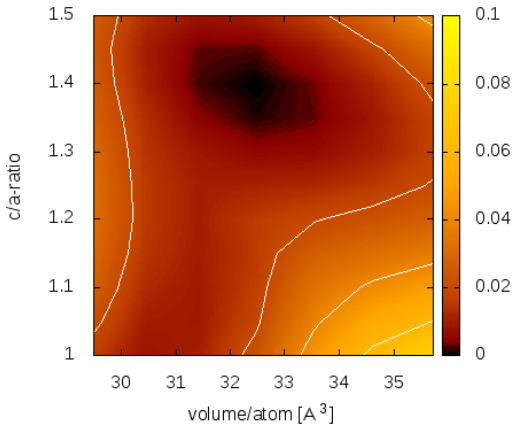

Figure 12: *Total energy of tellurium as a function of the volume/atom and the c/a-ratio, calculated with D2.*

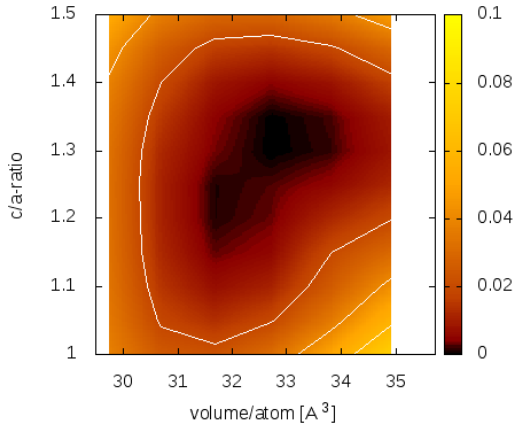

Figure 13: *Total energy of tellurium as a function of the volume/atom and the c/a-ratio, calculated with TS.*

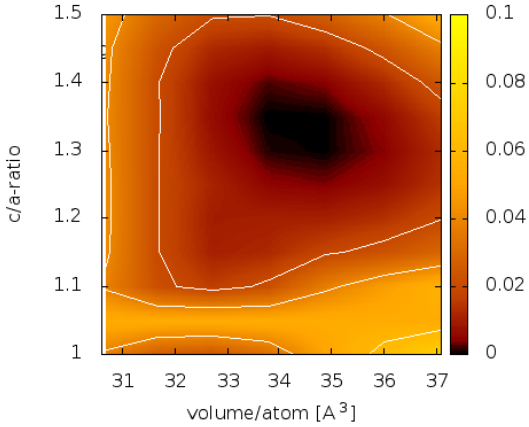

Figure 14: *Total energy of tellurium as a function of the volume/atom and the c/a-ratio, calculated with vdW-DFT.*

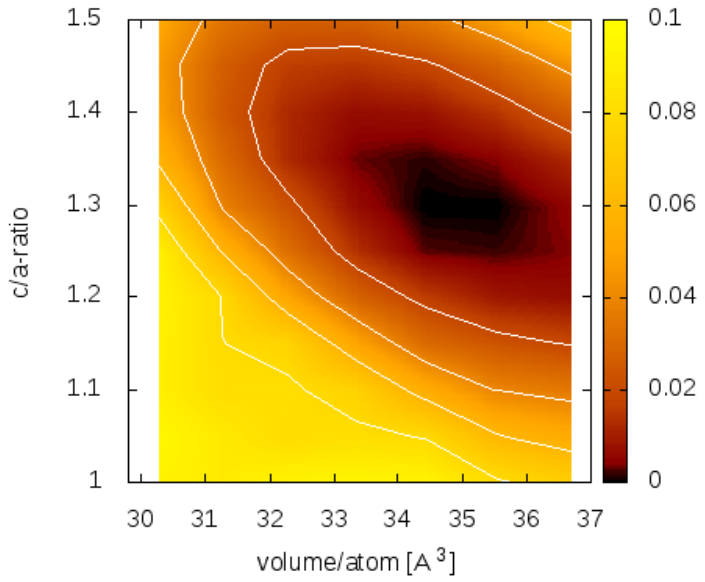

Figure 15: *Total energy of tellurium as a function of the volume/atom and the c/a-ratio, calculated with the RPA.*

The following table presents the structure properties of the tellurium calculations and compare them with experimental data of reference [**31**]. For the RPA calculations the u parameter was determined for each c/a-ratio and each volume using the PBE functional.

Table 3: *Crystal structure properties of tellurium calculated with different methods compared with the experimental values (Expt).*

	volume/atom (Å^3)	c/a-ratio (Å)	u	θ (deg)	$\frac{d_2}{d_1}$
PBE	34.57	1.31	0.275	100.3	1.19
D2	32.38	1.4	0.281	102.6	1.16
TS	32.77	1.32	0.29	97.9	1.14
vdW	34.22	1.34	0.279	98.9	1.16
RPA	34.51	1.29	0.273	101.3	1.23
Expt	33.74	1.33	0.264	103	1.23

15.2.1 Atomization energy

The cohesive energies were calculated as described in the section of selenium. Table 4 shows the final results.

Table 4: *Cohesive energies of tellurium calculated with different methods.*

	binding energies [eV]
PBE	2.374
D2	2.683
TS	2.608
vdW	2.641
RPA	2.054

15.2.2 Conclusion

For tellurium the trends are similar to selenium, however, this time the PBE prediction of the volume/atom and the c/a-ratio is almost correct. The $\frac{d_2}{d_1}$-ratio is already too small for PBE and with the vdW functional the ratio becomes even smaller. The vdW functionals D2 and TS, which both use an additive energy correction term to the DFT energy, yield a too small volume/atom and a small $\frac{d_2}{d_1}$-ratio. This is the same trend as for selenium. The vdW-DFT leads to a too large volume/atom, but a good c/a-ratio. The RPA again predicts the best $\frac{d_2}{d_1}$-ratio compared to the experimental value. For the cohesive energy we finally note that experimental results are not available. The trends for the cohesive energies are similar to the trends for selenium.

15.3 Arsenic

Arsenic and antimony have both the same crystal structure. It is a rhombohedral structure with the Pearson symbol hR2. The unit cell has two atoms and the structure can be seen as a layer structure. The structure can be described by the following vectors.

Primitive lattice vectors:

$$\mathbf{a}_1 = b \cdot \mathbf{x} + a \cdot \mathbf{y} + a \cdot \mathbf{z} \tag{175}$$

$$\mathbf{a}_2 = a \cdot \mathbf{x} + b \cdot \mathbf{y} + a \cdot \mathbf{z} \tag{176}$$

$$\mathbf{a}_3 = a \cdot \mathbf{x} + a \cdot \mathbf{y} + b \cdot \mathbf{z} \tag{177}$$

Basis vectors:

$$\mathbf{b}_1 = u(\mathbf{a}_1 + \mathbf{a}_2 + \mathbf{a}_3) = u(2a + b)(\mathbf{x} + \mathbf{y} + \mathbf{z}) \tag{178}$$

$$\mathbf{b}_2 = -u(\mathbf{a}_1 + \mathbf{a}_2 + \mathbf{a}_3) = -u(2a + b)(\mathbf{x} + \mathbf{y} + \mathbf{z}) \tag{179}$$

In the last equations the vectors $\mathbf{x}$, $\mathbf{y}$ and $\mathbf{z}$ are the unit vectors of the Cartesian coordinate system. a,b and u are scalars. The following figure shows the hP3 crystal structure.

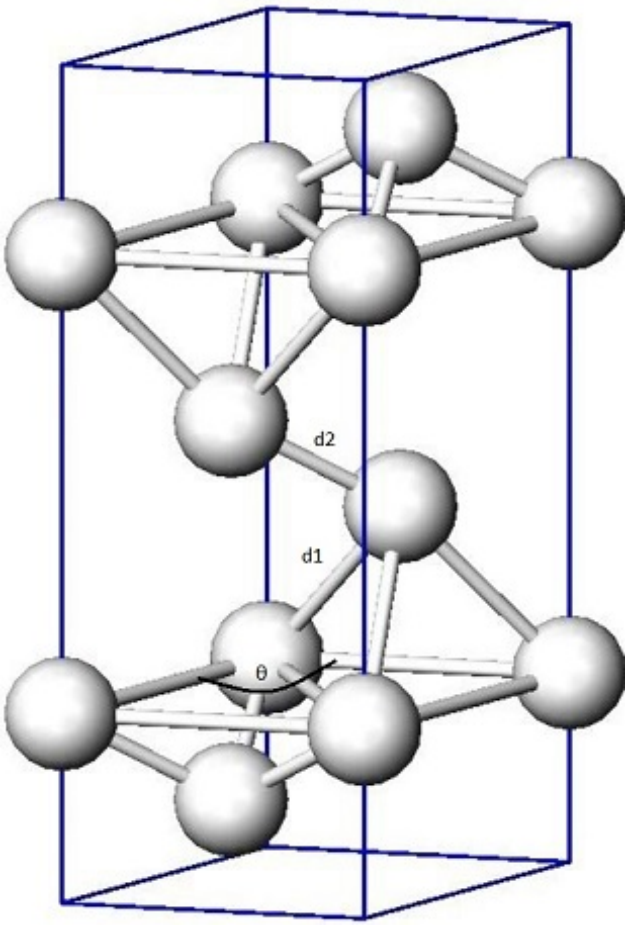

Figure 16: *Properties of crystal structure hR2*

Figure 16 shows two layers of the arsenic structure. The figure also presents some structure properties. Distance d_1 is called the interlayer distance, it describes the length from one atom to the neighbor atom in the same layer. d_2 is called the interlayer distance and it describes the nearest distance from one atom to another atom of a different layer. Then we have θ which is the binding angle. Other important properties are the volume per atom and the z parameter. The z parameter is the z-component of the primitive lattice vectors.

To calculate the structure of the arsenic unit cell we pursue the same strategy as for selenium in section 12.1. Only our two dimensional uniform grid depends now on the volume/atom and on the z parameter. In the RPA simulations, arsenic was treated as a metal and for the calculations, the `POTCAR` file *PAW _PBE As _GW 20Mar2012* was used.

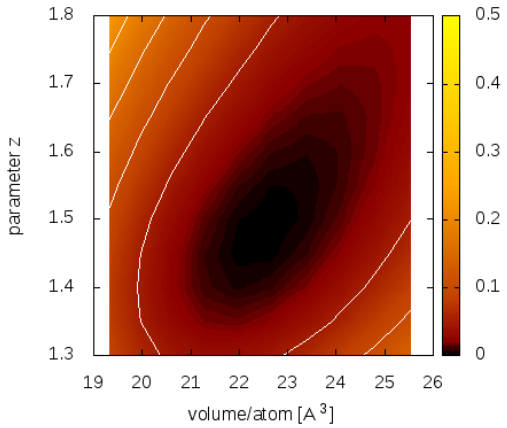

Figure 17: *Total energy of arsenic as a function of the volume/atom and the z parameter, calculated with PBE.*

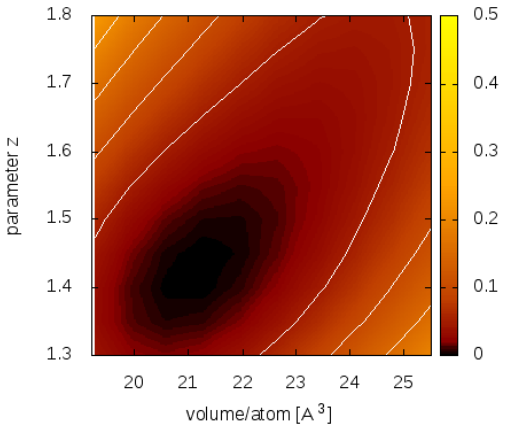

Figure 18: *Total energy of arsenic as a function of the volume/atom and the z parameter, calculated with D2.*

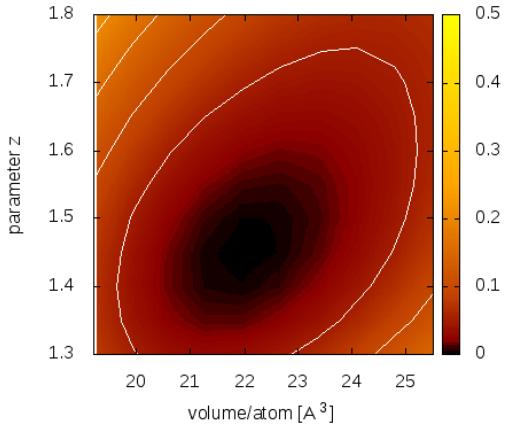

Figure 19: *Total energy of arsenic as a function of the volume/atom and the z parameter, calculated with TS.*

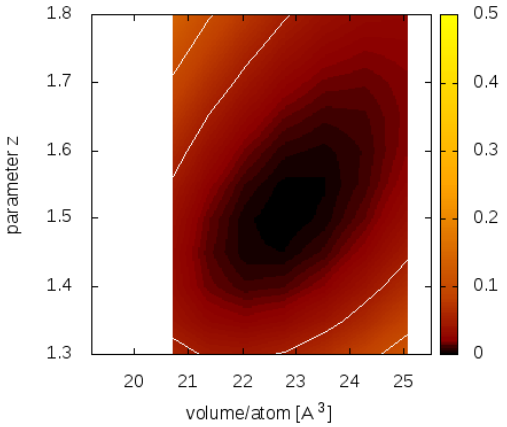

Figure 20: *Total energy of arsenic as a function of the volume/atom and the z parameter, calculated with vdW-DFT.*

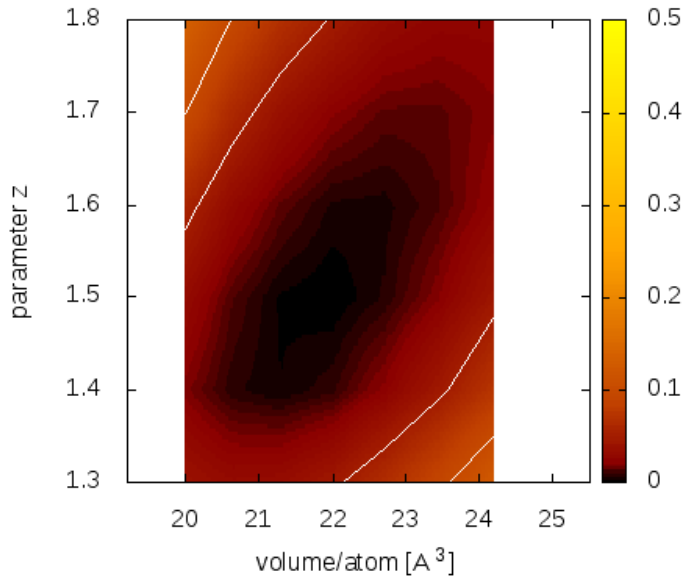

Figure 21: *Total energy of arsenic as a function of the volume/atom and the z parameter, calculated with the RPA.*

The structure properties of the smallest energy corresponds to the structure properties of the relaxed ground state. In these energy plots the z parameter is scaled by a constant, in table 5 the unscaled value of the parameter is presented. We also performed a HSE06 calculations, with `ISIF=3`. The results of the calculations compared to the experimental results [**33**] are shown in table 5.

Table 5: *Crystal structure properties of arsenic calculated with different methods and compared with the experimental values (Expt).*

	volume/atom (Å^3)	lattice constant a (Å)	z parameter (Å)	θ (deg)	$\frac{d_2}{d_1}$
PBE	22.51	4.22	3.56	93.8	1.252
D2	21.13	4.06	3.39	92.6	1.212
TS	22.01	4.12	3.49	92.8	1.224
vdW	22.75	4.2	3.59	93.4	1.245
HSE06	22.07	4.29	3.62	96.8	1.243
RPA	21.87	4.18	3.57	94.3	1.249
Expt	21.53	4.13	3.35	93.5	1.251

15.3.1 Atomization energy

The cohesive energies were calculated as described in the section of selenium. Table 6 presents the results.

Table 6: *Cohesive energies of arsenic calculated with different methods*

	binding energies [eV]
PBE	3.000
D2	3.327
TS	3.219
vdW	3.403
HSE06	2.751
RPA	2.816

15.3.2 Conclusion

As for selenium and tellurium we find the trend that the $\frac{d_2}{d_1}$-ratio is very small for the vdW functionals, specially for the D2 and TS method. This trend is expected from the vdW functionals, because vdW functionals add a pairwise interaction between the layers. The vdW functionals seem to overestimate this interaction. However the D2 method predicts about 1.9% smaller volume/atom and about 1.2% larger z parameter compared to the experiment. The TS method predicts an almost perfect lattice constant. The vdW-DFT leads to a too large volume/atom as for tellurium. Interesting is that the PBE functional predicts a good $\frac{d_2}{d_1}$-ratio, which means that the vdW interaction between the layers is already captured well by PBE. The HSE06 functional overestimates the volume/atom and the z parameter is too large. In terms of the volume/atom and the lattice constant the RPA improves the PBE functional. For the cohesive energy experimental results are not avoidable. As before the trend that the vdW functionals predict the largest cohesive energies is the same as for selenium and tellurium.

15.4 Antimony

Antimony has the same crystal structure as arsenic. The calculations were performed in the same way as for arsenic. In the RPA simulations antimony was also treated as a metal and for the calculations, the `POTCAR` file *PAW_PBE Sb_GW 21Mar2012* was used.

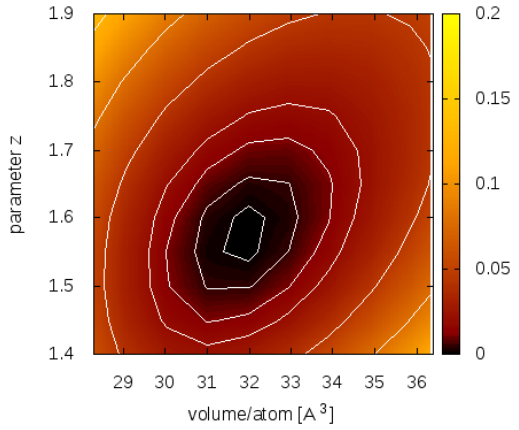

Figure 22: *Total energy of antimony as a function of the volume/atom and the z parameter, calculated with PBE.*

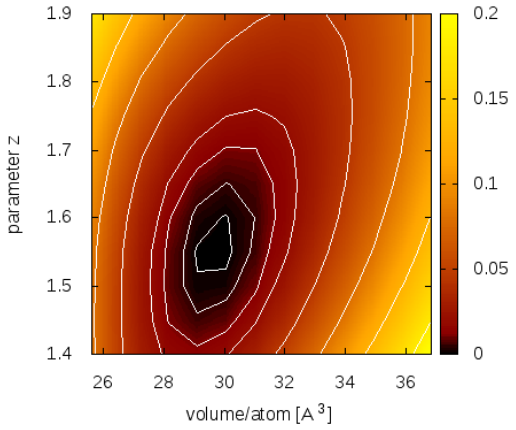

Figure 23: *Total energy of antimony as a function of the volume/atom and the z parameter, calculated with D2.*

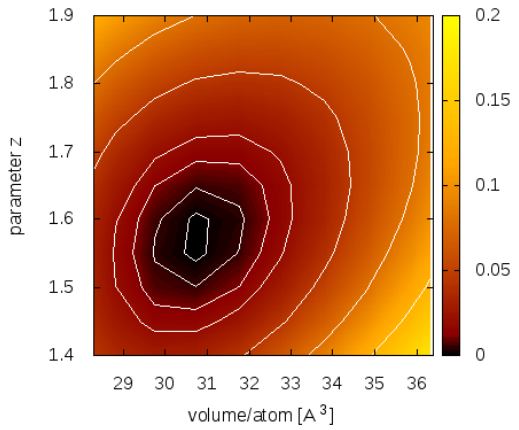

Figure 24: *Total energy of antimony as a function of the volume/atom and the z parameter, calculated with TS.*

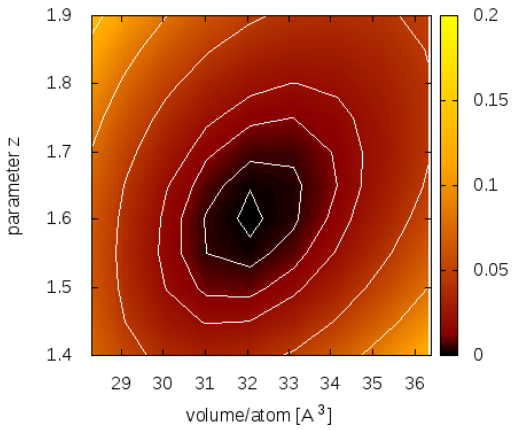

Figure 25: *Total energy of antimony as a function of the volume/atom and the z parameter, calculated with vdW-DFT.*

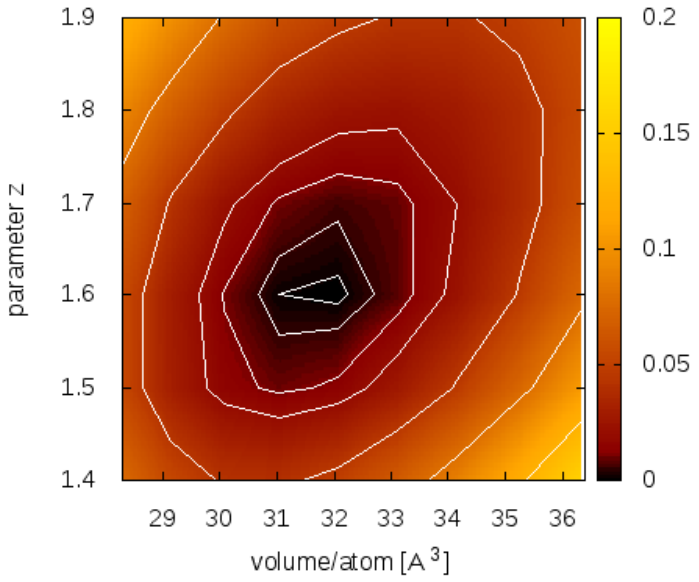

Figure 26: *Total energy of antimony as a function of the volume/atom and the z parameter, calculated with the RPA.*

The following table presents the structure properties of the antimony calculations and compare them with experimental data of [**33**].

Table 7: *Crystal structure properties of antimony calculated with different methods and compared with the experimental values (Expt).*

	volume/atom (Å^3)	lattice constant a (Å)	z parameter (Å)	θ (deg)	$\frac{d_2}{d_1}$
PBE	31.84	4.64	3.852	92.7	1.177
D2	29.65	4.44	3.725	91.9	1.124
TS	30.73	4.48	3.734	90.6	1.127
vdW	32.06	4.61	3.871	92	1.167
HSE06	30.95	4.52	3.852	92.5	1.18
RPA	31.74	4.61	3.869	92.3	1.172
Expt	30.2	4.51	3.784	91.7	1.158

15.4.1 Atomization energy

The cohesive energies were calculated as described in the section of selenium. Table 8 presents the results.

Table 8: *Cohesive energies of antimony calculated with different methods.*

	cohesive energies [eV]
PBE	2.445
D2	2.862
TS	2.728
vdW	3.484
HSE06	2.51
RPA	2.492

15.4.2 Conclusion

In antimony the trend that the vdW functionals D2 and TS overestimate the vdW interaction between the crystal layers, can be seen recognized again at the too small $\frac{d_2}{d_1}$-ratios. The D2 and the TS method yield this time to similar results for the $\frac{d_2}{d_1}$-ratio, the z parameter and the lattice constant a. The D2 method underestimates the volume/atom and the TS method overestimates it. The vdW-DFT method predicts a too large volume and overestimates the $\frac{d_2}{d_1}$-ratio. In terms of the volume/atom and the lattice constant a, the HSE06 functional really improves upon the PBE functional. For this improvement the short range Hartree-Fock exchange energy term of the HSE06 functional is most likely responsible. For the $\frac{d_2}{d_1}$-ratio the HSE06 functional is similar to the PBE functional, this can be explained by the long range part of the HSE06 functional, which does not include the Hartree-Fock exchange energy. The RPA hardly improves upon the PBE functional in terms of volume/atom, lattice constant a and $\frac{d_2}{d_1}$-ratio.

16 Melting temperature of silicon

The prediction of the melting temperature of silicon is a huge challenge to ab-initio technics. Previous investigations on this problem led to a melting temperature far below the experimentally measured melting temperature of 1687 K, for example the prediction of Osamu Sugino and Roberto Car [**35**]. They used a DFT-LDA technic, which resulted in a melting temperature of 1351 K. We believe that with the HSE06 functional the predicted melting temperature will be closer to the experimental melting temperature than predictions using the LDA or GGA functional. This assumption is based on the investigation of the silicon β-tin structure. The β-tin structure appears when a diamond crystal is under pressure. The β-tin structure has a similar short range order as the liquid. Therefore the energy difference between the β-tin phase and the diamond phase of silicon can be seen as a prognosis for the energy difference between the liquid phase and the diamond phase of silicon. We assume that the liquid phase will have a slightly higher internal energy than the β-tin phase. In the next two figures we show the internal energy as a function of the volume/atom of the β-tin structure and the diamond structure calculated with the PBE and with the HSE06 functional.

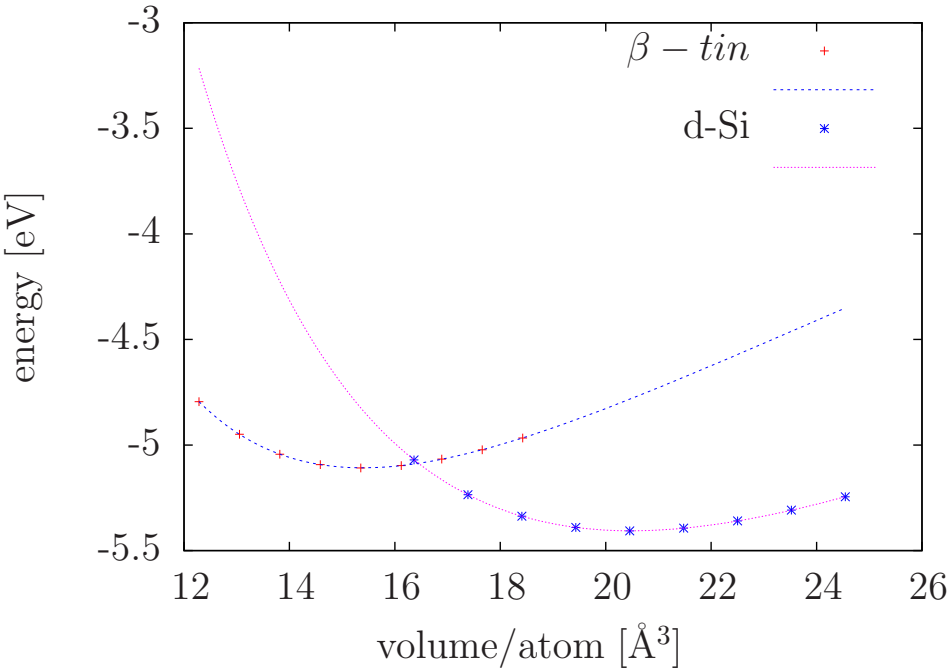

Figure 27: *Energy as a function of volume/atom for β-tin and diamond silicon calculated with the* PBE *functional.*

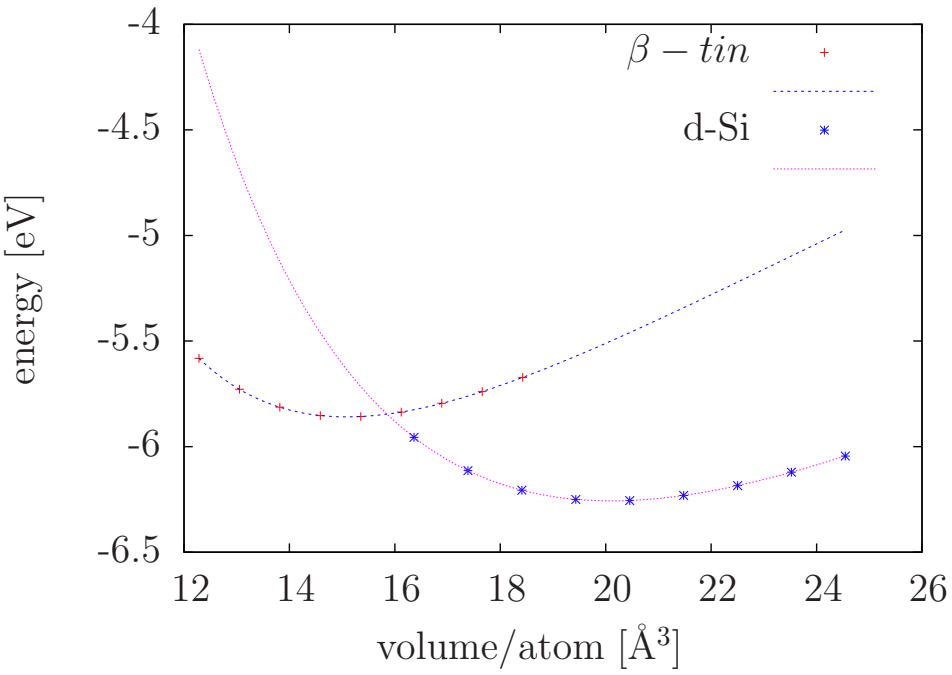

Figure 28: *Energy as a function of volume/atom for β-tin and diamond silicon calculated with the* HSE06 *functional.*

We calculated the energy difference between the β-tin phase and the diamond phase, with the PBE and the HSE06 functional. The energies are calculated for the equilibrium volume/atom of both phases. This results in $\Delta E_{\text{PBE}} = 0.29$ eV and in $\Delta E_{\text{HSE06}} = 0.39$ eV. We can see from these results that ΔE_{HSE06} is larger then ΔE_{PBE}. Previously the DFT-LDA calculations underestimated the melting temperature of silicon. According to the energy difference between the β-tin phase and the diamond phase calculated with the HSE06 functional, we assume that the melting temperature of silicon calculated with the HSE06 functional will be larger than the melting temperature calculated with the LDA functional.

The strategy for the melting temperature prediction is to calculate the Helmholtz free energy difference between silicon in the liquid phase and silicon in the solid phase. Our system consists of 64 atoms and has a diamond structure in the solid configuration. The Helmholtz free energy will be calculated for the solid and the liquid configurations at their equilibrium volume. For the calculation of the Helmholtz free energy we used thermodynamic integration and thermodynamic perturbation theory. The Helmholtz free energy will be calculated for both configurations for HSE06 using 3×3×3 k-points and a monkhorst pack grid. With the free energy difference between the two phases at the calculation temperature of 1687 K and the internal energies of both phases, the melting temperature can be predicted. As we will show below, the predicted melting temperature is 1798 K, which is 111 K above the experimental melting temperature. [**36**].

16.1 Equilibrium volume of silicon (Si)

In this section we try to predict the equilibrium volume of a cell of 64 silicon atoms. The volume should be predicted for 64 silicon atoms in a liquid configuration and for 64 silicon atoms in a diamond crystal structure configuration. The equilibrium volumes of these two configurations are interesting for the prediction of the silicon melting point. The strategy to predict the melting point is to calculate the Gibbs free energy for the solid and the liquid phase at a certain temperature. The Gibbs free energy is lower, at the more stable phase. With the Gibbs free energies of the two phases the melting temperature can be approximated. The equilibrium volume is important for these calculations, because at this volume the pressure is approximately zero. In this certain case, the Gibbs free energy is equal to the Helmholtz free energy G=F. Predicting the melting temperature with the Helmholtz free energy makes the calculations less expensive. The idea of the equilibrium volume prediction is to calculate the total pressure for 3 different volumes. With these pressure points we can interpolate a function, which depends on the volume. Then we have to find the point where the function is zero. For the prediction of the equilibrium volume the HSE06 hybrid functional was used.

16.1.1 Equilibrium volume of liquid silicon (l-Si)

A diamond structure cell with 64 Si atoms was set up. Then we performed a molecular dynamics (MD) simulation at a very high temperature, to melt the crystal and to obtain a liquid configuration. Starting from this liquid configuration, MD simulations for 3 different volumes were performed at a temperature of $T = 1687$ K. For these simulations we used the Langevin thermostat, with the friction coefficient of $\gamma = 5\frac{1}{ps}$. The MD simulations were performed for 3000 time steps, with a time step of 3 fs. In these simulations the hybrid functional HSE06 was used. An additional flag called `NKRED=2` was set, which should reduce the computing time. The simulations were performed with 2×2×2 k-points, `ISIF=2` to calculate the pressure, `EDIFF=10`$^{-4}$ and an energy cutoff of 245.34 eV. The flags `ISMEAR=-1` and the `SIGMA`, which can be calculated through $\sigma = k_B T$, were set. For these calculations `SIGMA=0.149` was set. The flags which are used are described in section 11. For the `POTCAR` file we used the *PAW_PBE Si_GW_new 19Mar2013* file.

First we look at the configuration after it was heated up. To be sure that the system is in a liquid phase, one can look at the mean square displacement (MSD).

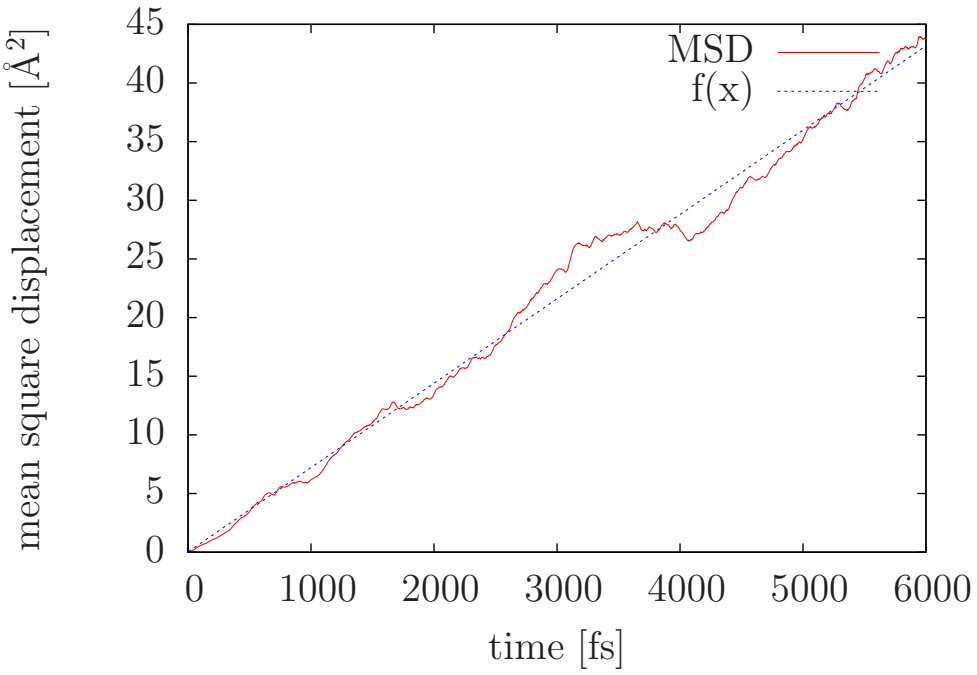

Figure 29: *Mean squared displacement (MSD) at a temperature of 1687* K*, f(x) linear fit of the MSD*

Figure 29 shows the MSD of the simulation. The linear behavior of the MSD and the high diffusion constant $D = 7.196 \cdot 10^{-5} \frac{m^2}{s}$, are typical signs of a liquid phase. In figure 30 we can see the pair correlation function.

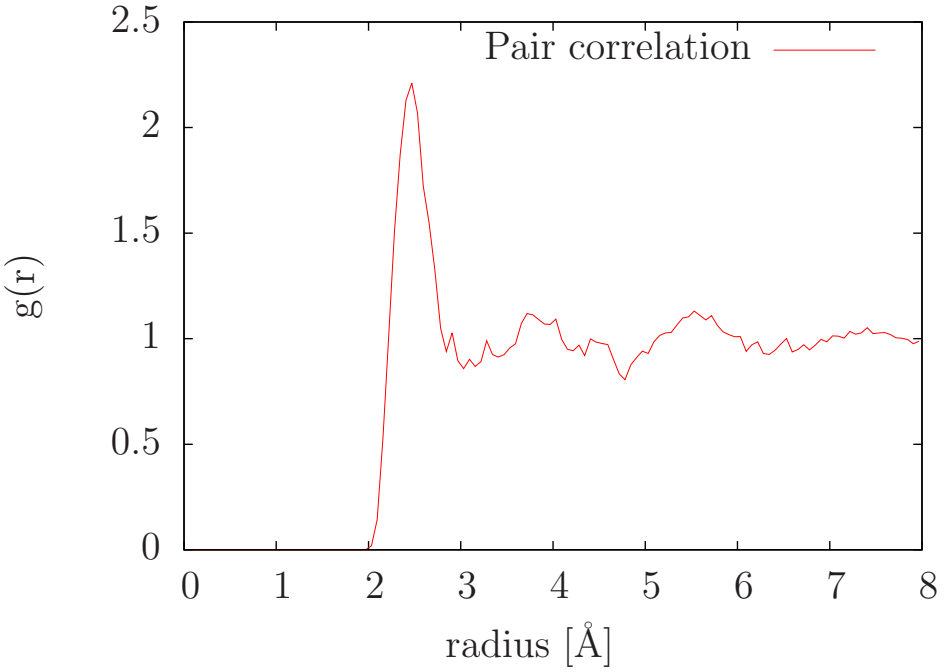

Figure 30: *Pair correlation function of liquid silicon at a temperature of 1687* K*.*

The pair correlation function shows a short range ordered ensemble, which we expect for a liquid. We are therefore pretty confident that the simulation conditions correspond to a phase point in the liquid region of silicon.

The volumes per atom where the calculations were performed are 17.29 Å^3, 18.15 Å^3 and 19.06 Å^3. Now we will inspect the average pressures at these three volumes.

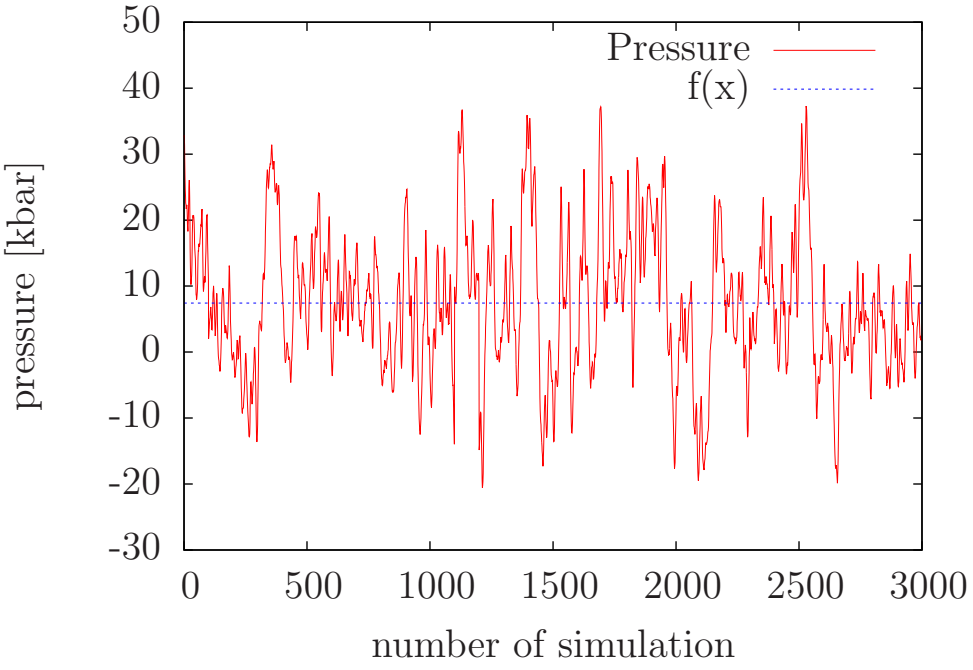

Figure 31: *Instantaneous pressure of liquid silicon at a volume per atom of 17.29* Å^3 *and a temperature of 1687* K*, f(x) is the average pressure.*

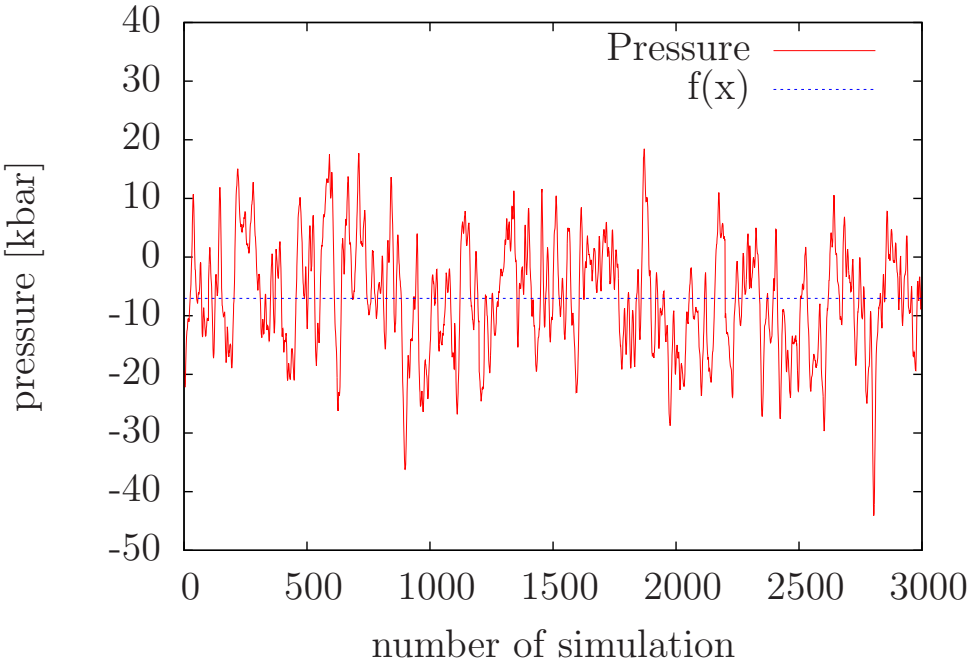

Figure 32: *Instantaneous pressure of liquid silicon at a volume per atom of 18.15* Å^3 *and a temperature of 1687* K*, f(x) is the average pressure.*

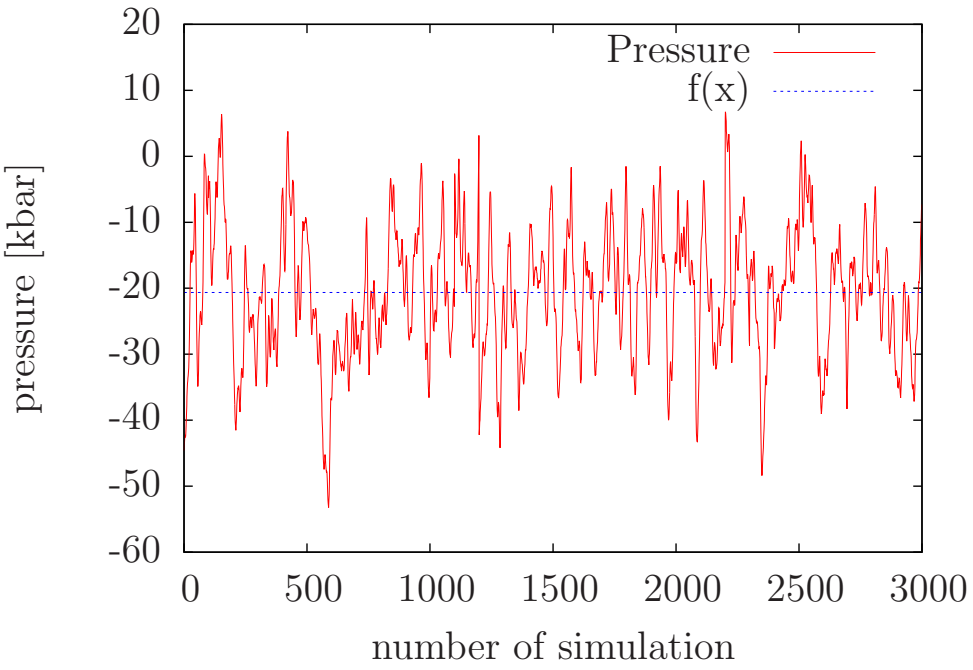

Figure 33: *Instantaneous pressure of liquid silicon at a volume per atom of 19.06* Å^3 *and a temperature of 1687* K*, f(x) is the average pressure.*

Figures 31, 32 and 33 show the microscopic pressure of the silicon liquid simulations at different volumes per atom. The results for the average pressures are $\langle p \rangle = 7.4$ kbar for a volume per atom of 17.29 Å^3, $\langle p \rangle = -7.1$ kbar for a volume per atom of 18.15 Å^3 and $\langle p \rangle = -20.6$ kbar for a volume per atom of 19.06 Å^3. To obtain the standard deviation of the pressure, a block-average analysis, like it is described in section 10, was performed for each of these three MD simulations.

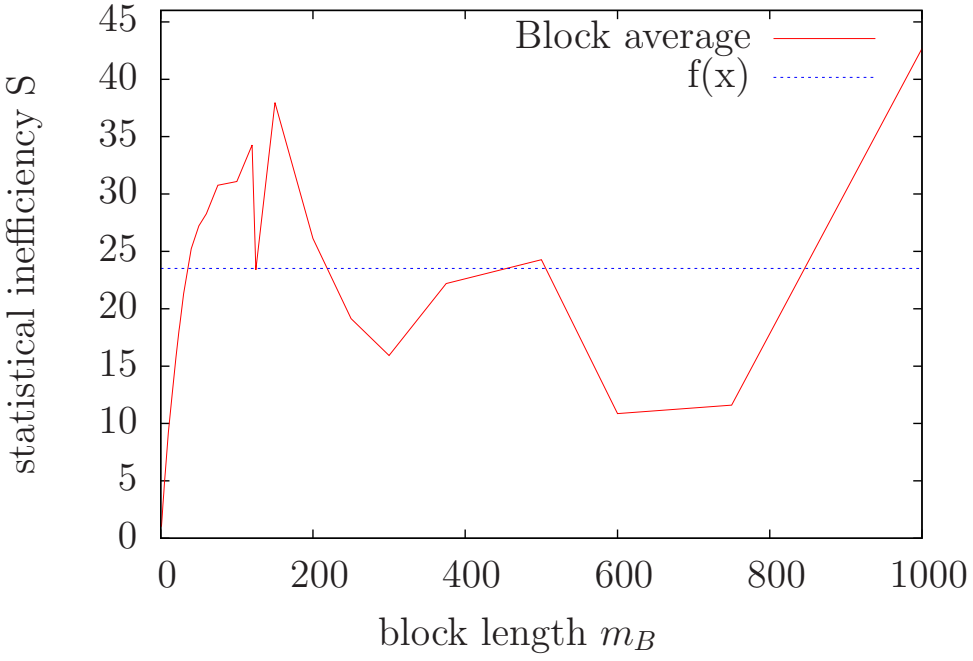

Figure 34: *Block-average analysis of liquid silicon at a volume per atom of 17.29* Å^3 *and a temperature of 1687* K*.*

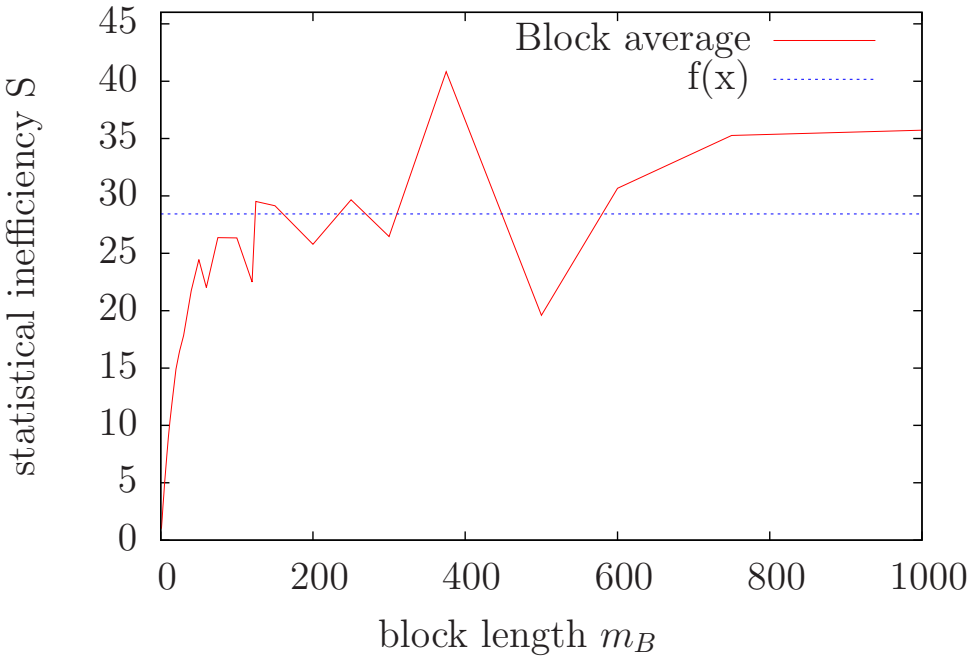

Figure 35: *Block-average analysis of liquid silicon at a volume per atom of 18.15* Å^3 *and a temperature of 1687* K.

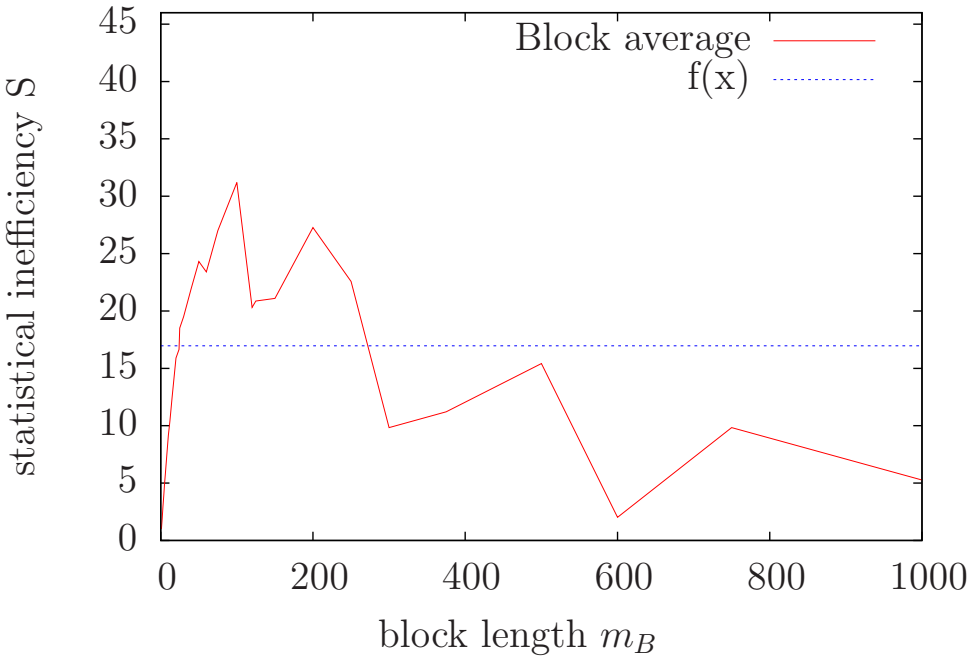

Figure 36: *Block-average analysis of liquid silicon at a volume per atom of 19.06* Å^3 *and a temperature of 1687* K.

The figures 34, 35 and 36 represent the block-average analysis for each volume. It can be seen that the block averages become reasonably uncorrelated at a block length of $m_B = 60$ for a volume per atom of 17.29 Å^3, at a block length of $m_B = 50$ for a volume per atom of 18.15 Å^3 and at a block length of $m_B = 60$ for a volume per atom of 19.06 Å^3. Therefore the standard deviations of the pressures are, $\sigma_s = 1.52$ kbar for 17.29 Å^3, $\sigma_s = 1.22$ kbar for 18.15 Å^3 and $\sigma_s = 1.4$ kbar for 19.06 Å^3.

Since we have used a reduced k-point set to evaluate the non-local exchange potential we did this with the `NKRED` flag and since errors are introduced by the finite energy cutoff, it is important to correct the pressure for these errors. Therefore we took some statistically independent configurations of the MD simulations. For these configurations, one calculation with the hybrid functional HSE06 at `ENCUT=250` eV and another calculation with HSE06 at `ENCUT=350` eV were performed. Both simulations were calculated without the `NKRED` flag. Between the pressures of the MD simulations and pressures of the calculations, with `ENCUT=350` eV and without the `NKRED` flag, we could detect a constant shift. Table 9 shows the pressure shifts and the final results for the pressures.

Table 9: *Pressures of liquid silicon by different volumes and a temperature or 1687* K.

volume/atom [Å^3]	pressure shift Δp [kbar]	final pressure [kbar]
17.29	10.1	17.6 ± 1.52
18.15	9.4	2.3 ± 1.22
19.06	7.7	-12.1 ± 1.4

For calculating the equilibrium volume, we can now plot the three average pressure points of table 9 against the volume.

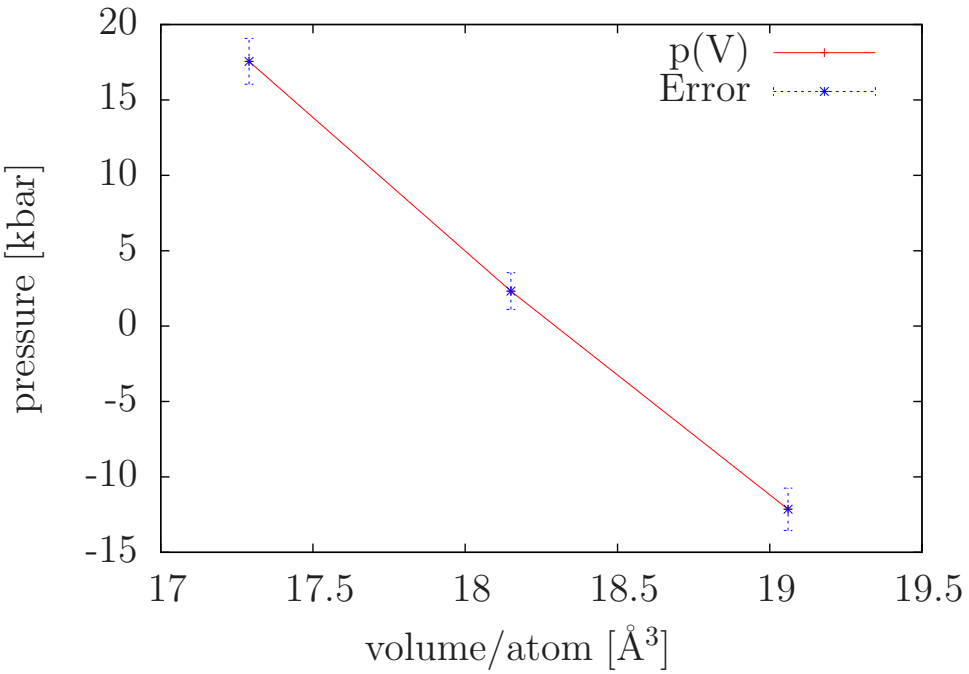

Figure 37: *Pressure as a function of the volume per atom of liquid silicon.*

With the function p(V) the equilibrium volume can be determined. It is the volume where the pressure is zero (p(V)=0). The result of the equilibrium volume in liquid silicon at a temperature of 1687 K is $V_{\text{eq}} = (18.29 \pm 0.077)$ Å^3.

16.1.2 Equilibrium volume of solid silicon (s-Si)

To calculate the equilibrium volume of solid silicon, we pursue two different strategies. The first one is, similar to the section of l-Si, to perform an MD simulation for three different volumes. The other one is the quasi harmonic approximation to perform phonon frequency calculations for different volumes. In the next section the first strategy is presented.

16.1.3 MD simulation of solid silicon (s-Si)

For this simulation a diamond super cell of 64 Si atoms was set up. To keep the solid configuration, we did not heat the system up, we just performed an MD simulation at the experimental temperature $T = 1687$ K. The flags, the thermostat and the `POTCAR` file for these simulations are the same as for the liquid. So we used the Langevin thermostat, the HSE06 functional with the `NKRED` flag and the simulations were performed at 2×2×2 k-points. We performed 3 MD simulations for different volumes, where each simulation had 3000 time steps of 3 fs.

First we look at the MD simulation for the volume per atom of 20.02Å^3. To be sure that the system did not melt, we checked the mean square displacement (MSD).

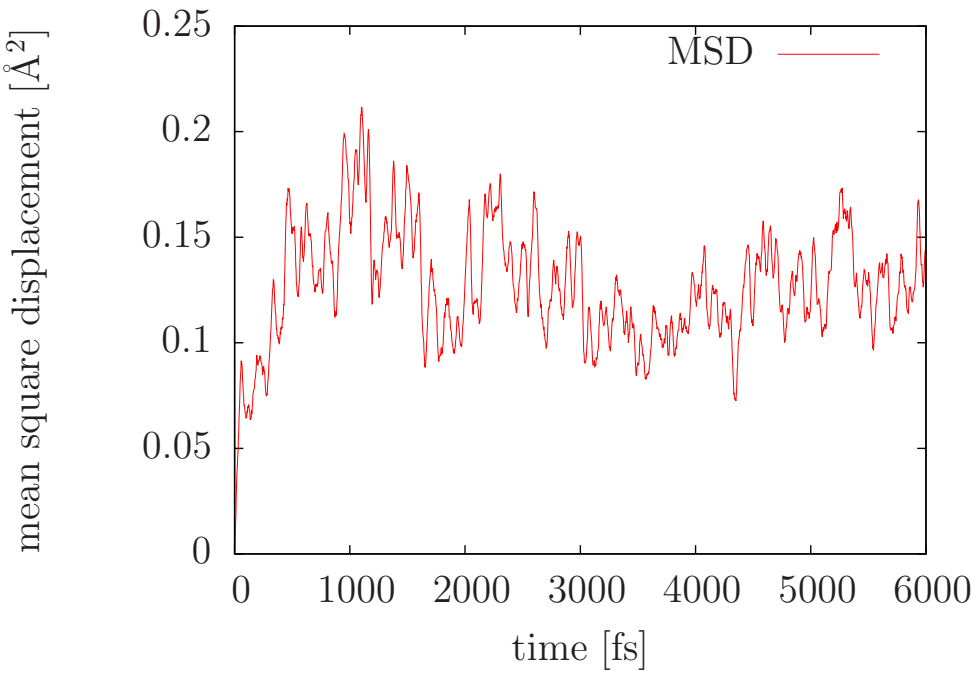

Figure 38: *Mean square displacement of solid silicon at a volume per atom of 20.02* Å^3 *and a temperature of 1687* K.

The shape and the magnitude of the MSD in figure 29 compared to figure 38 is very different. The mean square displacement rises to about 0.13 Å^2, but then it remains constant. Which is a sign for a solid phase. In figure 39 the pair correlation function can be seen.

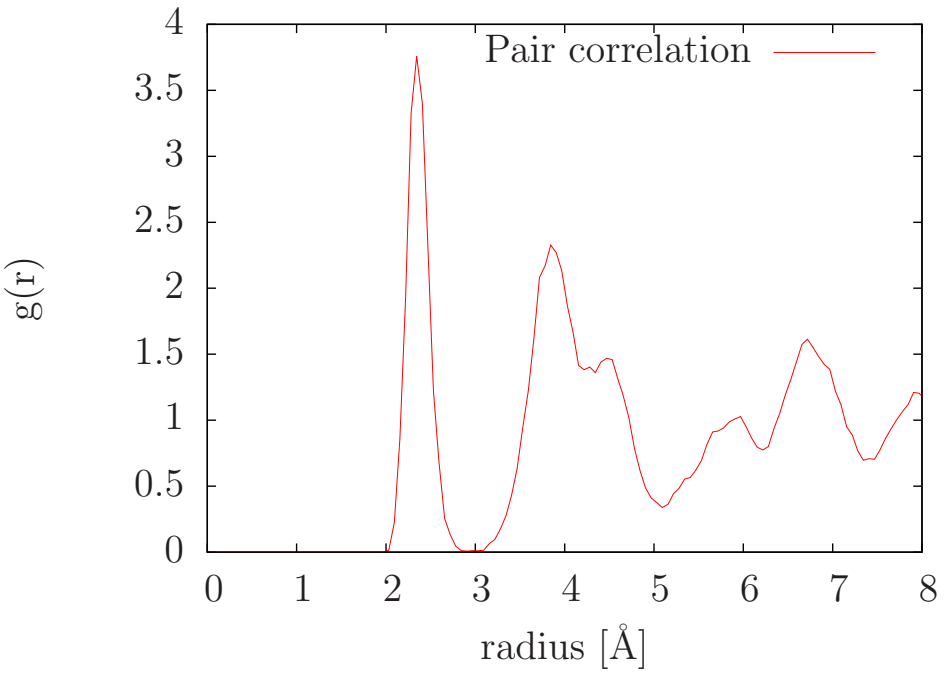

Figure 39: *Pair correlation function of solid silicon at a volume per atom of 20.02* Å^3 *and a temperature of 1687* K.

The pair correlation function shows a fairly well ordered structure, which we expect for a solid. We are now confident, that we have performed the MD simulation in the solid phase. Now we can present the result for the average pressure for the different volumes. The volumes per atom where the calculations were performed are 20.02 Å^3, 21 Å^3 and 22 Å^3.

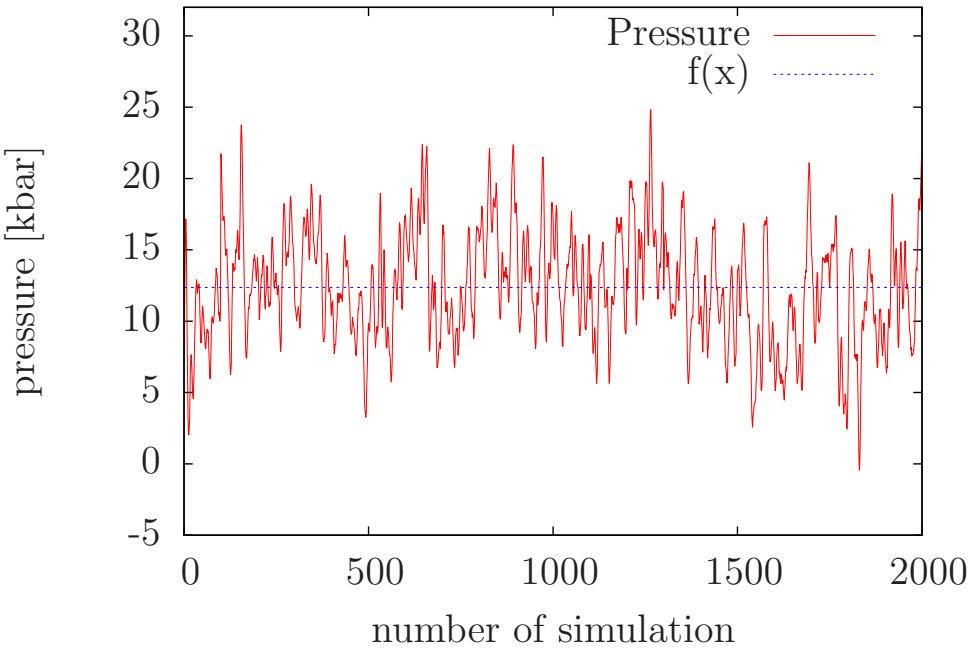

Figure 40: *Instantaneous pressure of liquid silicon at a volume per atom of 20.02* Å^3 *and a temperature of 1687* K*, f(x) is the average pressure.*

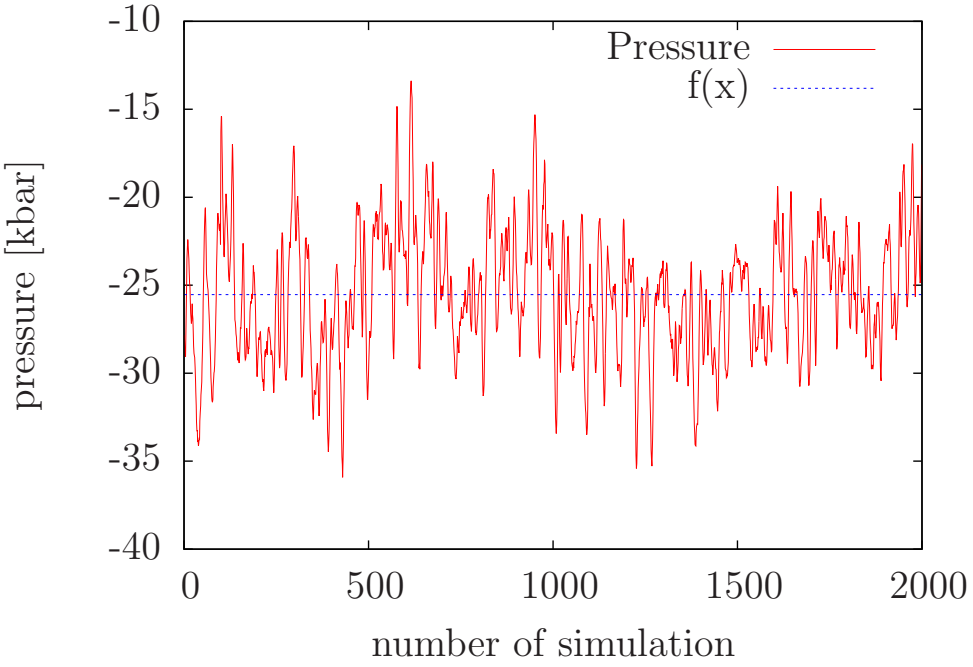

Figure 41: *Instantaneous pressure of solid silicon at a volume per atom of 21* Å^3 *and a temperature of 1687* K*, f(x) is the average pressure.*

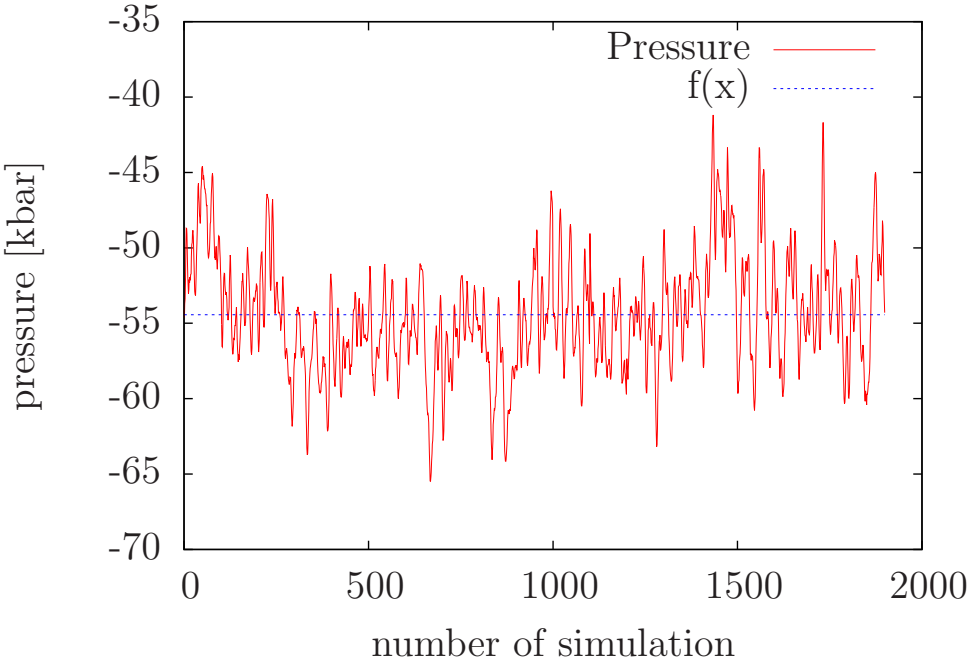

Figure 42: *Instantaneous pressure of solid silicon at a volume per atom of 22* Å^3 *and a temperature of 1687* K*, f(x) is the average pressure.*

Figures 40, 41 and 42 show the microscopic pressure of the solid silicon simulations at different volumes per atom. The results for the average pressures are $\langle p \rangle = 12.3$ kbar for a volume per atom of 20.02 Å^3, $\langle p \rangle = -25.5$ kbar for a volume per atom of 21 Å^3 and $\langle p \rangle = -54.4$ kbar for a volume per atom of 22 Å^3. To obtain the standard deviation of the pressure, a block-average analysis was performed for each of these MD simulations.

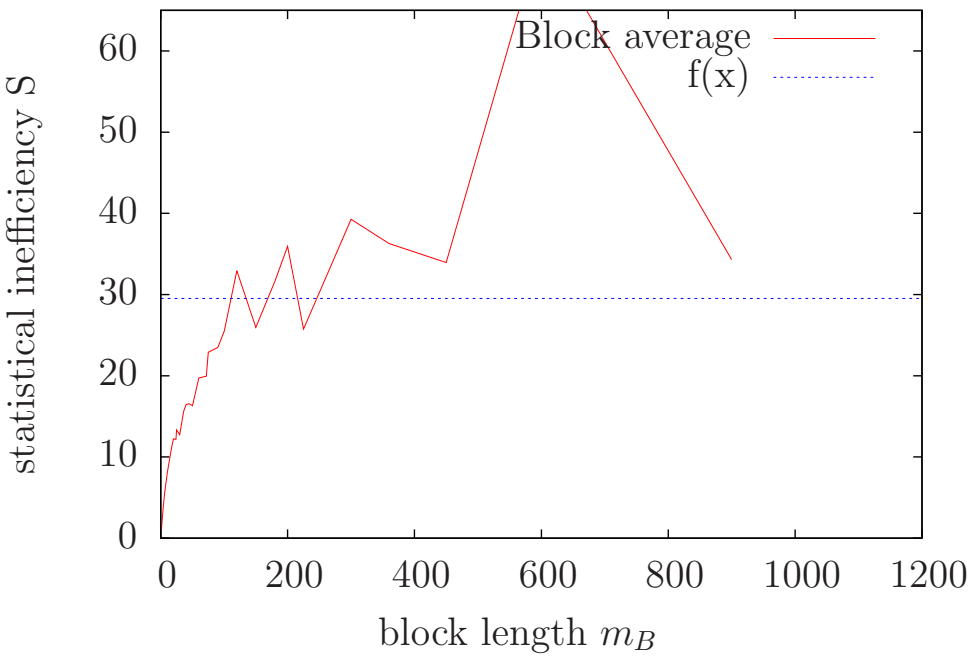

Figure 43: *Block-average analysis of solid silicon at a volume per atom of 20.02* Å^3 *and a temperature of 1687* K.

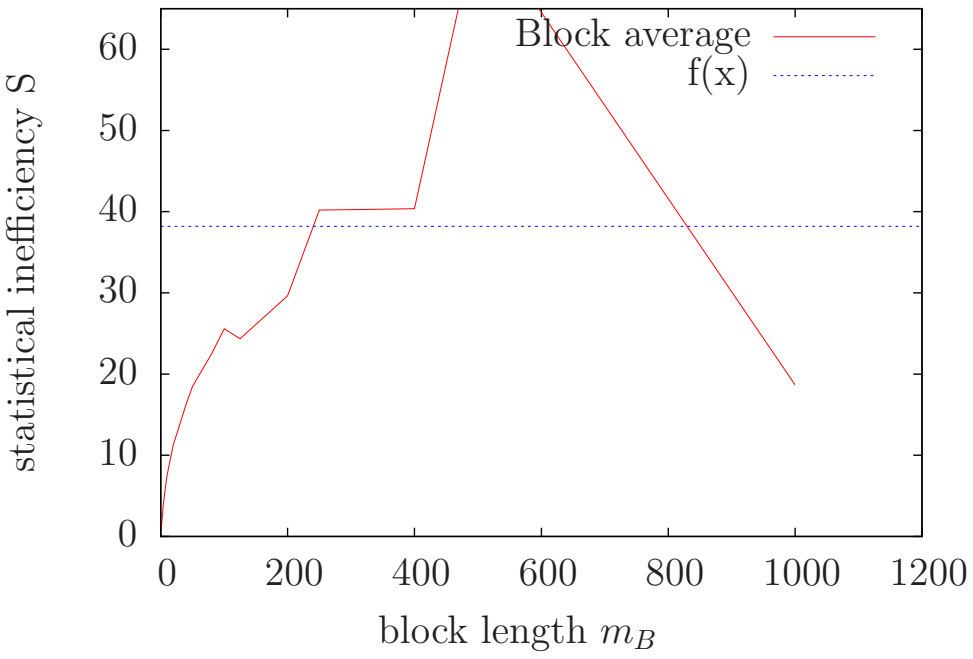

Figure 44: *Block-average analysis of solid silicon at a volume per atom of 21* Å^3 *and a temperature of 1687* K.

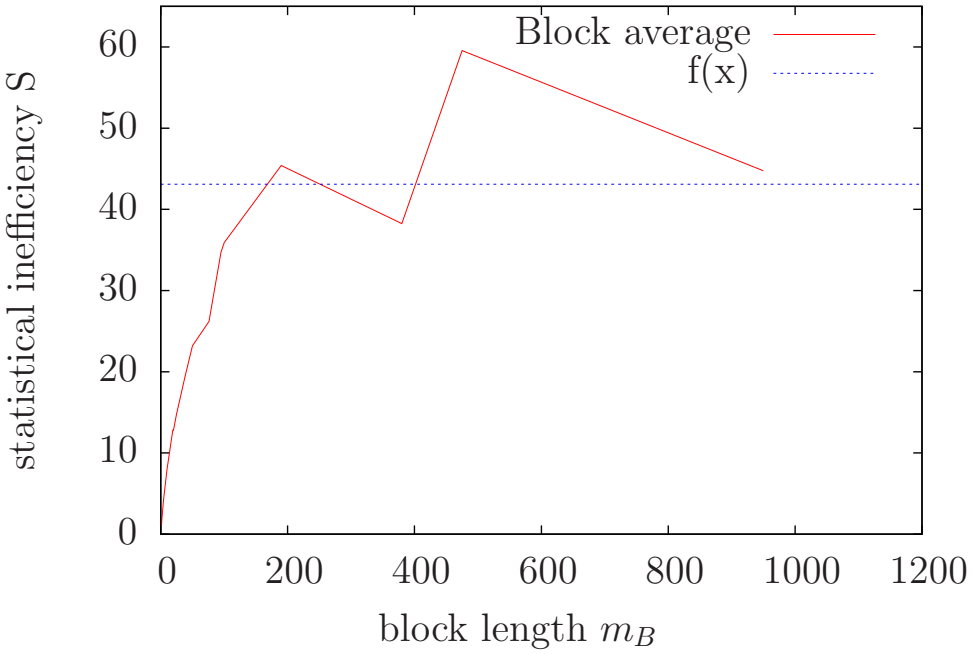

Figure 45: *Block-average analysis of solid silicon at a volume per atom of 22* Å^3 *and a temperature of 1687* K.

The figures 43, 44 and 45 represent the block-average analysis for each volume. It can be seen that the block averages become reasonably uncorrelated at a block length of $m_B = 40$ for a volume per atom of 20.02 Å^3, at a block length of $m_B = 80$ for a volume per atom of 21 Å^3 and at a block length of $m_B = 76$ for a volume per atom of 22 Å^3. Therefore the standard deviations of the pressures are, $\sigma_s = 0.55$ kbar for 20.02 Å^3, $\sigma_s = 0.79$ kbar for 21 Å^3 and $\sigma_s = 0.76$ kbar for 22 Å^3.

Then we took some statistically independent configurations of the MD simulations, as it is described for liquid silicon in section 15.1.1. For these configurations, one calculation with the hybrid functional HSE06 at `ENCUT=250` eV and another calculation with HSE06 at `ENCUT=350` eV were performed. Both simulations were calculated without the `NKRED` flag. Between the pressures of the MD simulations and pressures of the calculations, with `ENCUT=350` eV and without the `NKRED` flag, we could detect a constant shift. Table 10 shows the pressure shifts and the final results for the pressures.

Table 10: *Pressures of solid silicon by different volumes and a temperature or 1687* K.

volume/atom [Å^3]	pressure shift Δp [kbar]	final pressure [kbar]
20.02	6.2	18.5 ± 0.55
21	5.7	-19.8 ± 0.79
22	5.4	-49.1 ± 0.76

For calculating the equilibrium volume, we plot the three pressure points against the volume.

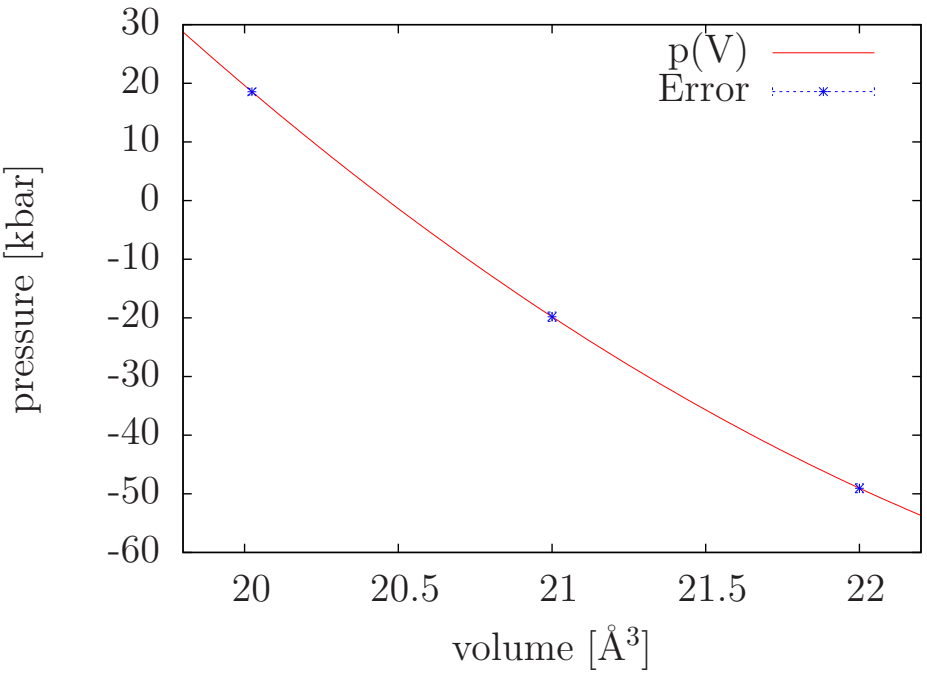

Figure 46: *Pressure as a function of the volume per atom of solid silicon.*

Now the equilibrium volume can be determined. It is the volume where the pressure is zero. The result of the equilibrium volume is $V_{\text{eq}} = (20.49 \pm 0.073)$ Å^3.

16.1.4 Phonon frequencies calculation (s-Si)

In this section we like to present the results of our quasi harmonic calculations. We performed five calculations, each of them at a different volume. The volume points were chosen around the volume of $V = 20.02$ Å^3. For every volume point the flag `IBRION=6` was used, with this flag `VASP` calculates the phonon frequencies. These frequencies can be used to calculate the free energy of the harmonic lattice vibrating Si crystal. For the free energy calculations we used the Phonopy program. With Phonopy the free energy F(T) between $T = 0$ K to $T = 2000$ K, in steps of 200 K, was calculated. The free energy F(T) for the five volumes is shown in figure 47.

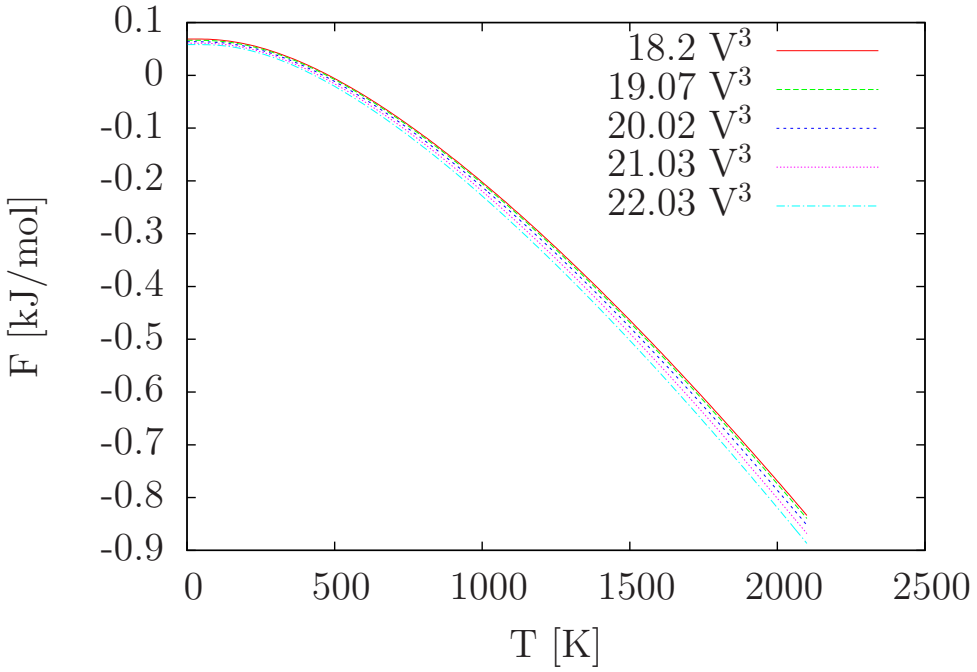

Figure 47: *Free energy of the phonon system as a function of the temperature, for five different volumes per atom of solid silicon.*

Further calculations for the electronic structure were performed for each volume, to obtain the electronic ground state energy. We can now inspect a certain temperature and plot the free energy of the phonon system plus the total energy of the electron system against the volume. For the temperature of 400 K, this is shown in figure 48.

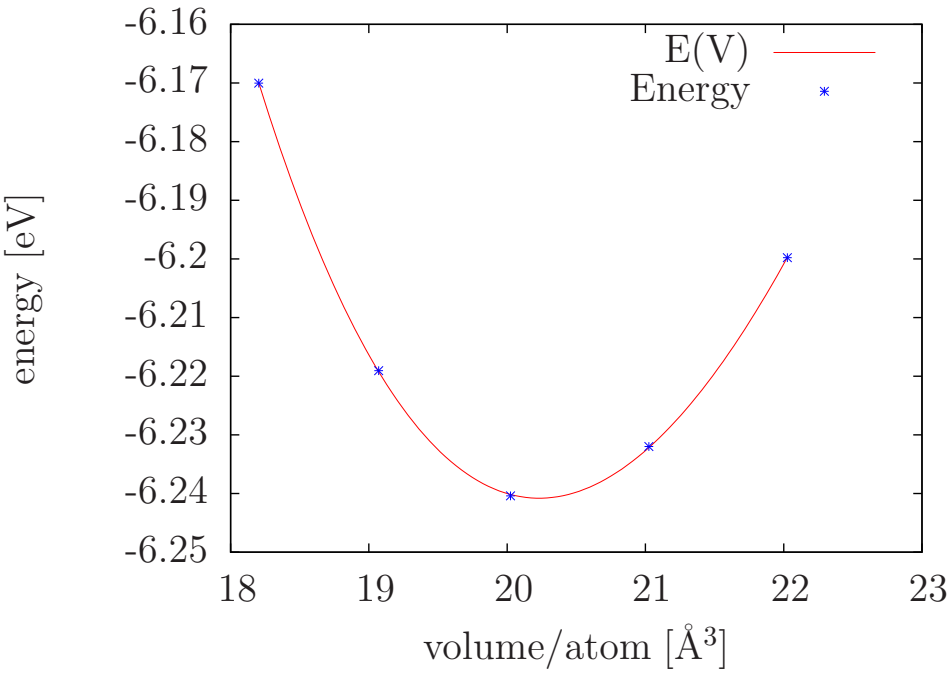

Figure 48: *Free energy as a function of the volume per atom, at a temperature of 400* K*, for solid silicon.*

In figure 48 we used a Murnaghan fit. The minimum of this fit is by 20.23 Å^3. This volume is a prediction of the equilibrium volume at a temperature of 400 K. For the next plot we calculated the equilibrium volumes for every temperature step and plotted the volumes against the temperature (figure 49).

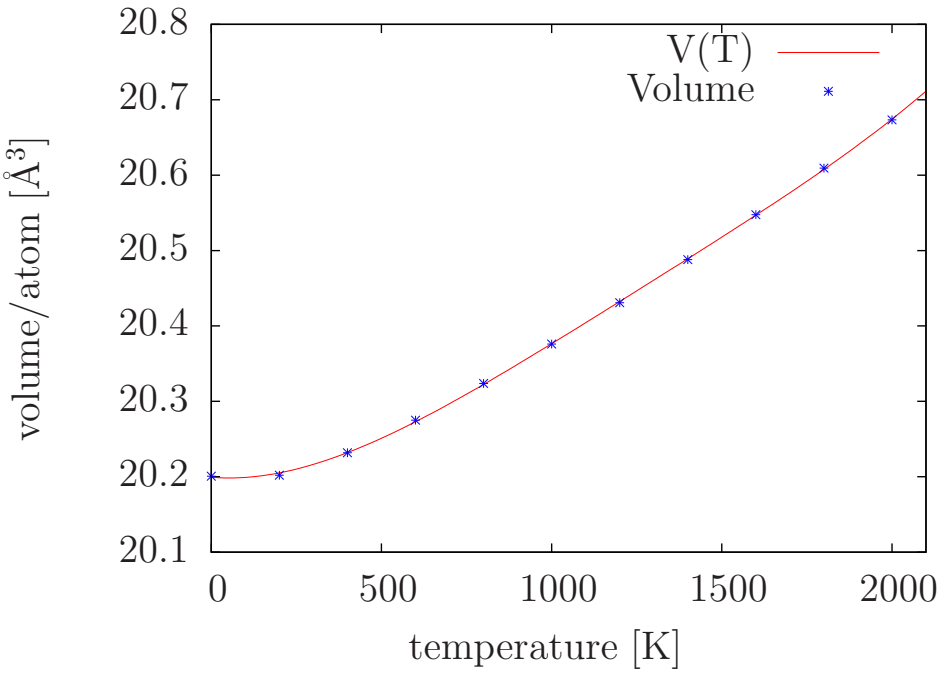

Figure 49: *Temperature as a function of the volume per atom, for solid silicon.*

With this plot the equilibrium volume at the temperature $T = 1687$ K can be predicted. The result of this prediction is $V_{\text{eq}} = 20.44$ Å^3 This prediction of the equilibrium volume was only made to verify the result of the equilibrium volume from section 15.1.3. In general the result of 15.1.3 is expected to be more accurate than the result of 15.1.4, because in 15.1.4 we did not consider the anharmonic contribution. By comparing these to results for the equilibrium volume, we can see that the difference is only 0.05 Å^3 and therefore practically irrelevant. For all the following simulations we used a volume per atom of $V = 20.49$ Å^3.

16.2 Free Energy of liquid silicon

For the prediction of the melting temperature it is important to calculate the Helmholtz free energy for the liquid phase. In this section we use thermodynamic integration theory and thermodynamic perturbation theory to calculate the free energy of a silicon liquid. The liquid was calculated using the HSE06 functional at 3×3×3 k-points. From now on this liquid will be called the HSE_{3k} liquid. The next subsection will introduce the calculation step by step. Our system consists of 64 Si atoms, it is calculated at a temperature of 1687 K and a volume per atom of 20.49 $Å^3$.

16.2.1 Free energy of the Ideal Gas

We start with the calculation of an ideal gas. The free energy can be calculated analytically. The free energy in a canonical ensemble can be calculated through equation

$$F = -\frac{1}{\beta} ln\left(Z(T,V,N)\right), \tag{180}$$

where $Z(T,V,N)$ is the partition function. The partition function for a mono atomic ideal gas is

$$Z(T,V,N) = \frac{V^N}{\Lambda^{3N} N!}, \tag{181}$$

with the thermal de-Broglie wavelength Λ, which is defined as

$$\Lambda = \frac{h}{\sqrt{\frac{2\pi m}{\beta}}}. \tag{182}$$

Using formula (180) and the partition function (181) we obtain

$$F = -\frac{1}{\beta} ln\left[\frac{V^N}{\Lambda^{3N} N!}\right] \approx -\frac{1}{\beta} N\left(ln\left[\frac{V}{\Lambda^3 N}\right] + 1\right). \tag{183}$$

In the last formula we used the Stirling approximation. We now present the calculation of the free energy of the Si gas. The system consists of 64 atoms (N=64), where the mass of an Si atom is $m = 28.085 \cdot u = 4.664 \cdot 10^{-26}$ kg. With formula (183) the free energy per atom of $F_{\text{ideal}} = -1.668$ eV/atom was calculated.

16.2.2 Integration form an ideal gas to PBE at the Γ point

Thermodynamic integration theory was used to calculate the free energy difference between a system of an ideal Si gas and a system which has been calculated with the PBE functional and sampled at the Γ point. From now on this setup will be called the PBE_Γ liquid. Both systems the ideal gas and the PBE_Γ consists of 64 Si atoms, a volume per atom of 20.49 $Å^3$ and are calculated at the temperature 1687 K. We obtained the free energy difference by performing 7 MD simulations where each consisted of 60000 time steps, with a step of 0.5 fs. For the first simulation at $\lambda = 0.0000010846$ the Langevin thermostat, with the friction coefficient of $\gamma = 5\frac{1}{ps}$ was used. For the other 6 simulations the Nosé-Hoover thermostat with `SMASS=5` was used. The flags `ISMEAR=-1` and `SIGMA=0.145` were set. The energy cutoff was the default value of 245.34 eV. For the `POTCAR` file we used the *PAW_PBE Si_GW_new 19Mar2013* file. Additional the `SCALEE` flag was set. The `SCALEE` flag sets the $\lambda \in [0, 1]$ parameter. The λ parameter specifies the amount of ab-initio energy in the simulations. This parameter scales the ab-initio energy $\lambda U^{\text{ab-inito}}$ as well as the ab-initio forces $\lambda F^{\text{ab-inito}}$. Each of the MD simulations was performed with a different λ value. We had to choose the λ parameter in a way that a 8 point Gauss-Lobatto quadrature can be used.

When we plot the λ parameter of each simulation versus the average energies per atom of each simulation, we obtain figure 50.

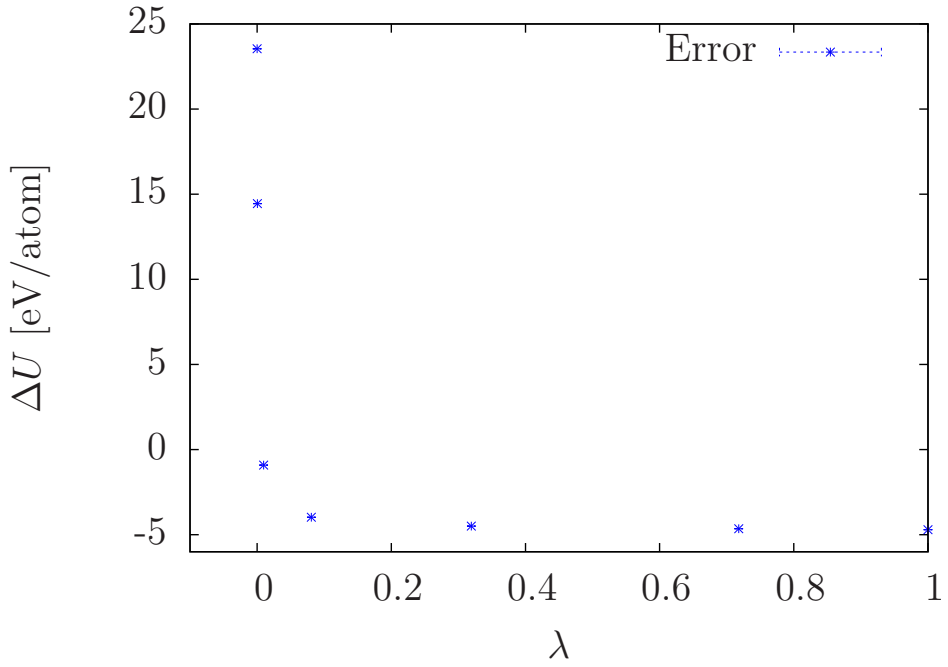

Figure 50: *Energy difference between an ideal gas and a PBE Γ point liquid as a function of the λ parameter.*

The Gauss-Lobatto quadrature integrates from $x \in [-1, 1]$, but $\lambda \in [0, 1]$, so we used the variable transformation

$$\lambda(x) = (\frac{x+1}{2})^{\frac{1}{1-k}}. \tag{184}$$

With the variable transformation of (184) the following integral transformation can be obtained.

$$\int_{-1}^{1} F(\lambda(x))\frac{d\lambda(x)}{dx}dx = \frac{1}{2(1-k)}\int_{-1}^{1} F(\lambda(x))\lambda(x)^k dx \tag{185}$$

In (185) $F(\lambda)$ is the energy difference as a function of the λ parameter. $F(\lambda)$ is shown in figure 50. Using the Gauss-Lobatto quadrature the integral turns into the sum

$$\frac{1}{2(1-k)}\int_{-1}^{1} F(\lambda(x))\lambda(x)^k dx = \frac{1}{2(1-k)}\sum_{i=0}^{n} \omega_{x_i} F(\lambda(x_i))\lambda(x_i)^k. \tag{186}$$

The right choice for the transformation (184) and a good choice for the k value are important. In figure 50 it can be seen that the energy becomes very large and positive at small λ. This is close to the ideal gas. Atoms in the ideal gas come very close to each other, which is forbidden by the Pauli repulsion in real systems. For the point $\lambda = 0$ atoms can even overlap, and then `VASP` fails. Therefore we have to choose the transformation in a way that the energy at the point $\lambda = 0$ is never considered. The transformation is chosen such that the transformed function $F(\lambda(x))\lambda(x)^k$ can be set to 0 at the $\lambda = 0$ ($x = -1$) point (figure 51). The transformation should also satisfy that the λ density is large at small λ's and becomes very coarse at $\lambda = 1$. In figure 51 we can see that the function $F(\lambda(x))\lambda(x)^k$ has to map the Gauss-Lobatto integration points x such that the point $x = -1$ ($\lambda = 0$) can be set to 0. This behavior of the transformed function can be obtained with the variable transformation (184) and the right choice of k. In test calculations $k = 0.8$ was found to be an excellent choice although $k = 0.75$ or $k = 0.7$ fields within 1 meV to the same results as we obtain for $k = 0.8$.

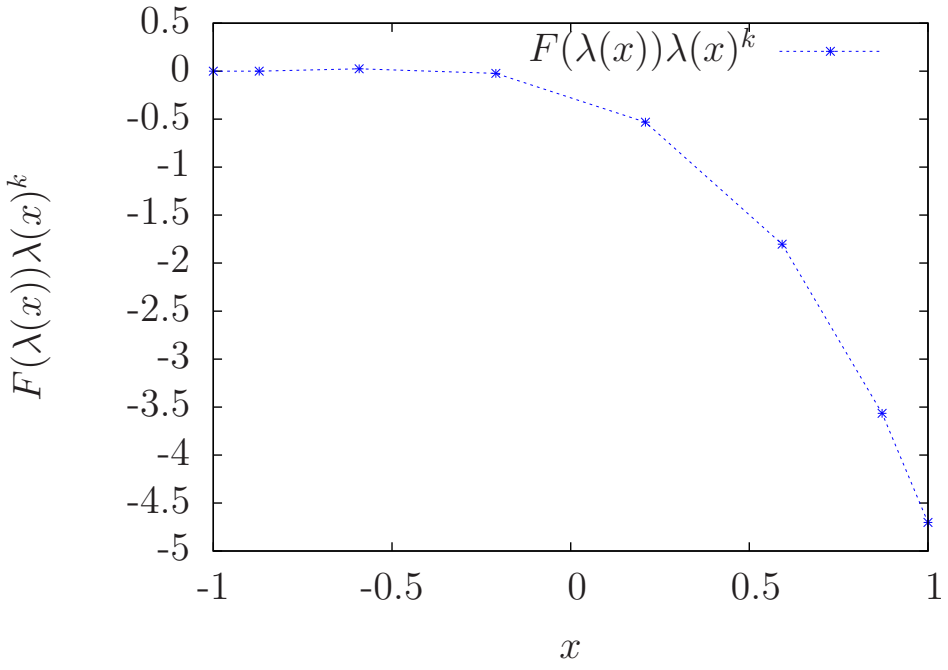

Figure 51: *Transformed integrand as a function of the Gauss-Lobatto points x.*

To use the Gauss-Lobatto quadrature, we had to calculate the weight functions ω_{x_i}.

$$\omega_{x_i} = \frac{2}{n(n-1)[P_{n-1}(x_i)]^2} \tag{187}$$

Where P_n are the Legendre polynomials. In the following table we listed the weight functions ω_x for x values which belong to the eight λ-values. In the table there are also the terms of the integral listed and the statistical error that is introduced by the finite runtime of the MD simulation. The error was calculated using the block average method.

Table 11: *Gauss-Lobatto quadrature*

ω_{x_i}	$\lambda(x_i)^k$	$F(\lambda(x_i)) \cdot \frac{\lambda(x_i)^k \cdot \omega_{x_i}}{2(1-k)}$	standard error [eV/atom]
0.0357143	0	0	0
0.2107042	0.0000169	0.000201009	0.0179
0.3411227	0.0017370	0.021446859	0.00689
0.4124588	0.0244303	-0.023321233	0.00105
0.4124588	0.1336642	-0.546851007	0.00014
0.3411227	0.4011669	-1.538547213	0.000035
0.2107042	0.7671774	-1.878741763	0.000034
0.0357143	1	-0.419900535	0.00004

By summing up the third row of table 11 we obtain the result for the integral. In the fourth row the error has to be multiplied by the weight $\frac{\lambda(x_i)^k \omega_{x_i}}{2(1-k)}$ and then add up to obtain the error of the free energy difference. The result for the free energy difference between ideal gas and the PBE_Γ liquid is $\Delta F = (-4.3857 \pm 0.0011)$ eV/atom.

16.2.3 Integration from the PBE_Γ liquid to PBE at 2×2×2 k-points

In this section we use thermodynamic integration theory to integrate from the PBE_Γ liquid to a liquid system, which has been calculated with the PBE functional at 2×2×2 Gamma centered k-points. The PBE system at 2×2×2 k-points will be called the PBE_{2k} liquid. The volume, temperature and the number of atoms are the same as in section 15.2.2. Also the flags we used are the same as in 15.2.2. Except of the `SCALEE` flag, we did not use that in this section. The `POTCAR` file is the same as in 15.2.2. In this section we used the Langevin thermostat with the same parameters as in 15.2.2, but also the Nosé Hoover thermostat with the `SMASS=5` flag. The additional flags `VCAIMAGES` and `IMAGES` are set for some simulations and the use of them will be discusses below. For this integration we used the Milne quadrature formula. With the Milne quadrature, we can approximate the integral from (121) as:

$$\begin{aligned}\Delta F \approx \frac{1}{90}(&\underbrace{7\langle U^{\mathrm{PBE_{2k}}} - U^{\mathrm{PBE_\Gamma}}\rangle_{\mathrm{PBE_\Gamma}}}_{1} + \underbrace{32\langle U^{\mathrm{PBE_{2k}}} - U^{\mathrm{PBE_\Gamma}}\rangle_{\frac{0.25\mathrm{PBE_\Gamma}+0.75\mathrm{PBE_{2k}}}{2}}}_{2} + \\ &\underbrace{12\langle U^{\mathrm{PBE_{2k}}} - U^{\mathrm{PBE_\Gamma}}\rangle_{\frac{\mathrm{PBE_\Gamma}+\mathrm{PBE_{2k}}}{2}}}_{3} + \underbrace{32\langle U^{\mathrm{PBE_{2k}}} - U^{\mathrm{PBE_\Gamma}}\rangle_{\frac{0.75\mathrm{PBE_\Gamma}+0.25\mathrm{PBE_{2k}}}{2}}}_{4} + \\ &\underbrace{7\langle U^{\mathrm{PBE_{2k}}} - U^{\mathrm{PBE_\Gamma}}\rangle_{\mathrm{PBE_{2k}}}}_{5}).\end{aligned} \tag{188}$$

The first, two MD simulations were performed at the end-points: one with PBE_Γ and one with PBE_{2k}. Both of these simulations consisted of 2000 time steps with a step of 3 fs. They were performed with the Langevin thermostat. For part 1 of the approximation (188), we used every 10th configuration of the PBE_Γ MD simulation and performed for each of these configurations a PBE_{2k} calculation. For contribution 5 we did the same, but then the MD was performed with PBE_{2k} and every 10th configuration was used to perform a PBE_Γ calculation. For contribution 3, we performed a MD simulation where the forces are calculated by $F = \frac{F(\mathrm{PBE}_\Gamma)+F(\mathrm{PBE_{2k}})}{2}$. We obtain this by setting the flags `VCAIMAGES=0.5` and `IMAGES=2`. For contribution 2 and contribution 4 the flag `VCAIMAGES` was set to 0.25 and 0.75. These simulations were performed with the Nosé Hoover thermostat and run for 2000 steps.

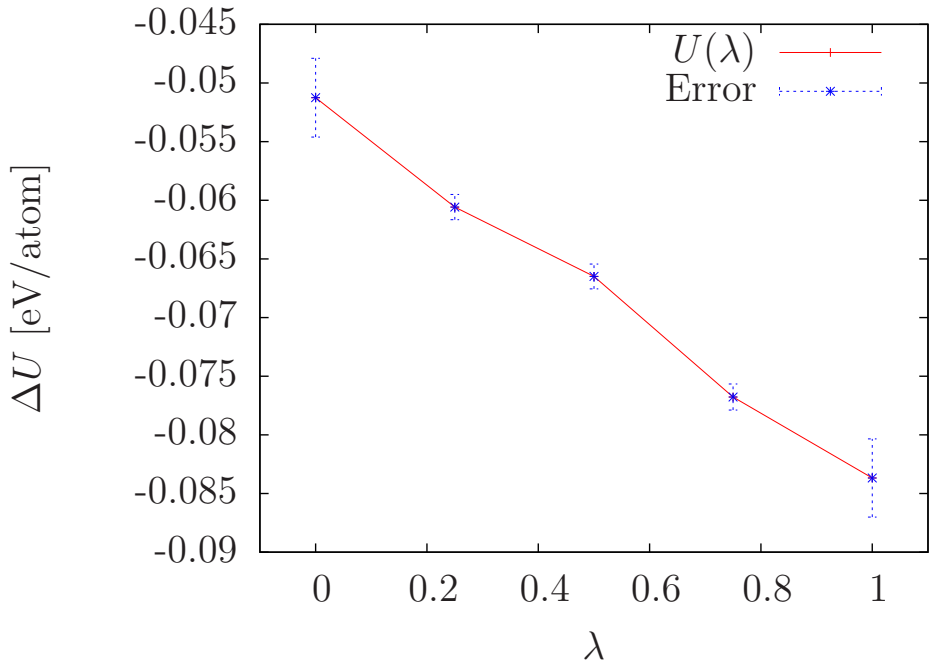

Figure 52: *Difference of internal energy U between a PBE_{Γ} liquid and a PBE_{2k} liquid as a function of the λ parameter.*

Figure 52 shows the average difference of the internal energy U between PBE_{Γ} and PBE_{2k} as a function of the λ parameter. Using formula (188) we obtain a result for the free energy difference of $\Delta F = (-0.0682 \pm 0.0014)$ eV/atom. The result was verified with the mid point rule and the simpson rule leading practically to the same result within the error bar. The result of the mid point rule is $\Delta F = (-0.0668 \pm 0.0011)$ eV/atom and the result of the simpson rule is $\Delta F = (-0.0682 \pm 0.0018)$ eV/atom

16.2.4 Integration from the PBE_{2k} liquid to HSE at 2×2×2 k-points with NKRED

In this section we integrate from the PBE_{2k} liquid to a system which has been calculated with the HSE06 functional and using the `NKRED=2` flag at 2×2×2 Gamma centered k-points. This system will be called the HSE_{NKRED} liquid. System size, temperature and number of atoms are the same as in 15.2.2. Also all flags and the `POTCAR` file stay the same. For this integration we used the Simpson quadrature formula. With the Simpson quadrature, we can approximate the integral from (121) as:

$$\Delta F \approx \underbrace{\frac{1}{6}\langle U^{\mathrm{HSE_{NKRED}}} - U^{\mathrm{PBE_{2k}}}\rangle_{\mathrm{PBE_{2k}}}}_{1} + \underbrace{\frac{4}{6}\langle U^{\mathrm{HSE_{NKRED}}} - U^{\mathrm{PBE_{2k}}}\rangle_{\frac{\mathrm{PBE_{2k}}+\mathrm{HSE_{NKRED}}}{2}}}_{2} + \underbrace{\frac{1}{6}\langle U^{\mathrm{HSE_{NKRED}}} - U^{\mathrm{PBE_{2k}}}\rangle_{\mathrm{HSE_{NKRED}}}}_{3}. \tag{189}$$

The strategy to calculate the contributions of (189) is the same as in the previous section. Contribution 1 and 3 were calculated by performing MD simulations using the Langevin thermostat with the same parameters as in 15.2.2. Contribution 2 was calculated by the Nosé Hoover thermostat and the additional flags `VCAIMAGES=0.5` and `IMAGES=2`. This means that `VASP` performed two simulations for identical positions and averaged the forces according to $F = \frac{F(\mathrm{PBE_{2k}})+F(\mathrm{HSE_{NKRED}})}{2}$.

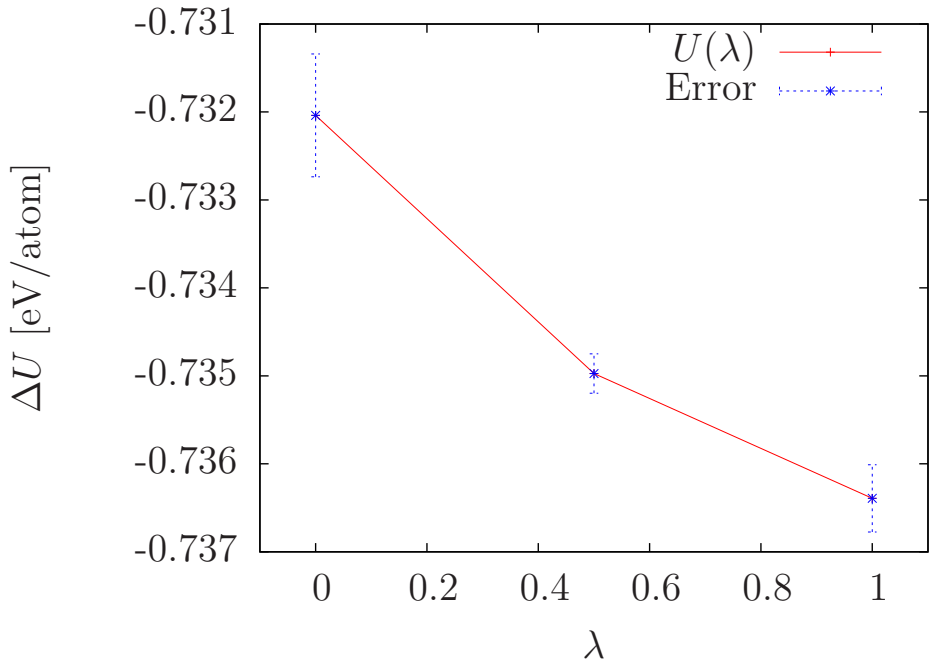

Figure 53: *Difference between a PBE_{2k} liquid and a HSE_{NKRED} liquid as a function of the λ parameter.*

Figure 53 shows the average energy difference between PBE_{2k} and HSE_{NKRED} liquid as a function of the λ parameter. Using formula (189) we obtain a result for the free energy difference $\Delta F = (-0.7347 \pm 0.0013)$ eV/atom. We also could use the mid point rule, which leads to the result of $\Delta F = (-0.7349 \pm 0.0022)$ eV/atom. The result of the mid point rule lies in the error bar of the result from the simpson rule and is therefore practically the same.

16.2.5 Thermodynamic Perturbation from a HSE_{NKRED} liquid to a HSE system with 3×3×3 Monkhorst-Pack k-points

We used thermodynamic perturbation theory to calculate the free energy difference between a HSE_{NKRED} liquid and a HSE system with 3×3×3 Monkhorst-Pack k-points. We will call this system the HSE_{3k} liquid. First we performed an MD simulation with the HSE06 functional and the `NKRED=2` flag. The system properties and the `VASP` flags stayed the same as in the previous section. From this simulation we took the configuration of every 20th step, to get statistically reasonably independent configurations. For these configurations we performed a HSE06 calculation at 3×3×3 Monkhorst-Pack k-points without setting NKRED. To determine whether thermodynamic perturbation theory is reliable in this case we adopted both the exact relation as well as the quadratic Taylor expansion (129).

$$-\frac{1}{\beta}\ln\langle e^{-\beta\Delta U}\rangle = 0.021739 \tag{190}$$

$$\langle\Delta U\rangle - \frac{\beta}{2}\langle(\Delta U)^2\rangle + \frac{\beta}{2}\langle\Delta U\rangle^2 = 0.021738 \tag{191}$$

The results of (190) and (191) are almost exactly the same suggesting that TPT is very accurate. The result of the free energy difference between a HSE_{NKRED} liquid and a HSE_{3k} liquid is $\Delta F = (0.0217 \pm 1.8 \cdot 10^{-4})$ eV/atom.

16.2.6 Free Energy of the HSE_{3k} liquid

In this subsection we summarize the results for the free energy differences and the result of the free energy of a HSE_{3k} liquid.

Table 12: *Free energy of HSE_{3k} liquid*

	eV/atom	standard error eV/atom
F_{ideal}	-1.6685	
ΔF (ideal gas → PBE_{Γ})	-4.3857	± 0.0011
ΔF (PBE_{Γ} → PBE_{2k})	-0.0682	± 0.0014
ΔF (PBE_{2k} → HSE_{NKRED})	-0.7347	± 0.0013
ΔF (HSE_{NKRED} → HSE_{3k})	0.0217	± $1.8 \cdot 10^{-4}$
F_{liquid}	-6.8354	± 0.0039

16.3 Free Energy of solid silicon

For the prediction of the melting temperature it is also important to calculate the free energy of the system in the solid phase. In this section the free energy of a solid Si crystal is calculated using the HSE06 functional. The crystal consists of 64 Si atoms, it has a diamond structure and the volume per atom is 20.496 Å^3. All calculations in this section were performed with the `POTCAR` file *PAW_PBE Si_GW_new 19Mar2013*. The free energy of a crystal consists of three parts. The internal energy of the Si crystal at $T = 0$ K and free energy correction of electrons at $T = 1687$ K. The free energy of a harmonic vibrating crystal and the free energy correction related to anharmonic contributions. The calculations of these three energies will be discussed in the next sections.

16.3.1 Internal energy of a silicon crystal at $T = 0$ plus free energy correction of the electronic system

This calculation was performed for a Si crystal with a diamond structure and 64 atoms. The volume per atom was 20.496Å^3. To obtain the internal energy and the electronic free energy we performed HSE simulations. For the correction of the electronic system the flags `ISMEAR=-1` and `SIGMA=0.11` were set. With `ISMEAR=-1` the partial occupancies of the electrons are set from a Fermi Dirac statistic and `SIGMA=0.11` determines the width of the Fermi smearing, which corresponds to the temperature $T = 1687$ K. Also the flag `PRECFOCK=Fast` and `LREAL=Auto` was set. This simulation was performed using 2×2×2 Monkhorst-Pack k-points. The result of the simulation and the error which was determined by Gaussian error propagation is $F_{\text{ideal}} = (-6.2548 \pm 5.3 \cdot 10^{-7})$ eV/atom.

16.3.2 Harmonic component of the free energy

To calculate the harmonic component of the free energy a calculation of the phonon frequencies, with `IBRION=6` and 2×2×2 Monkhorst-Pack k-points was performed. The system and the `VASP` flags are the same as in the previous section. With the resulting `DYNMATFULL` file, the program Phonopy calculated the free energy as a function of the temperature.

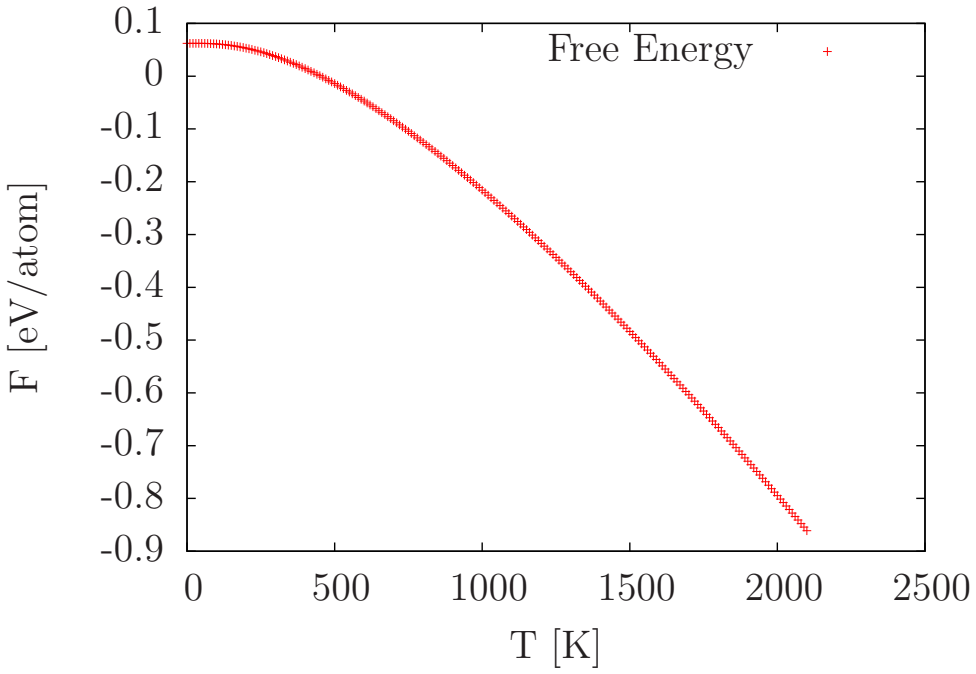

Figure 54: *Harmonic component of the free energy as a function of the temperature*

Figure 54 shows the free energy as a function of the temperature. The free energy at the temperature $T = 1687$ K is $\Delta F = -0.5955$ eV/atom. For the next part we need an additional file, the `DYNMATFULL` file. It contains all the normal modes and the frequencies of the silicon cell. We obtained this by performing the same simulation with the additional flag `ISPECIAL=-1`. Note that the calculation of the harmonic component were performed with the flag `PRECFOCK=Normal` and the other solid calculations with `PRECFOCK=Fast`. The use of another FFT grid could cost inaccurateness in the result. We repeated the calculation with `PRECFOCK=Fast` and obtained practically the same result.

16.3.3 Anharmonic component of the free energy

To calculate the anharmonic component, we used thermodynamic integration. We integrated from a system with harmonic oscillations to a fully interacting system. Under a fully interacting system we understand an ab-initio calculation with the PBE or HSE06 functionals. For the integration we used a three point Gauss-Legendre-Integration. For this integration we had to perform three MD simulations. For the MD simulations the `SCALEE` flag was set. The `SCALEE` flag controls the λ parameter. In these MD simulations the internal energy and the forces were calculated as

$$U = (1-\lambda)U^{\text{harm}} + \lambda U^{\text{ab-initio}} \tag{192}$$

Where U^{harm} is the harmonic part of the internal energy, which is calculated from the `DYNMATFULL` file. The ab-initio energy $U^{\text{ab-initio}}$ is calculated with the PBE or HSE06 functional at 2×2×2 Monkhorst-Pack k-points. An MD simulation with HSE06 would be fairly time-consuming, however we decided to use a hybrid Monte Carlo strategy [**34**]. In this strategy one starts with an initial configuration and random velocities. For this initial configuration a HSE calculation, with the same flags as in 16.1. is performed. Then 40 MD steps using the PBE functional are performed. For the final configuration another HSE06 calculation is done. This final step is accepted with the following probability.

$$p_{acc} = min\left[1, \frac{exp(-\beta(E_{\text{HSE}}(\mathbf{r}^f) + E_{\text{kin}}(\mathbf{p}^f)}{exp(-\beta(E_{\text{HSE}}(\mathbf{r}^i) + E_{\text{kin}}(\mathbf{p}^i)}\right] \tag{193}$$

Where $\mathbf{r}^f$,$\mathbf{p}^f$ are the final positions and momenta and $\mathbf{r}^i$,$\mathbf{p}^i$ are the initial positions and momenta. This Monte Carlo strategy creates a canonical ensemble for the HSE functional. To use the Gauss-Legendre-quadrature, we had to change the interval from $x \in [-1,1]$ to $\lambda \in [0,1]$, with a linear transformation

$$\lambda(x) = \frac{x+1}{2}. \tag{194}$$

This leads to the points $\lambda_1 = 0.1127016653$, $\lambda_2 = 0.5$ and $\lambda_3 = 0.8872983346$. For each of these points a hybrid Monte Carlo simulation was performed. With the transformation we also have to rewrite the integral (125).

$$\int_{-1}^{1} F(\lambda(x))\frac{d\lambda}{dx}dx = \frac{1}{2}\int_{-1}^{1} F(\lambda(x))dx \approx \frac{1}{2}\sum_{i=1}^{3}\omega_{x_i}F(\lambda(x_i)) \tag{195}$$

The next figure shows the internal energy difference per atom between the ab-initio calculation and the harmonic approximation, for every integration point.

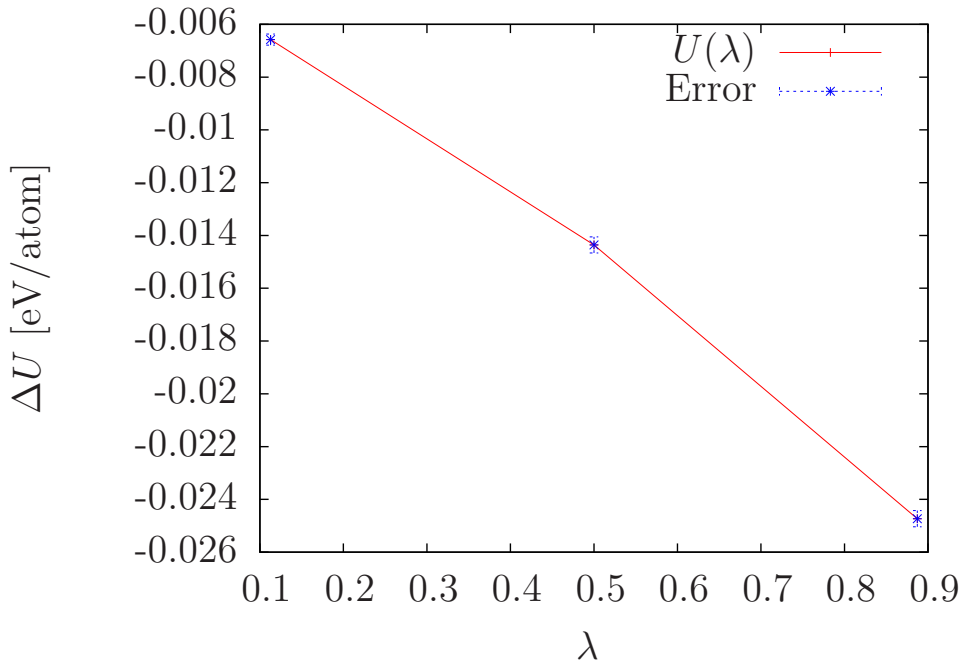

Figure 55: *Internal energy difference per atom between the ab-initio calculation and the harmonic approximation as a function of the λ parameter.*

In the following table we present the results of this integration.

Table 13: *Gauss-Legendre-quadrature*

ω_x	$\frac{1}{2}F(\lambda(x_i)) \cdot \omega_{x_i}$	standard error
0.555555	-0.001825	0.00021
0.888888	-0.006375	0.0003
0.555555	-0.006863	0.00031

By summing up the third row of table 13 we obtain the result for the integral. In the fourth row the error has to be multiplied by the weight $\frac{\omega_{x_i}}{2}$ and then add up to obtain the error of the free energy difference. The result of the integral is $\Delta F = (-0.01506 \pm 0.00074)$ eV/atom.

16.3.4 Thermodynamic Perturbation from the HSE_{2k} solid to a HSE system with 3×3×3

In this section we used thermodynamic perturbation theory to calculate the free energy difference between the fully interacting HSE system at 2×2×2 k-points to a HSE system at 3×3×3 k-points. We performed an hybrid Monte Carlo simulation for the fully interacting system at 2×2×2 Monkhorst-Pack k-points, with the same flags as in the previous sections. From this simulation we took 10 statistical independent configurations and performed for each of them a HSE06 simulation at 3×3×3 Monkhorst-Pack k-points. With the exact relation and the Taylor expansion (129) we checked if thermodynamic perturbation theory is reliable.

$$-\frac{1}{\beta}\ln\langle e^{-\beta\Delta U}\rangle = -0.00091519 \tag{196}$$

$$\langle\Delta U\rangle - \frac{\beta}{2}\langle(\Delta U)^2\rangle + \frac{\beta}{2}\langle\Delta U\rangle^2 = -0.00091809 \tag{197}$$

With the results of (196) and (197) we suggest that TPT is very accurate. The free energy difference between the systems is $\Delta F = (-0.0092 \pm 7.1 \cdot 10^{-5})$.

16.3.5 Free energy of the HSE solid

In this subsection we summarize the results for the free energy differences and the result of the free energy of the solid for the HSE06 functional.

Table 14: *Free energy of the solid using the HSE06 functional*

	eV/atom	standard error eV/atom
F_{ideal}	-6.2548	$\pm\ 5.3 \cdot 10^{-7}$
F_{harm}	-0.5955	
F_{anharm}	-0.0151	$\pm\ 7.4 \cdot 10^{-4}$
ΔF ($\text{HSE}_{2\text{k}} \rightarrow \text{HSE}_{3\text{k}}$)	-0.0009	$\pm\ 7.1 \cdot 10^{-5}$
F_{solid}	-6.8663	$\pm\ 8.1 \cdot 10^{-4}$

16.4 Melting point of silicon

We have now the free energy and the internal energy of both phases for a certain thermodynamic state point. It is possible to estimate F for other thermodynamic state points. For this calculation we start with the free energy.

$$F = U - TS \tag{198}$$

By differentiating F with respect to T we obtain

$$\begin{aligned} \frac{\partial F}{\partial T} &= \frac{\Delta F}{\Delta T} = -S \\ \Delta F &= -S\Delta T. \end{aligned} \tag{199}$$

This means that for a small temperature change ΔT, the linear approximation of the free energy changes by ΔF. We can take this derivation for the free energy of the liquid

$$\frac{\partial F_{\text{liquid}}}{\partial T} = -S_{\text{liquid}} \tag{200}$$

and for the solid

$$\frac{\partial F_{\text{solid}}}{\partial T} = -S_{\text{solid}}. \tag{201}$$

When we now subtract equation (201) from equation (202) we obtain:

$$\frac{\partial (F_{\text{liquid}} - F_{\text{solid}})}{\partial T} = \frac{(F_{\text{liquid}} - F_{\text{solid}})}{\Delta T} = -(S_{\text{liquid}} - S_{\text{solid}}) \rightarrow \tag{202}$$

$$\Delta T = \frac{(F_{\text{liquid}} - F_{\text{solid}})}{-(S_{\text{liquid}} - S_{\text{solid}})}. \tag{203}$$

When we now plug in formula (198) in formula (204) we obtain

$$\Delta T = \frac{(F_{\text{liquid}} - F_{\text{solid}})}{-(U_{\text{liquid}} - F_{\text{liquid}} - U_{\text{solid}} + F_{\text{solid}})} \cdot T. \tag{204}$$

We can use equation (205), to calculate the melting temperature. First the internal energies for both phases are required. We obtain the internal energy $U_{\text{liquid}} = -5.49938$ eV for the liquid phase from the simulations of section 15.2.5 and the internal energy $U_{\text{solid}} = -6.00008$ eV for the solid phase from the simulations of section 15.3.4. The free energy difference between both phases is $\Delta F = F_{\text{liquid}} - F_{\text{solid}} = 30.9$ meV (section 15.2.6, 15.3.5) and the simulation temperature is $T = 1687$ K.

With equation (205) we obtain the result $\Delta T = (111 \pm 7)$ K. The temperature where the free energies of both phases will be roughly equal is $T_{\text{melt}} = T + \Delta T$. We finally obtain the result for the melting temperature $T_{\text{melt}} = (1798 \pm 7)$ K.

17 Conclusion

In the first part of this master thesis, the crystal structure and the binding energy of the materials selenium, tellurium, arsenic and antimony were investigated. The materials were simulated with three different vdW functionals the D2 method of Grimme, the method of Tkatchenko Scheffler (TS) and the vdW-DFT method. Additional simulations using the PBE functional, the HSE06 functional and the RPA were performed. What is conspicuous about the simulations is that the vdW functionals overestimate the vdW interactions, which results in a 5% smaller interchain distance for selenium and tellurium and in a 3% smaller interlayer distance in arsenic and antimony compared to the experimental value. The volume per atom calculated with the D2 method and TS method tend to be about 4% smaller for selenium and tellurium and about 2% smaller for arsenic and antimony. However the vdW-DFT tends to overestimate the volume per atom, especially for arsenic and antimony. In antimony the volume per atom is even about 6% larger than the experimental value. The PBE functional does not include vdW interactions. Calculations with this method result in too large volumes per atom for all four materials. For antimony the volume per atom is even 7% larger than the experimental value. With the HSE06 functional we only considered arsenic and antimony. For both materials in the cases of the volume per atom the HSE06 functional improves upon the PBE functional. The HSE06 functional predicted for arsenic and antimony volumes per atom about 2.5% larger than the experimental value. Conspicuous is that the interlayer distance is predicted about 0.5% closer to the experimental value using the PBE functional than the HSE06 functional. The RPA leads to excellent crystal structure predictions for the materials selenium, tellurium and arsenic. In the case of antimony the RPA hardly improves the volume per atom and the ratio between interchain and intrachain distance from PBE functional. Still the RPA is a promising method for crystal structure prediction of materials that include vdW interactions, but the RPA is also the method, which needs the most compute time. The computationally cheaper vdW functionals tend to overestimate the vdW interactions.

In the second part the free energy of liquid silicon and solid silicon were calculated using the HSE06 hybrid functional. With these free energies the melting temperature of silicon was predicted. The melting temperature lies 111 K above the experimental measured melting temperature. This is certainly a substantial improvement compared to LDA which predicts a melting temperature of 1351 K, 336 K below the experimental value of 1687 K. This shows, that the HSE06 functional prefers solid phases. A future goal for the melting temperature prediction of silicon would be to calculate the free energies for the liquid and the solid using the RPA. For the free energy of silicon thermodynamic perturbation theory between the HSE06 and the RPA functional might be used.

References

[1] P. Hohenberg and W. Kohn. "The Inhomogeneous Electron Gas". In: Phys. Rev. 136 (1964), B864. issn: 01631829. doi: 10.1103/PhysRevB.7.1912.

[2] W Kohn and L J Sham. "Self-consistent equations including exchange and correlation effects". In: Physical Review 140.4A (1965). issn: 0031899X. doi: 10.1103/PhysRev.140.A1133.

[3] Alexander L Fetter and John Dirk Walecka. Quantum Theory of Many-Particle Systems. Courier Corporation, 2003. isbn: 0-486-42827-3.

[4] D. M. Ceperley and B. J. Alder. "Ground state of the electron gas by a stochastic method". In: Physical Review Letters 45.7 (1980), pp. 566-569. issn: 00319007. doi: 10.1103/PhysRevLett.45.566.

[5] John P. Perdew and Yue Wang. "Accurate and simple analytic representation of the electron-gas correlation energy". In: Physical Review B 45.23 (1992), pp. 13244-13249. issn: 01631829. doi: 10.1103/PhysRevB.45.13244.

[6] John P. Perdew, Kieron Burke, and Matthias Ernzerhof. Generalized Gradient Approximation Made Simple. 1996. doi: 10.1103/PhysRevLett.77.3865.

[7] S. Grimme, "Semiempirical gga-type density functional constructed with a long-range dispersion correction.", J. Comp. Chem. 27, 1787 (2006).

[8] Alexandre Tkatchenko and Matthias Scheffler, "Accurate Molecular Van Der Waals Interactions from Ground-State Electron Density and Free-Atom Reference Data", DOI: 10.1103/PhysRevLett.102.073005

[9] Lampros Andrinopoulos, "Using van der Waals Density Functionals in ONETEP"

[10] Stefan Zahn "Vorlesung Hartree-Fock" Wilhelm-Ostwald-Institut für Physikalische und Theoretische Chemie, Universität Leipzig, Linnéstr. 2, D-04103 Leipzig, Germany

[11] VASP wiki "Hartree-Fock and HF/DFT hybrid functionals"

[12] David Langreth and John Perdew. "Exchange-correlation energy of a metallic surface: Wave-vector analysis". In: Physical Review B 15.6 (1977), pp. 2884-2901. issn: 0556-2805. doi: 10.1103/PhysRevB.15.2884.

[13] L.D. Landau and E.M. Lifshitz, Statistical Mechanics, (Addison-Wesley, Reading 1969).

[14] K. Yabana et al. "Real-time, real-space implementation of the linear response time-dependent density-functional theory". In: Physica Status Solidi (B) Basic Research. Vol. 243. 5. 2006, pp. 1121-1138. isbn: 0370-1972. doi: 10.1002/pssb.200642005.

[15] Mark S. Hybertsen and Steven G. Louie. "Ab initio static dielectric matrices from the density-functional approach. I. Formulation and application to semiconductors and insulators". In: Physical Review B 35.11 (1987), pp. 5585-5601. issn: 01631829. doi: 10.1103/PhysRevB.35.5585.

[16] VASP manual. "A general recipe to calculate ACFDT-RPA total energies". `https://cms.mpi.univie.ac.at/vasp/vasp/general_recipe_calculate_ACFDT_RPA_total_energies.html`

[17] Arthur Bialon "The Iron-Boron System: Ordered Structures and Point Defects"

[18] VASP manual. "Automatic k-mesh generation" https://cms.mpi.univie.ac.at/vasp/vasp/Automatic_k_mesh_generation.html

[19] DR Hamann. Generalized norm-conserving pseudopotentials. Physical Review B, 40(5):2980, 1989.

[20] VASP manual. "Thermodynamic integration" https://cms.mpi.univie.ac.at/vasp/vasp/Thermodynamic_integration_free_energy_gradients.html

[21] Wolfram MathWorld "Fundamental Theorem of Calculus" http://mathworld.wolfram.com/FirstFundamentalTheoremofCalculus.html

[22] Free-energy perturbation theory https://www.nyu.edu/classes/tuckerman/stat.mechII/lectures/lecture_9/node2.html

[23] Rudolf Gross, Achim Marx "Festkörper-physik"

[24] Wallace, D. C. "Thermodynamics of crystals" (Dover, 1998) Rec

[25] VASP Wiki. Langevin https://cms.mpi.univie.ac.at/wiki/index.php/MDALGO

[26] Nosé, S. A unified formulation of the constant temperature molecular dynamics methods. The Journal of Chemical Physics 81, 511-519 (1984)

[27] Daan Frenkel & Berend Smit "Understanding Molecular Simulation from Algorithm to Application"

[28] VASP manual. "Flags" http://cms.mpi.univie.ac.at/vasp/vasp/vasp.html

[29] Cherin, P. and Unger, P. The crystal structure of trigonal selenium Locality: synthetic, Inorganic Chemistry 6, 1588-1589 (1967)

[30] D. Vanderbilt and J. D. Joannopoulos, Phys. Rev. B 27, 6296 (1983).

[31] Adenis, C., Langer, V. and Lindqvist, O., Reinvestigation of the structure of tellurium, Acta Crystallographica, Section C: Crystal Structure Communications 45, 941-942 (1989)

[32] Pedersen, U. R., Hummel., F., Kresse, G., Kahl, G. & Dellago, C. "Computing gibbs free energy differences by interface pinning. Phys. Rev. B 88, 094101 (2013)

[33] Wyckoff, R. W. G., Second edition. Interscience Publishers, New York, CRYSTA1,7-7(1963)

[34] Nakayama A., Taketsugu T., Shiga M., "Speed-up of ab initio hybrid Monte Carlo and ab Initio path integral hybrid Monte Carlo simulations by using an auxiliary potential energy surface" Chemistry letters Vol. 38 5-Oct-2009 doi: 10.1246/cl.2009.976

[35] Osamu Sugino and Roberto Car "Ab Initio Molecular Dynamics Study of First-Order Phase Transitions: Melting of Silicon" Received 11 July 1994

[36] Physics of Group IV Elements and III VCompounds, - edited by K.-H. Hellwege and O. Madelung, Numerical "Data and Functional Relationship in Science and Technology", Landolt-Bornstein, New Series, Group III, Vol. 17, subvolume a (Springer-Verlag, Berlin, 1982)

[37] (C. Chipot "Free-energy calculations Measuring free-energy differences using computer simulations" University of Illinois)

[38] (Xiao-Lin Li, Guang-Han Cao, Chun-Mu Feng and Ya-Dong Li "Synthesis and magnetoresistance measurement of tellurium microtubes" Journal of Materials Chemistry)